

**Foundations and Trends® in Electric Energy
Systems**

Distribution System Optimization to Manage Distributed Energy Resources (DERs) for Grid Services

Suggested Citation: Anamika Dubey and Sumit Paudyal (2023), "Distribution System Optimization to Manage Distributed Energy Resources (DERs) for Grid Services", Foundations and Trends® in Electric Energy Systems: Vol. 6, No. 3-4, pp 120–264. DOI: 10.1561/3100000030.

Anamika Dubey
Washington State University
anamika.dubey@wsu.edu

Sumit Paudyal
Florida International University
spaudyal@fiu.edu

This article may be used only for the purpose of research, teaching, and/or private study. Commercial use or systematic downloading (by robots or other automatic processes) is prohibited without explicit Publisher approval.

now
the essence of knowledge
Boston — Delft

Contents

1	Introduction	122
1.1	Motivation for Optimizing Distribution Systems Operations	124
1.2	DGs/DERs for Grid Services and D-OPF Formulations	125
1.3	Organization of Monograph	129
2	Network Modeling and Distribution Power Flow Formulation	131
2.1	Power Distribution Systems	131
2.2	Defining Device Models	133
2.3	Distribution Power Flow Models	136
2.4	Illustrated Example	139
2.5	Algorithms to Solve Distribution Power Flow Model	142
2.6	Distribution System Simulators	148
2.7	Summary and Discussions	150
3	Distribution Optimal Power Flow (D-OPF) Formulations	151
3.1	Introduction	151
3.2	Notations	152
3.3	Basics D-OPF Problem	152
3.4	Distribution Nonlinear Optimal Power Flow Models	155
3.5	Approximation and Relaxation Techniques	157
3.6	Multi-period Optimization: D-OPF problems	163

3.7	Illustrated Example	163
3.8	Modeling Tools and Solvers	174
3.9	Summary and Discussions	177
4	Mixed-Integer D-OPF Model	180
4.1	Introduction	180
4.2	Mixed-Integer Non-Linear Formulation	181
4.3	Mixed-Integer Convex Formulation	181
4.4	Performance of MISOCP DOPF Formulation	187
4.5	Performance of MILP DOPF Formulation	190
4.6	Summary and Discussion	190
5	Distribution Voltage Control: Conservation Voltage Reduction	194
5.1	Optimization Problem Formulation	196
5.2	Solution Approach	201
5.3	Large-feeder Simulation Results	203
5.4	Summary and Discussions	212
6	Resilient Distribution Systems Operations	214
6.1	DG-assisted Distribution System Restoration	216
6.2	Optimization Problem Formulation	217
6.3	Results and Discussions	224
6.4	GridAPPS-D Integration of FLISR Application	231
6.5	Summary and Discussions	237
7	Conclusions and Future Directions	238
7.1	Algorithmic Challenges with Grid-Edge Optimization	239
7.2	Learning-for-Control for DGs/DERs Coordination	242
7.3	Open-source Grid Optimization Packages/Simulator Interface	243
Acknowledgements		245
References		247

Distribution System Optimization to Manage Distributed Energy Resources (DERs) for Grid Services

Anamika Dubey¹ and Sumit Paudyal²

¹ Washington State University, USA; anamika.dubey@wsu.edu

² Florida International University, USA; spaudyal@fiu.edu

ABSTRACT

The proliferation of distributed energy resources (DERs) and the deployment of advanced sensing and control technologies in electric power distribution systems calls for coordinated management of the grid's resources. This has sparked a growing interest in optimization methods for large-scale unbalanced power distribution systems, with the goal of improving grid's operational efficiency and resilience. The current fast-paced research in this domain is driven by the challenging mathematical problem of three-phase optimal power flow (OPF). This monograph introduces the state-of-the-art optimization methods applied to unbalanced power distribution systems for the provisioning of grid services from DERs. To that end, fundamentals of D-OPF methods are introduced along with the unique challenges and differences compared to the bulk grid and related aspects of computational complexity due to mutual coupling, unbalanced loading conditions, and control of legacy devices. Different models for formulating D-OPF problems are described in

Anamika Dubey and Sumit Paudyal (2023), "Distribution System Optimization to Manage Distributed Energy Resources (DERs) for Grid Services", Foundations and Trends® in Electric Energy Systems: Vol. 6, No. 3-4, pp 120–264. DOI: 10.1561/3100000030.

©2023 A. Dubey and S. Paudyal

detail, as are methods for relaxing or approximating the formulations to achieve computational tractability. Finally, the use of D-OPF formulations to solve distribution-level operational problems via advanced distribution-level applications is described in detail. The specific applications discussed in this monograph include: (1) Volt-VAR control and Conservation Voltage Reduction using legacy voltage control devices and DERs, and (2) Solutions for Tomorrow's Grid Reconfiguration and Restoration using DERs.

1

Introduction

With the integration of numerous actionable agents, distributed generation resources, and sensing devices, the electric power distribution system is rapidly evolving into an autonomous and intelligent system. For example, behind-the-meter photovoltaic (PV) output has reached 71.3 GW in the U.S. power grid, with over 2.5 million PV panels installed. Likewise, a recent study shows California's fleet of light-duty plug-in EVs could double the total transportation electricity demand, from under 5,000 GWh in 2019 to over 10,000 GWh by 2030. Simultaneously, the grid is also getting overwhelmed with extreme weather events that are happening at a higher frequency and causing greater damage. Recent fire-related damages and fatalities caused by high-voltage transmission lines combined with dry weather are costing billions of dollars each year, with the only practical solution being de-energizing the lines and disrupting the power supply to millions of customers. The recent advances in the distribution systems, including the integration of distributed generation (DGs), distributed energy resources (DERs), and microgrids provide potential means to improve the grid's operational resilience. An advanced decision-support system is needed to plan and manage grid operations by proactively managing the grid's variable,

uncertain, and distributed resources. Consequently, resilient operational solutions for power distribution grids have drawn significant attention. These applications range from leveraging recent advances in smart grid technology, such as remote control capabilities and DERs, to enable advanced grid services such as frequency and voltage support for the bulk grid and resilient operations through intentional islanding to support critical services during disruptions.

The need for advanced grid support functionality from a large number of DERs has sparked increased interest in optimization methods for large-scale unbalanced power distribution systems. This monograph provides a much-needed primer on optimization methods used in active power distribution systems for advanced operations, with the goal of benefiting researchers working in this field. The graduate students and young researchers working in the area of DERs and distribution systems operations need a background on not only topics related to power distribution engineering but also a wide variety of interdisciplinary subjects to address the upcoming challenges. The monograph will benefit a diverse pool of researchers and industry practitioners by building the necessary background on modeling the distribution systems (with DERs) and system optimization methods for provisioning grid services.

Specifically, we introduce the state-of-the-art optimization methods applied to unbalanced power distribution systems for the provisioning of grid services for efficient and resilient grid operations. We begin with mathematical descriptions of the unbalanced power flow and optimal power flow (OPF) models and describe a systematic approach to problem formulation using an example test feeder. Our discussion also includes a mathematical description of distribution system components and controllable devices. We describe the mathematical complexity of resulting optimization problems and introduce commonly used relaxation and approximation techniques for computational tractability. We also detail the limitations of the existing formulations. The mathematical formulations are complemented by open-source codes using example distribution systems. Following that, we will describe the problem formulation for multiple grid service application cases that use distribution OPF. These algorithms are tested with large-scale distribution test systems, and the implications of using DGs/DERs for specific grid

services are discussed. Finally, we summarize outstanding challenges and the need for additional research in this area.

1.1 Motivation for Optimizing Distribution Systems Operations

The utility distribution systems are designed to deliver reliable electric power economically to the electrical consumers at their place of consumption. However, over the last decade, the electric power grid has been transforming unprecedentedly, necessitating a significant change in how we design, operate, and control traditional power systems. Starting with the high penetration of DERs, the integration of electric vehicles (EVs), bi-directional power flow, and smart metering, the power grid, as we know, is changing. The inherent variability of renewable generation and the vulnerability of traditional power systems to the demand and generation stochasticity can potentially result in system-level problems. However, if deployed and controlled purposefully, these new technologies can provide multiple crucial grid services that can help improve the efficiency, reliability, and resilience of the power grid.

Historically, distribution system operations have been mostly passive, with rule-based methods primarily used to control the feeder's few legacy voltage control devices, such as capacitor banks and voltage regulators. These control rules were pre-designed and acted based on local measurements. Since the loads were predictable and the system lacked any local generation resources, the rule-based controls were sufficient to ensure desirable system operations. However, the integration of DERs led to added variability and uncertainty in distribution system operations rendering rule-based and local-control-only algorithms inapplicable. Multiple studies showed that the integration of active grid-edge resources such as photovoltaic generation (PVs) or new load types, such as EVs may lead to multiple system-level challenges, including, but not limited to, voltage limit violations (overvoltages/undervoltages), increased voltage variability and three-phase voltage unbalance, and thermal limit violations [42]–[44], [88], [137]. It was also shown that the local control might result in unnecessary tap changes and capacitor bank operations; these are mechanical devices, and a higher number of operations can lead to mechanical failures [1]. Mitigating these system-

level operational challenges requires a coordinated operation of systems' controllable devices, including the new resources. It was also recognized that the new grid-edge resources could provide additional grid services, such as capacity, flexibility, ramping, voltage support, and so on, that were previously not possible in a passive power distribution system. This resulted in the development of new methods and advanced applications to actively manage grid-edge resources [41].

With the evolution of active power distribution systems and new grid requirements, optimal power flow (OPF) methods emerged as a potential mechanism to optimize distribution system operations for different grid service requirements. A comprehensive review of OPF methods is provided in the following articles [26], [63], [95], [97]. When compared to the bulk power grid, distribution-level OPF (D-OPF) presents distinct challenges due to three-phase unbalanced loading, mutual coupling among the different phases of the line, the presence of single-phase and two-phase branches, and radial topology with a high R/X ratio, which causes significant voltage drops. Furthermore, grid-edge optimization necessitates the integration of various technologies such as battery storage, smart inverters, capacitor banks, voltage regulators, and secondary voltage controllers resulting in mixed-integer decision variables and inter-temporal constraints. Besides that, distribution-level optimization necessitates the inclusion of multiple sources of uncertainty from model and measurement data, resulting in computationally intractable stochastic optimization formulations. As a result, D-OPF formulations and approaches require separate consideration than bulk-grid models.

1.2 DGs/DERs for Grid Services and D-OPF Formulations

In this section, we identify the commonly discussed grid services that DERs could potentially provide. These services are identified as those that originated for the distribution system or for the bulk-grid level. We also identify the possible class of objective functions associated with each grid service, controllable devices, and DER control variables, see Table 1.1. It is worth noting that many of these DER-enabled grid services are currently being validated through field demonstrations or are in the process of being deployed in the field, see [5], [6], [40], [78],

Table 1.1: Grid Services from DGs/DERs that can benefit from Distribution Optimal Power Flow Models and Algorithms

Grid Services	Problem Objective	Controllable Devices
Improved support for voltage and power quality	Manage feeder voltages (magnitude, variability, unbalance), reduce losses	Voltage regulators, capacitor banks, DG active/reactive power
Network congestion management service	Manage network thermal limit constraints via network reconfiguration, network tariff design and flexibility procurement	Tie switches, sectionalizing switches, Building energy management system (BMS), active/reactives power from DGs and other DERs (BESS, EVs)
Avoided or deferred distribution capacity costs	Conservation voltage reduction, reduce system peak, manage system constraints	DG active/reactive power from DGs and other DERs (BESS, EVs), voltage control devices
Leverage demand response capability	Reduce system peak Manage system constraints	Building energy management system (BMS), active power from DGs and other DERs (BESS, EVs)
Reduce wholesale energy costs	Distribution market to optimize social welfare cost	Building energy management system (BMS), active power from DGs and other DERs (BESS, EVs)
Reliability via DG-assisted restoration	Reduce outage duration	Tie switches, sectionalizing switches, grid-forming DGs, microgrids
Resilience via Intentional Islanding	Reduce outage duration, Stable islands	Tie switches, sectionalizing switches, grid-forming DGs, microgrids
Ancillary service (Bulk-grid frequency support)	Active power control for frequency support	Active power support from DGs and other DERs (BESS, EVs, BMS)
Ancillary service (Bulk-grid voltage support)	Reactive power control for voltage support	Reactive power support from DGs and other DERs (BESS, EVs, BMS)
Black-start regulation	Reduce system peak, Manage system constraint	Grid forming DERs
Flexibility reserve	Manage renewable variability	BESS, BMS, EVs
Energy and Ancillary service markets	Generate revenue by market participation	BESS, BMS, EVs

[143]. The procurement of these grid services can be formulated as an OPF problem with a specified objective function and constraints. The optimization problem type is dictated by control variables, the optimization time horizon, and the problem objective. Some grid services, such as bulk grid frequency and voltage support, may require a closed-loop formulation instead of an open-loop OPF model. Additionally, the problem formulation may involve multiple decision-making

hierarchies, such as coordinating distribution-level markets with wholesale markets. Although such applications can be modeled as one large optimization problem, they require hierarchical or distributed optimization approaches to manage the resulting computational complexity and information and data privacy requirements.

Mathematically, D-OPF is a constrained optimization problem. In its most general form, this results in a nonlinear mixed-integer optimization problem. However, several versions of the general model are solved depending on the decision variables and power flow models used in the problem definition [67]. A nonlinear D-OPF formulation is often solved where only continuous decision variables are modeled, excluding any discrete control devices in the formulation. These models can use bus-injection or branch-flow power flow models, resulting in different D-OPF formulations. In this case, the primary source of nonlinearity is due to nonlinear power flow equations. Given the difficulty of solving nonlinear optimization problems, power flow equations can be approximated or relaxed to produce a simpler linear or convex optimization formulations. Real-world D-OPF problems often require optimizing for both discrete and continuous control variables, resulting in a mixed-integer nonlinear optimization problem. These are some of the most difficult optimization problems to solve.

A list of problem types is described in Table 1.2. The control variables and optimization horizon will define the problem type. DG control parameters, such as active and reactive power dispatch from DGs, are modeled as continuous variables. However, integers, especially binary variables, are often included to model the connectivity/availability statuses of DG/DER devices; for example, the on/off status of EV charging, and the charge/discharge status of BESS are modeled as binary variables. Likewise, tap settings for voltage regulators and capacitor bank switch status are modeled as discrete decisions. The optimization time horizon is defined by the type of controllable device and whether they result in inter-temporal constraints. For example, the state-of-charge for BESS at future time intervals is a function of the current decision requiring a multi-time period optimization formulation. On the contrary, the reactive power dispatch from smart inverters connected to PVs does not carry any memory for the next time step and hence a single-

Table 1.2: Taxonomy of D-OPF Problem Types

D-OPF type	Power flow model	Optimization model	Decision variables
Nonlinear models	Bus-injection model [26]	NLP	Continuous
	Branch flow model [10], [11]	NLP	
Linear Approximate model	Lin-dist flow [46], [50]	LP	Continuous
	Other linearized models [58], [68], [127], [141]	LP	
Convex Relaxation models	Semi-definite relaxation [8], [46]	SDP	Continuous
	Second-order cone relaxation [46], [65], [68]	SOCP	
Mixed-integer models	Nonlinear power flow model [108], [148]	MINLP	Continuous, discrete
	Linear approximate model [99], [128]	MILP	
	Convex relaxation [4], [129], [134], [153]	MISOCP, MISDP	

period optimization will suffice. A stochastic optimization problem can be considered when it is important to incorporate uncertainty in the model parameters and measurements.

Table 1.3 details the controllable devices at the distribution level, corresponding controllable variables, and their types. Distribution systems primarily include legacy voltage control devices such as capacitor banks and voltage regulators, and feeder-level switches. Active distribution systems are integrated with various DER technologies, including PVs, BESS, EVs, BMS, etc. In the past decade, several power-electronics-based devices have also emerged as a viable option to control voltage and power flow in the distribution systems [13], [73], [91], [107]. Some examples include Low-voltage Distribution Static Compensator (D-STATCOM) [105], Static Var Compensator (SVC) [106], Unified power flow controller (UPFC) [33], [104], and Soft open points [70].

Table 1.3: Distribution-level Controllable Devices

Controllable Device	Controllable Parameter	Decision Variable
Voltage regulator	Tap setting	Discrete
Capacitor bank	On/Off status	Discrete
Feeder Switches	Connect/disconnect	Discrete
PVs with smart inverters	Active and/or reactive power	Continuous
	Connect/disconnect	Discrete
BESS with smart inverters	Active and/or reactive power	Continuous
	Charge/discharge status	Discrete
EVs	Active power	Continuous
	Charge/discharge	Discrete
BMS	Active power setpoints	Continuous
Other DGs (grid-following)	Active and/or reactive power	Continuous
	Connect/disconnect	Discrete
Other DGs (grid-forming)	Voltage and frequency	Continuous
	Connect/disconnect	Discrete
<i>Other Power Electronics Devices</i>		
Low-voltage Distribution STATCOM	Reactive power	Continuous
Unified power flow controller	Voltage and reactive power	Continuous
	Mode of operation	Discrete
Static Var Compensator (SVC)	Capacitor stages	Discrete
Soft Open Point (back-to-back VSCs, multiterminal VSCs)	Active and reactive power flow	Continuous

1.3 Organization of Monograph

The monograph is organized as follows. Section 1 introduces the concept of active power distribution systems, motivates the optimization for grid services, and describes the taxonomy for distribution-level optimization problems. Section 2 briefly reviews the distribution systems network and DER models for quasi-static analysis and optimization, including the distribution power flow models and algorithms. Section 3 develops the analytical framework for modeling distribution optimal power flow problems and introduces different approximation and relaxation techniques for scalability. Section 4 introduces discrete decisions into the distribution-level optimization problems and develops different mixed-integer distribution optimal power flow models. Sec-

tion 5 develops application cases for distribution-level services using DERs under normal operating conditions, namely services for voltage optimization. This section uses different OPF models introduced in Sections 3 and 4. Section 6 develops multiple application cases for resilient distribution systems operations using DERs in active power distribution systems. Section 7 presents some concluding remarks and future research directions.

2

Network Modeling and Distribution Power Flow Formulation

2.1 Power Distribution Systems

Power Distribution System refers to the section of an electric power system between the sub-transmission system and the customer's end. Distribution systems are generally considered to be electricity supply network operating at voltage levels of 132 kV and below; the typical distribution voltages in North America are 4.16 kV, 7.2 kV, 12.47 kV, 13.2 kV, 14.4 kV, 23.9 kV, 34.5 kV, and others [72]. A schematic diagram depicting various components of a distribution system is shown in Figure 2.1 [53], [72]. These components are:

- Feeders: These are the main three-phase wires which originate from the substation transformers to supply energy to the load centers. The feeders often branch out to three-phase, two-phase, and single-phase laterals. The wires could be overhead conductors or underground cables.
- Transformers: These step down the voltage to a distribution system voltage level. Three-phase as well as single-phase transformers are found in distribution systems. The three-phase transformer connections could be a wye grounded-wye grounded, delta-wye

grounded, open delta-wye grounded, and others. The substation transformer steps down the transmission/sub-transmission voltage to distribution level voltages. The distribution/service transformer further steps down the distribution level voltage to the voltage levels appropriate for utilization at the customer end.

- **Control and Protection Devices:** Distribution systems include a variety of control devices such as voltage regulators, switched capacitors (SCs), switches, etc. Voltage regulating elements such as load tap changers (LTCs) may be available in some transformers to regulate the customer end voltage. SCs are used for reactive power supply. Devices such as circuit breakers, reclosers,

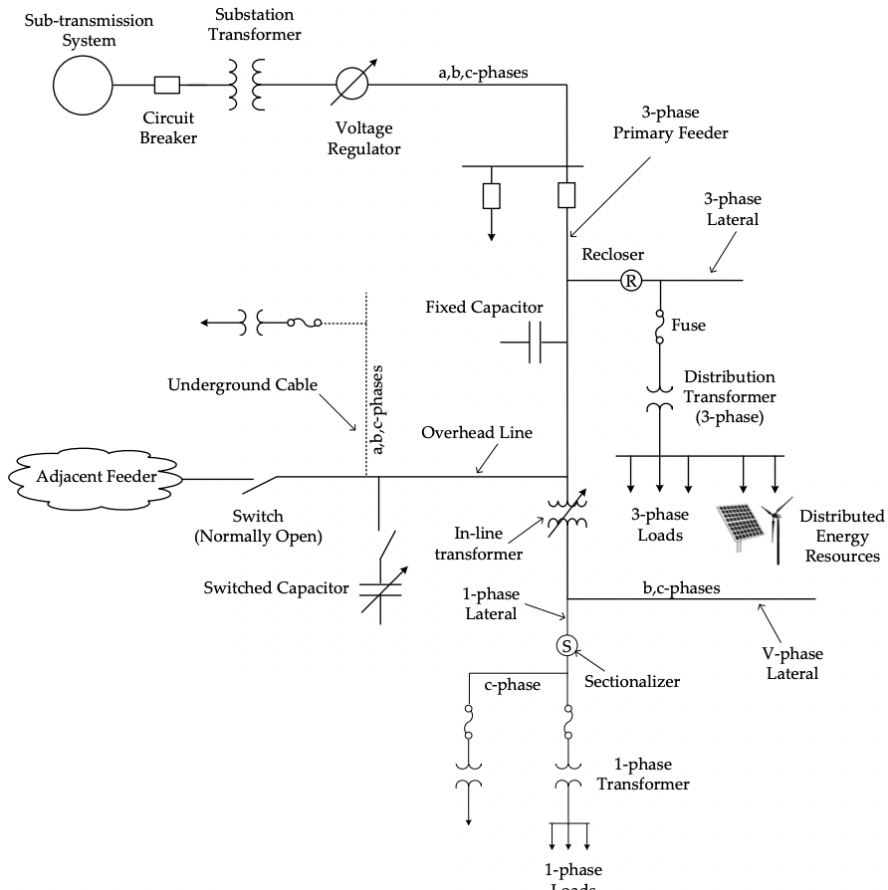


Figure 2.1: A typical North American Distribution Feeder [53], [72].

sectionalizers and fuses are used for the system and equipment protection. Switches and sectionalizers are often used to reconfigure the distribution system feeders.

- Other Components: These include the customer loads, fixed capacitors, and DERs connected at various nodes. Distribution systems are also equipped with metering equipment at substation and feeder levels. Present day distribution systems are also equipped with a communication infrastructure and the various components that make up the Advanced Metering Infrastructure (AMI), and new power electronics-based controllable devices (see Table 1.3).

2.2 Defining Device Models

This section details the mathematical models for some commonly available devices at the distribution level, including, capacitor banks, voltage regulators, smart inverters, BESS, and voltage-dependent customer loads.

2.2.1 Notations for Network Modeling

A radial distribution system can be represented as a directed graph $\mathcal{G} = (\mathcal{N}, \mathcal{E})$ where \mathcal{N} denotes set of buses and \mathcal{E} denotes set of edges. An edge (i, j) joins two adjacent nodes i and j where i is the parent node for node j . The three phase $\{a, b, c\}$ for a node i in the distribution system is denoted by $\Phi_i \subseteq \{a, b, c\}$. For each bus $i \in \mathcal{N}$ and phase $\psi \in \Phi_i$, let V_i^ψ , $s_{L,i}^\psi$, and $s_{DG,i}^\psi$ be complex voltage, complex power demand and complex DG power generation, respectively. Let, $V_i := [V_i^\psi]_{\psi \in \Phi_i}$, $s_{L,i} := [s_{L,i}^\psi]_{\psi \in \Phi_i}$ and $s_{DG,i} := [s_{DG,i}^\psi]_{\psi \in \Phi_i}$. For each line, let ψ phase current be I_{ij}^ψ and define, $I_{ij} := [I_{ij}^\psi]_{\psi \in \Phi_i}$. $(\cdot)^H$ represents the conjugate transpose and $\mathbf{j} = \sqrt{-1}$. Let z_{ij} be the phase impedance matrix for the two terminal devices such as distribution lines or transformers; kindly refer to [72] for details on line and transformer models.

2.2.2 Voltage Regulator

A 32-step voltage regulator with a voltage regulation range of $\pm 10\%$ is assumed. The series and shunt impedance of the voltage regulator are ignored as these have very small value [72]. Let, a^ψ be the turn ratio for the voltage regulator connected to phase ψ of line (i, j) . Then a^ψ can take values between 0.9 to 1.1 with each step resulting in a change of 0.00625 pu. An additional node i' is introduced to model the current equations. The control for regulator is defined using binary variables. Let, for $u_{tap,i}^\psi \in \{0, 1\}$ be a binary variable defined for each regulator step position i.e. $i \in \{1, 2, \dots, 32\}$. Also define a vector $b_i \in \{0.9, 0.90625, \dots, 1.1\}$. Then V_i^ψ , V_j^ψ , $I_{ii'}^\psi$, and $I_{i'j}^\psi$ where $\psi \in \Phi_i \cap \Phi_j$ are given as follows:

$$V_j^\psi = V_i^\psi = a^\psi V_i^\psi \text{ and } I_{ii'}^\psi = a^\psi I_{i'j}^\psi \quad (2.1)$$

$$\text{where, } a^\psi = \sum_{i=1}^{32} b_i u_{tap,i}^\psi \text{ and } \sum_{i=1}^{32} u_{tap,i}^\psi = 1.$$

In order to express (2.1) as a function of $v_i^\psi = (V_i^\psi)^2$, $v_j^\psi = (V_j^\psi)^2$, $l_{ii'}^{\psi\psi} = (I_{ii'}^\psi)^2$, and $l_{i'j}^{\psi\psi} = (I_{i'j}^\psi)^2$ we take square of (2.1) and define $(a^\psi)^2 = A^\psi$ and $b_i^2 = B_i$. Further realizing that $(u_{tap,i}^\psi)^2 = u_{tap,i}^\psi$, (2.1) can be reformulated as (2.2).

$$v_j^\psi = A^\psi \times v_i^\psi \text{ and } l_{ii'}^{\psi\psi} = A^\psi l_{i'j}^{\psi\psi} \quad (2.2)$$

2.2.3 Capacitor Banks

The per-phase model for capacitor banks is developed. The reactive power generated by capacitor bank, $q_{cap,i}^\psi$, is defined as a function of binary control variable $u_{cap,i}^\psi \in \{0, 1\}$ indicating the status (ON/OFF) of the capacitor bank, its rated per-phase reactive power $q_{cap,i}^{rated,\psi}$, and the square of the bus voltage at bus i for phase ψ , v_i^ψ .

$$q_{cap,i}^\psi = u_{cap,i}^\psi q_{cap,i}^{rated,\psi} v_i^\psi \quad (2.3)$$

The capacitor bank model is assumed to be voltage dependent and provides reactive power as a function of v_i^ψ when connected, i.e. $u_{cap,i}^\psi = 1$. For a three-phase capacitor bank, a common control variable, $u_{cap,i}^\psi$, is defined for each phase.

2.2.4 Distributed Generation with Smart Inverters

A per-phase model for reactive power support from smart inverter connected to DGs is developed. The DGs are modeled as negative loads with a known active power generation equal to the forecasted value. The reactive power support from DG depend upon the rating of the smart inverter. Let, the rated per-phase apparent power capacity for smart inverter connected to i^{th} DG be $s_{DG,i}^{rated,\psi}$ and the forecasted active power generation be $p_{DG,i}^\psi$. The available reactive power, $q_{DG,i}^\psi$ from the smart inverter is given by (2.4) which is a box constraint.

$$-\sqrt{(s_{DG,i}^{rated,\psi})^2 - (p_{DG,i}^\psi)^2} \leq q_{DG,i}^\psi \leq \sqrt{(s_{DG,i}^{rated,\psi})^2 - (p_{DG,i}^\psi)^2} \quad (2.4)$$

2.2.5 Voltage-Dependent Model for Customer Loads

The most widely acceptable load model is the ZIP model which is a combination of constant impedance (Z), constant current (I) and constant power (P)) characteristics of the load [20]. The mathematical representation of the ZIP model for the load connected at phase ψ of bus i is given by (2.5)-(2.6).

$$p_{L,i}^\psi = p_{i,0}^\psi \left[k_{p,1} \left(\frac{V_i^\psi}{V_0} \right)^2 + k_{p,2} \left(\frac{V_i^\psi}{V_0} \right) + k_{p,3} \right] \quad (2.5)$$

$$q_{L,i}^\psi = q_{i,0}^\psi \left[k_{q,1} \left(\frac{V_i^\psi}{V_0} \right)^2 + k_{q,2} \left(\frac{V_i^\psi}{V_0} \right) + k_{q,3} \right] \quad (2.6)$$

where, $k_{p,1} + k_{p,2} + k_{p,3} = 1$, $k_{q,1} + k_{q,2} + k_{q,3} = 1$, $p_{i,0}^\psi$ and $q_{i,0}^\psi$ are per-phase load consumption at nominal voltage, V_0 . Note that the ZIP load model represented in (2.5)-(2.6) are a function of both V_i^ψ and $v_i^\psi = (V_i^\psi)^2$.

2.2.6 Battery Energy Storage [64]

A generic BESS model considers a four-quadrant operation capability having the ability to inject and absorb both active and reactive power during its charging and discharging cycles (2.7). The use of separate terms for power injected into ($p_{i,CHA}^{\psi,t}$) or drawn from ($p_{i,DIS}^{\psi,t}$) the BESS

allows for a roundtrip efficiency of less than 100% which realistically accounts for BESS-to-grid interactions [29].

$$\begin{aligned} \text{SOC}_i^{\psi,t} &= \text{SOC}_i^{\psi,t-1} \\ &\quad - \Delta t \left(\eta_{i,\text{CHA}}^{\psi} p_{i,\text{CHA}}^{\psi,t} + p_{i,\text{DIS}}^{\psi,t} / \eta_{i,\text{DIS}}^{\psi} \right) \end{aligned} \quad (2.7)$$

The BESS state of charge (SOC), which indicates the available capacity in the BESS, should be maintained within pre-specified limits in order to preserve the lifespan of the BESS indicated by (2.8a). The initial SOC and final SOC are kept the same using (2.8b). The rate of charging or discharging of the BESS should not exceed its specified rating as indicated by (2.8c)-(2.8d). The binary variable, $b_i^{\psi,t}$ are included to avoid the simultaneous charging and discharging.

$$\underline{\text{SOC}}_i^{\psi} \leq \text{SOC}_i^{\psi,t} \leq \overline{\text{SOC}}_i^{\psi} \quad (2.8a)$$

$$\text{SOC}_i^{\psi,1} = \text{SOC}_i^{\psi,T} \quad (2.8b)$$

$$-\bar{p}_{i,\text{BESS}}^{\psi} b_i^{\psi,t} \leq p_{i,\text{CHA}}^{\psi,t} \leq 0 \quad (2.8c)$$

$$0 \leq p_{i,\text{DIS}}^{\psi,t} \leq \bar{p}_{i,\text{BESS}}^{\psi} (1 - b_i^{\psi,t}) \quad (2.8d)$$

$$\forall i \in \mathcal{B}^{\mathcal{B}}, \forall \psi \in \Psi_i, \forall t \in \mathcal{T}, b_i^{\psi,t} \in \{0, 1\}.$$

The apparent power of the BESS should limit its active and reactive power capability indicated by (2.9).

$$\sqrt{(p_{i,\text{CHA}}^{\psi,t} + p_{i,\text{DIS}}^{\psi,t})^2 + (q_{i,\text{BESS}}^{\psi,t})^2} \leq \bar{s}_{i,\text{BESS}}^{\psi}, \quad \forall i \in \mathcal{B}^{\mathcal{B}}, \forall \psi \in \Psi_i. \quad (2.9)$$

2.3 Distribution Power Flow Models

This section details two popular formulations used to model distribution power flow in optimization problems: a bus-injection model (BIM) and a branch-flow model (BFM). The BIM model is expressed in terms of bus injection variables, such as active and reactive power injections or current injections at network buses. On the contrary, the BFM model is formulated using variables defined on the network branches i.e. active and reactive power flows or current flowing in distribution lines.

2.3.1 Bus-injection Model (Power Injection Form)

In the power injection form, the distribution power flow model could be written as,

$$\mathbf{S} = \mathbf{V} (\mathbf{YV})^* = \mathbf{V} \left(\sum_{j=1}^N Y_{ji} V_j \right)^H \quad (2.10)$$

where,

$$\mathbf{V} = \begin{bmatrix} V_1 \\ V_2 \\ \vdots \\ V_n \end{bmatrix}, \mathbf{Y} = \begin{bmatrix} Y_{11} & Y_{12} & \cdots & Y_{1n} \\ Y_{21} & Y_{22} & \cdots & Y_{2n} \\ \vdots & \vdots & \ddots & \vdots \\ Y_{n1} & Y_{n2} & \cdots & Y_{nn} \end{bmatrix} \quad (2.11)$$

are bus voltage vector, and the bus admittance matrix of the network, respectively. The equations shown in (2.10) is non-linear and based on nodal voltage and power injections. (2.10) consists of $2n$ non-linear equations when real and imaginary components are separated. With voltage and admittance bus represented in polar coordinates, (2.10) can be written as the following:

$$P_m = V_m \sum_{n=1}^N V_n Y_n \cos(\delta_m - \delta_n - \theta_{mn}) \quad (2.12)$$

$$Q_m = V_m \sum_{n=1}^N V_n Y_{mn} \sin(\delta_m - \delta_n - \theta_{mn}) \quad (2.13)$$

2.3.2 Bus-injection Model (Current Injection Form)

In the current injection form, the following linear set of network equations are used:

$$\mathbf{I} = \mathbf{YV} = \left(\sum_{j=1}^N Y_{ji} V_j \right) \quad (2.14)$$

where,

$$\mathbf{I} = \begin{bmatrix} I_1 \\ I_2 \\ \vdots \\ I_n \end{bmatrix}, \quad (2.15)$$

where, I is the current injection vector. Then, the following power injection equations are used for non-zero injection buses.

$$\text{diag}(\mathbf{S}) = \text{diag}(\mathbf{V}) \text{diag}(\mathbf{I})^H \quad (2.16)$$

Note that the number of non-linear equations in current injection form depends on the number of non-zero injection buses, while on the power injection form this depends on the total number of buses on the network.

2.3.3 Branch Flow Model

Nonlinear BFM Model (BFM) The mathematical formulation for a power flow model based on branch flow equations for a radial distribution system is detailed in (2.17)-(2.19) [50]. The voltage drop and power balance equations are given by (2.17) and (2.19), respectively. The relationship between the branch power flow, nodal voltages, and branch currents is defined using (2.19). Note that $(\cdot)^H$ represents the conjugate transpose.

$$V_j = V_i - z_{ij} I_{ij} \quad (2.17)$$

$$\text{diag}(S_{ij} - z_{ij} l_{ij}) = \sum_{k:j \rightarrow k} \text{diag}(S_{jk}) + s_{L,j} \quad (2.18)$$

$$S_{ij} = V_i I_{ij}^H \quad (2.19)$$

The aforementioned model can be modified to incorporate the DERs. For $j \in \mathcal{N}_{DG}$, (2.18) is modified by (2.20).

$$\text{diag}(S_{ij} - z_{ij} l_{ij}) = \sum_{k:j \rightarrow k} \text{diag}(S_{jk}) + s_{L,j} - s_{DG,j} \quad (2.20)$$

LinDistFlow - Linearized Three-Phase AC Power Flow This linear power flow approximation assumes that the branch power losses are relatively smaller than the branch power flows [50]. The impact of power loss on active and reactive branch flow equations and on voltage drop equations is ignored. After approximating (2.17)-(2.19), we obtain linearized AC branch flow equations as shown in (2.21)-(2.22). Here (2.21) corresponds to linearized active and reactive power flow and (2.22) corresponds to voltage drop equations.

$$P_{ij}^{\psi\psi} = \sum_{k:j \rightarrow k} P_{jk}^{\psi\psi} + p_{L,j}^{\psi} \text{ and } Q_{ij}^{\psi\psi} = \sum_{k:j \rightarrow k} Q_{jk}^{\psi\psi} + q_{L,j}^{\psi} \quad (2.21)$$

$$v_j^{\psi} = v_i^{\psi} - \sum_{\phi \in \Phi_j} 2\Re \left[S_{ij}^{\psi\phi} (z_{ij}^{\psi\phi})^* \right] \quad (2.22)$$

The *LinDistFlow* model is reasonably accurate in representing bus voltages under normal loading conditions. Although this model does not include the impact of power losses on voltage drops, it does incorporate the impacts of power flows due to load on voltage drop calculations. Because power losses are small in comparison to power flow in the branches, the obtained feeder voltages are a good approximation of the actual feeder voltages [50].

2.4 Illustrated Example

Describing power flow formulation using a 5-bus example.

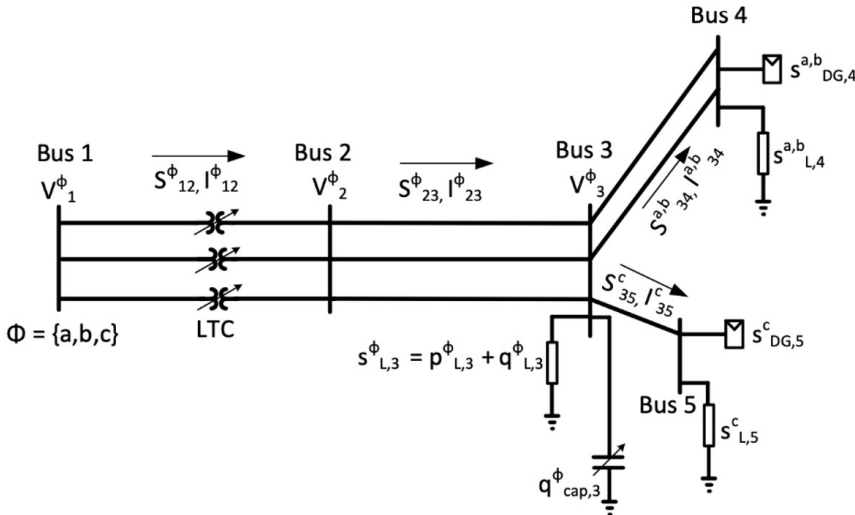


Figure 2.2: Five bus example test feeder.

2.4.1 Bus-injection Model

Bus injection model requires a Y-bus for the power flow formulation. For three-phase systems, readers are suggested follow [16] on how to derive the respective Y-bus. $Y = G + j B$.

Variable definitions: Let $\Phi_i \subseteq \{a, b, c\}$ defines set of phases corresponding to bus $i \in N$, $V_i^\psi = |V_i^\psi| \angle \theta_i^\psi$ denotes complex voltage phasor for phase $\psi \in \Phi_i$ of bus i , and $I_{ij}^\psi = |I_{ij}^\psi| \angle \delta_i^\psi$ denotes complex current phasor for branch (ij) for phase $\psi \in \Phi_i \cap \Phi_j$.

Then the power flow variables for the system shown in Figure 2.2 are defined as following,

- Bus 1: $\mathbf{V}_1 = [V_1^a, V_1^b, V_1^c]$
- Bus 2: $\mathbf{V}_2 = [V_2^a, V_2^b, V_2^c]$
- Bus 3: $\mathbf{V}_3 = [V_3^a, V_3^b, V_3^c]$
- Bus 4: $\mathbf{V}_4 = [V_4^a, V_4^b, 0]$
- Bus 5: $\mathbf{V}_5 = [0, 0, V_5^c]$
- Bus 1: $\mathbf{I}_1 = [I_1^a, I_1^b, I_1^c]$
- Bus 2: $\mathbf{I}_2 = [0, 0, 0]$
- Bus 3: $\mathbf{I}_3 = [I_3^a, I_3^b, I_3^c]$
- Bus 4: $\mathbf{I}_4 = [I_4^a, I_4^b, 0]$
- Bus 5: $\mathbf{I}_5 = [0, 0, I_5^c]$

Lets define the nodal voltage and current injection vectors as,

$$\begin{aligned}\mathbf{V} &= [\mathbf{V}_1, \mathbf{V}_2, \mathbf{V}_3, \mathbf{V}_4, \mathbf{V}_5]^T \\ \mathbf{I} &= [\mathbf{I}_1, \mathbf{I}_2, \mathbf{I}_3, \mathbf{I}_4, \mathbf{I}_5]^T\end{aligned}\tag{2.23}$$

Load and generation variables:

- Bus 3: (Load) $\mathbf{s}_{L,3} = [s_{L,3}^a, s_{L,3}^b, s_{L,3}^c]$, (DG) $\mathbf{s}_{DG,3} = [s_{DG,3}^a, s_{DG,3}^b, s_{DG,3}^c]$, (Cap bank) $\mathbf{q}_{cap,3} = [q_{cap,3}^a, q_{cap,3}^b, q_{cap,3}^c]$,
- Bus 4: (Load) $\mathbf{s}_{L,4} = [s_{L,4}^a, s_{L,4}^b, 0]$, (DG) $\mathbf{s}_{DG,4} = [s_{DG,4}^a, s_{DG,4}^b, 0]$
- Bus 5: (Load) $\mathbf{s}_{L,5} = [0, 0, s_{L,5}^c]$, (DG) $\mathbf{s}_{DG,5} = [0, 0, s_{DG,5}^c]$

Define net power injection vectors as the following:

$$\mathbf{S} = [\mathbf{0}, \mathbf{0}, -\mathbf{s}_{L,3} + \mathbf{j} q_{cap,3}, \mathbf{s}_{DG,4} - \mathbf{s}_{L,4}, \mathbf{s}_{DG,5} - \mathbf{s}_{L,5}]^T \quad (2.24)$$

$$\begin{aligned} \mathbf{I} &= \mathbf{YV} \\ &= \sum_{j \in \{1, 2, 3, 4, 5\}, \psi \in \{a, b, c\}} Y_{ji}^{\phi, \psi} V_j^\psi \end{aligned} \quad (2.25)$$

$$diag(\mathbf{S}) = diag(\mathbf{V}) diag(\mathbf{I})^H \quad (2.26)$$

2.4.2 Branch flow model

In addition to variables defined in Section 2.4.1, below we define additional variables for branch flow model.

- Branch 12: $\mathbf{I}_{12} = [I_{12}^a, I_{12}^b, I_{12}^c]$
- Branch 23: $\mathbf{I}_{23} = [I_{23}^a, I_{23}^b, I_{23}^c]$
- Branch 34: $\mathbf{I}_{34} = [I_{34}^a, I_{34}^b, 0]$
- Branch 35: $\mathbf{I}_{35} = [0, 0, I_{35}^c]$

The line or transformer model is given as:

- Branch 12: $\mathbf{a}_{12} = \begin{bmatrix} a_{12}^a & 0 & 0 \\ 0 & a_{12}^b & 0 \\ 0 & 0 & a_{12}^c \end{bmatrix}$
- Branch 23: $\mathbf{Z}_{23} = \begin{bmatrix} Z_{23}^{aa} & Z_{23}^{ab} & Z_{23}^{ac} \\ Z_{23}^{ba} & Z_{23}^{bb} & Z_{23}^{bc} \\ Z_{23}^{ca} & Z_{23}^{cb} & Z_{23}^{cc} \end{bmatrix}$
- Branch 34: $\mathbf{Z}_{34} = \begin{bmatrix} Z_{34}^{aa} & Z_{34}^{ab} & 0 \\ Z_{34}^{ba} & Z_{34}^{bb} & 0 \\ 0 & 0 & 0 \end{bmatrix}$
- Branch 35: $\mathbf{Z}_{35} = \begin{bmatrix} 0 & 0 & 0 \\ 0 & 0 & 0 \\ 0 & 0 & Z_{35}^{cc} \end{bmatrix}$

The power flow equations using branch flow model is given as the following:

- Branch 12:
 (Voltage Equation) $\mathbf{V}_2 = \mathbf{a}_{12}\mathbf{V}_1$;
 (Current Equation) $\mathbf{I}_{12} = \mathbf{a}_{12}\mathbf{I}_{23}$
- Branch 23:
 (Voltage Equation) $\mathbf{V}_3 = \mathbf{V}_2 - \mathbf{Z}_{23}\mathbf{I}_{23}$;
 (Power balance equation) $\text{diag}(\mathbf{S}_{23} - \mathbf{Z}_{23}\mathbf{I}_{23}\mathbf{I}_{23}^H) = \text{diag}(\mathbf{S}_{34}) + \text{diag}(\mathbf{S}_{35}) + \mathbf{s}_{L,3} - \mathbf{s}_{DG,3} - u_{cap,3}\mathbf{q}_{cap,3}$,
 where, $\mathbf{S}_{23} = \mathbf{V}_2\mathbf{I}_{23}^H$
- Branch 34:
 (Voltage Equation) $\mathbf{V}_4 = \mathbf{V}_3 - \mathbf{Z}_{34}\mathbf{I}_{34}$;
 (Power balance equation) $\text{diag}(\mathbf{S}_{34} - \mathbf{Z}_{34}\mathbf{I}_{34}\mathbf{I}_{34}^H) = \mathbf{s}_{L,4} - \mathbf{s}_{DG,4}$,
 where, $\mathbf{S}_{34} = \mathbf{V}_3\mathbf{I}_{34}^H$
- Branch 35:
 (Voltage Equation) $\mathbf{V}_5 = \mathbf{V}_3 - \mathbf{Z}_{35}\mathbf{I}_{35}$;
 (Power balance equation) $\text{diag}(\mathbf{S}_{35} - \mathbf{Z}_{35}\mathbf{I}_{35}\mathbf{I}_{35}^H) = \mathbf{s}_{L,5} - \mathbf{s}_{DG,5}$,
 where, $\mathbf{S}_{35} = \mathbf{V}_3\mathbf{I}_{35}^H$

2.5 Algorithms to Solve Distribution Power Flow Model

In this section, we detail different algorithms that have been developed to solve distribution power flow equations. These algorithms differ in their approach to solving a nonlinear systems of equations defining the power flow model.

2.5.1 Forward-Backward Sweep Method

The Forward-Backward Sweep method exploits radial nature and overcome the challenges related to ill-conditioned nature of distribution networks. The algorithm consists of a nodal current calculation, a backward sweep and a forward sweep. At iteration n , the nodal current

injection at node i can be calculated as

$$I_i^n = \left(\frac{P_i^{sp} + jQ_i^{sp}}{V_i^{n-1}} \right)^* \quad (2.27)$$

where

$$P_i^{sp} = P_{G_i} - P_{L_i} \quad (2.28)$$

$$Q_i^{sp} = Q_{G_i} - Q_{L_i} \quad (2.29)$$

where P_i^{sp} , P_{G_i} and P_{L_i} are active component of scheduled, generated and load power at bus i respectively and Q_i^{sp} , Q_{G_i} and Q_{L_i} is reactive component of scheduled, generated and load power at bus i , respectively.

During backward sweep, the branch currents are calculated (with initialized voltages for first iteration). A current summation method is applied starting from nodes at far end of the feeder towards the source bus. The current in branch $\{ij\}$ connected between node i and j can be obtained as

$$I_{ij}^n = -I_j^n + \sum_{k:j \rightarrow k} (I_{jk}) \quad (2.30)$$

where I_{jk} is currents in all branches emanating from node j . If a voltage regulator with tap t is connected between node i and j the current in branch $\{ij\}$ is modified as

$$I_{ij}^n = (1 + 0.00625t) I_{ij}^n \quad (2.31)$$

The forward sweep calculates voltages using the calculated currents from backward sweep from the source bus till nodes at far end of feeder. The voltage at node j is obtained using current in branch $\{ij\}$ and updated voltage in node i as

$$V_j^n = V_i^n - Z_{ij} \times I_{ij}^n \quad (2.32)$$

where Z_{ij} is impedance of line $\{ij\}$. If a voltage regulator with tap t is connected between node i and j voltage at node j is modified as

$$V_j^n = (1 + 0.00625t) V_j^n \quad (2.33)$$

The voltages obtained using forward sweep are used for the next iteration in the backward sweep. The voltage mismatch is calculated as

$$\Delta V = V^n - V^{n-1} \quad (2.34)$$

The load flow iterations are repeated until voltage mismatches is lesser than a convergence tolerance.

2.5.2 Z-bus Approach (Fixed-Point Iteration)

In an electric power network with N buses, nodal current equation can be expressed according to the following matrix form:

$$\mathbf{I} = \mathbf{YV} = \sum_{j=1}^N Y_{ji} V_j \quad (2.35)$$

where

$$\mathbf{I} = \begin{bmatrix} I_1 \\ I_2 \\ \vdots \\ I_n \end{bmatrix}, \mathbf{V} = \begin{bmatrix} V_1 \\ V_2 \\ \vdots \\ V_n \end{bmatrix}, \mathbf{Y} = \begin{bmatrix} Y_{11} & Y_{12} & \cdots & Y_{1n} \\ Y_{21} & Y_{22} & \cdots & Y_{2n} \\ \vdots & \vdots & \ddots & \vdots \\ Y_{n1} & Y_{n2} & \cdots & Y_{nn} \end{bmatrix} \quad (2.36)$$

are the nodal injection current vector, bus voltage vector, and the bus admittance matrix of the network, respectively. Partitioning the matrices into slack and non-slack buses (2.35) can be expressed as

$$\begin{bmatrix} I_s \\ I_m \end{bmatrix} = \begin{bmatrix} Y_{ss} & Y_{sm} \\ Y_{ms} & Y_{mm} \end{bmatrix} \begin{bmatrix} V_s \\ V_m \end{bmatrix} \quad (2.37)$$

where I_s is the current injection at slack bus and V_s is the voltage at the slack bus and I_m is the current injection for all other buses and V_m is the voltage at all other buses. Therefore

$$I_m = Y_{ms} \cdot V_s + Y_{mm} \cdot V_m \quad (2.38)$$

At iteration n , the nodal current injection at node i can be calculated as

$$I_i^n = \frac{(P_i^{sp}) - j(Q_i^{sp})}{(V_i^*)} \quad (2.39)$$

where P_i^{sp} is active component of scheduled power at and Q_i^{sp} is reactive component of scheduled power at bus i . A fixed-point equation for voltages V_m can be obtained as

$$V_m^{n+1} = Y_{mm}^{-1} \cdot (I_m^n - Y_{ms} \cdot V_s^n) \quad (2.40)$$

The voltage mismatch is calculated as

$$\Delta V = V^n - V^{n-1} \quad (2.41)$$

The load flow iterations are repeated until voltage mismatches is lesser than a convergence tolerance.

2.5.3 Newton-Raphson Method (Power Injection Form)

The Newton Raphson method is a numerical method used to solve the non-linear power flow. By expressing the node voltage and admittance matrix in polar forms, the real and reactive power injections are given as the following:

$$P_i = V_i \sum_{j=1}^N Y_{ij} V_j \cos(\delta_i - \delta_j - \theta_{ij}) \quad (2.42)$$

$$Q_i = V_i \sum_{j=1}^N Y_{ij} V_j \sin(\delta_i - \delta_j - \theta_{ij}) \quad (2.43)$$

The power mismatch equations are

$$\Delta P_i = P_{i,sch} - P_{i, calc} \quad (2.44)$$

$$\Delta Q_i = Q_{i,sch} - Q_{i, calc} \quad (2.45)$$

By applying Taylor series expansion, this mismatch equations can be expanded as

$$\begin{bmatrix} \Delta \mathbf{P} \\ \Delta \mathbf{Q} \end{bmatrix} = \left[\begin{array}{c|c} \mathbf{J1} & \mathbf{J2} \\ \hline \mathbf{J3} & \mathbf{J4} \end{array} \right] \begin{bmatrix} \Delta \boldsymbol{\delta} \\ \Delta \mathbf{V} \end{bmatrix} \quad (2.46)$$

The Jacobian matrix is given by

$$\mathbf{J} = \left[\begin{array}{ccc|ccc} \frac{\partial P_2}{\partial \delta_2} & \dots & \frac{\partial P_2}{\partial \delta_N} & \frac{\partial P_2}{\partial V_2} & \dots & \frac{\partial P_2}{\partial V_N} \\ \vdots & & & \vdots & & \\ \frac{\partial P_N}{\partial \delta_2} & \dots & \frac{\partial P_N}{\partial \delta_N} & \frac{\partial P_N}{\partial V_2} & \dots & \frac{\partial P_N}{\partial V_N} \\ \hline \frac{\partial Q_2}{\partial \delta_2} & \dots & \frac{\partial Q_2}{\partial \delta_N} & \frac{\partial Q_2}{\partial V_2} & \dots & \frac{\partial Q_2}{\partial V_N} \\ \vdots & & & \vdots & & \\ \frac{\partial Q_N}{\partial \delta_2} & \dots & \frac{\partial Q_N}{\partial \delta_N} & \frac{\partial Q_N}{\partial V_2} & \dots & \frac{\partial Q_N}{\partial V_N} \end{array} \right] \quad (2.47)$$

The main diagonal elements of each submatrix of the Jacobian are computed in equations (2.48)-(2.51)

$$J1_{ii} = \frac{\partial P_i}{\partial \delta_i} = -V_i \sum_{\substack{j=1 \\ j \neq i}}^N Y_{ij} V_j \sin(\delta_i - \delta_j - \theta_{ij}) \quad (2.48)$$

$$J2_{ii} = \frac{\partial P_i}{\partial V_i} = V_i Y_{ii} \cos \theta_{ii} + \sum_{j=1}^N Y_{ij} V_j \cos(\delta_i - \delta_j - \theta_{ij}) \quad (2.49)$$

$$J3_{ii} = \frac{\partial Q_i}{\partial \delta_i} = V_i \sum_{\substack{j=1 \\ j \neq i}}^N Y_{ij} V_j \cos(\delta_i - \delta_j - \theta_{ij}) \quad (2.50)$$

$$J4_{ii} = \frac{\partial Q_i}{\partial V_i} = -V_i Y_{ii} \sin \theta_{ii} + \sum_{j=1}^N Y_{ij} V_j \sin(\delta_i - \delta_j - \theta_{ij}) \quad (2.51)$$

The off diagonal entries of each submatrix of the Jacobian are computed in equations (2.52)-(2.55)

$$J1_{ij} = \frac{\partial P_i}{\partial \delta_j} = V_i Y_{ij} V_j \sin(\delta_i - \delta_j - \theta_{ij}) \quad (2.52)$$

$$J2_{ij} = \frac{\partial P_i}{\partial V_j} = V_i Y_{ij} \cos(\delta_i - \delta_j - \theta_{ij}) \quad (2.53)$$

$$J3_{ij} = \frac{\partial Q_i}{\partial \delta_j} = -V_i Y_{ij} V_j \cos(\delta_i - \delta_j - \theta_{ij}) \quad (2.54)$$

$$J4_{ij} = \frac{\partial Q_i}{\partial V_j} = V_i Y_{ij} \sin(\delta_i - \delta_j - \theta_{ij}) \quad (2.55)$$

As the voltage vector is updated, the Jacobian is recalculated, and the power flow is said to converge when power mismatch vector is less than the tolerance value.

One drawback to the Newton Raphson method is that it may fail to converge for a large network with voltage regulators; in this case the nodes with voltage regulators have to be initialized by a pre-determined exact or approximate power flow.

2.5.4 Newton-Raphson Method (Current Injection Form)

In current injection based power flow, the complex current injection equations are expressed in terms of rectangular coordinates and bus admittance matrix is represented in terms of its real (G) and imaginary values (B). The Jacobian matrix is formed from the bus admittance matrix where each element in bus admittance matrix is replaced with 2×2 blocks. The off-diagonal blocks obtained in the Jacobian are fixed over iterations and diagonal blocks are updated at every iteration based on type of load model connected to that bus. The complex current mismatch at a bus i in a N bus distribution system is given as:

$$\Delta I_i = (I_i^{sp}) - (I_i^{calc}) \quad (2.56)$$

(2.56) can be expanded as

$$\Delta I_i = \frac{(P_i^{sp}) - j(Q_i^{sp})}{(V_i^*)} - \sum_{j=1}^n Y_{ji} V_j \quad (2.57)$$

where P_i^{sp} is active component of scheduled power at bus i and Q_i^{sp} is reactive component of scheduled power at bus i .

(2.57) which is in complex form can be represented in terms of real and imaginary component as

$$\Delta I_{ri} = \frac{P_i^{sp} V_{ri} + Q_i^{sp} V_{mi}}{V_{ri}^2 + V_{mi}^2} - \sum_{j=1}^N (G_{ij} V_{rj} - B_{ij} V_{mj}) \quad (2.58)$$

$$\Delta I_{mi} = \frac{P_i^{sp} V_{mi} - Q_i^{sp} V_{ri}}{V_{ri}^2 + V_{mi}^2} - \sum_{j=1}^N (G_{ij} V_{mj} - B_{ij} V_{rj}) \quad (2.59)$$

The Jacobian matrix can be calculated by differentiating (2.58) and (2.59) with respect to real and imaginary parts of all the bus voltages. Therefore the power flow formulation using current injections can be solved using (2.60) as

$$\begin{bmatrix} \Delta I_{m1} \\ \Delta I_{r1} \\ \vdots \\ \Delta I_{mn} \\ \Delta I_{rn} \end{bmatrix} = \begin{bmatrix} \frac{\partial I_{m1}}{\partial V_{r1}} & \frac{\partial I_{m1}}{\partial V_{m1}} & \cdots & \frac{\partial I_{m1}}{\partial V_{rn}} & \frac{\partial I_{m1}}{\partial V_{mn}} \\ \frac{\partial I_{r1}}{\partial V_{r1}} & \frac{\partial I_{r1}}{\partial V_{m1}} & \cdots & \frac{\partial I_{r1}}{\partial V_{rn}} & \frac{\partial I_{r1}}{\partial V_{mn}} \\ \vdots & \vdots & \vdots & \vdots & \vdots \\ \frac{\partial I_{mn}}{\partial V_{r1}} & \frac{\partial I_{mn}}{\partial V_{m1}} & \cdots & \frac{\partial I_{mn}}{\partial V_{rn}} & \frac{\partial I_{mn}}{\partial V_{mn}} \\ \frac{\partial I_{rn}}{\partial V_{r1}} & \frac{\partial I_{rn}}{\partial V_{m1}} & \cdots & \frac{\partial I_{rn}}{\partial V_{rn}} & \frac{\partial I_{rn}}{\partial V_{mn}} \end{bmatrix} \begin{bmatrix} \Delta V_{r1} \\ \Delta V_{m1} \\ \vdots \\ \Delta V_{rn} \\ \Delta V_{mn} \end{bmatrix} \quad (2.60)$$

The elements of Jacobian can be obtained using following equations.

$$\frac{\partial I_{mi}}{\partial V_{ri}} = B_{ii} - a_i \quad \frac{\partial I_{mi}}{\partial V_{rj}} = B_{ij}, \quad i \neq j \quad (2.61)$$

$$\frac{\partial I_{mi}}{\partial V_{mi}} = G_{ii} - b_i \quad \frac{\partial I_{mi}}{\partial V_{mj}} = G_{ij}, \quad i \neq j \quad (2.62)$$

$$\frac{\partial I_{ri}}{\partial V_{ri}} = G_{ii} - c_i \quad \frac{\partial I_{ri}}{\partial V_{rj}} = G_{ij}, \quad i \neq j \quad (2.63)$$

$$\frac{\partial I_{ri}}{\partial V_{mi}} = -B_{ii} - d_i \quad \frac{\partial I_{ri}}{\partial V_{mj}} = -B_{ij}, \quad i \neq j \quad (2.64)$$

where B and G are imaginary and real parts of admittance element and a, b, c, d can be obtained as in [52].

The voltage mismatch can be represented in compact form as

$$[\Delta V] = [J]^{-1} [\Delta I] \quad (2.65)$$

The updated voltage is given by

$$[V]^{k+1} = [V]^k + [\Delta V] \quad (2.66)$$

2.6 Distribution System Simulators

The analysis of power distribution systems requires a modeling software that can support detailed feeder and equipment modeling with advanced distribution system analysis capabilities. A mathematical description of a given distribution system and power flow algorithm discussed in this section can be easily developed using any programming language such as C++, python, or MATLAB. The power systems community has also developed dedicated distribution system modeling and simulation software to run the power systems analysis. For completeness, in this section we briefly summarize some of the existing simulators for detailed unbalanced power distribution system analysis. Given the focus of this monograph, our discussion is centered around the quasi-static analysis of power distribution systems.

Power (utility) industry uses different commercial software for the distribution system modeling and analysis including CYMDIST, Synergi, WindMIL, etc. However, these commercial software packages are proprietary and not easily accessible to the research community. Recognizing this challenge, the power systems community has developed open-source distribution system simulators that can model detailed distribution systems, provide flexibility for modeling new components and operational scenarios, and are simple to integrate into external packages such as optimization engines. Two of the most common open-source distribution simulators used by the power community are OpenDSS and GridLAB-D. Pandapower is another upcoming power flow simulator; however, it currently cannot model unsymmetrical lines commonly found in North American power distribution feeders. In what follows, we briefly describe these three simulators.

OpenDSS is an open-source simulator tool developed by Electric Power Research Institute (EPRI) to model and analyze electric power distribution systems [101]. The program supports all frequency domain (sinusoidal steady-state) and sequential power flow analyses commonly performed for utility distribution system planning and analysis. One of the major benefits of OpenDSS is its extraordinary capability to support modeling of end-use technologies, such as DGs/DERs, EVs, battery energy storage systems, thus serving as a valuable analysis platform for grid-edge integration. OpenDSS can be implemented as both a stand-alone executable program and an in-process Component Object Model (COM) server DLL designed to be driven by a variety of existing software platforms, such as MATLAB, Python, C++, etc. The executable version has a basic text-based user interface on the solution engine to assist users in developing scripts and viewing solutions. The COM interface is implemented on the in-process server DLL version of the program to allow users to use the features of the program to perform new types of studies and execute custom solution modes. The external execution of OpenDSS provides powerful analytical capabilities as well as excellent graphics for displaying results.

GridLAB-D is an open-source toolkit that supports three-phase unbalanced power distribution system simulation and analysis [56]. Pacific Northwest National Laboratory (PNNL) collaborated with industry and

academia to develop GridLAB-D. This effort was funded by the U.S. Department of Energy Office of Electricity Delivery and Energy Reliability (DOE/OE). GridLAB-D, uses agent-based and information-based modeling, to help develop detailed models for distribution systems with new grid-edge technologies, such as DGs/DERs, grid-interfacing buildings, EVs, etc. GridLAB-D, in its most basic form, allows interactions among all elements of a distribution system, from the substation to the end-use loads. It also serves as an excellent test bed for evaluating control strategies and researching the effects of smart grid technologies. Similar to OpenDSS, GridLAB-D is a flexible simulation environment that can be integrated with a variety of third-party data management and analysis tools.

Pandapower is yet another open source tool designed to perform steady-state analysis on three-phase power systems with symmetrical power line designs. It currently supports the analysis of balanced transmission and subtransmission systems, as well as three-phase distribution systems with symmetrical line designs common in Europe. Asymmetrical loads and generators can be considered with three-phase power flow. Distribution systems with asymmetrical power line designs, such as the feeder design popular in North America, cannot currently be analyzed with pandapower [138].

2.7 Summary and Discussions

This section introduced the approach to develop a mathematical model for power distribution system and components. Then it introduced different power flow formulations and described the power flow modeling with the help of an illustrated 5-bus example. We also discussed different algorithms to solve distribution power flow and introduced open-source distribution power flow simulators, including OpenDSS, GridLAB-D and Pandapower. The power flow formulation described in this section and network modeling details will be used in the following sections to formulate and solve distribution optimal power flow (D-OPF) problems.

3

Distribution Optimal Power Flow (D-OPF) Formulations

3.1 Introduction

In an active power distribution system, optimal power flow (OPF) algorithms find multiple applications, including, but not limited to, loss minimization, volt-var optimization, and effective management of distributed energy resources (DERs) [96]. The increasing penetration of DERs, the proliferation of proactive loads, and the interest in demand response programs require optimization methods for large-scale power distribution systems [41]. Lately, these new requirements have encouraged the rapid adoption of advanced distribution management systems (ADMS) and related ADMS applications [100]. As the distribution systems continue to become more active, the need for faster management of the grid's controllable assets will inevitably necessitate faster OPF algorithms [140]. Compared to the bulk power grid, distribution-level OPF (D-OPF) poses unique challenges due to three-phase unbalanced loading, mutual coupling among the different phases of the line, the existence of single-phase and two-phase branches, and radial topology with high R/X ratio leading to significant voltage drops. While earlier work focused on the balanced distribution systems [10], [46], lately, significant strides have been made regarding three-phase unbalanced D-OPF formulations [25], [50], [69], [109].

This section introduces the distribution-level OPF problem and details different models proposed in the literature. Our discussion in this section is limited to single-period D-OPF problems primarily aiming to control grid-following DGs. Control of devices with discrete decisions are introduced in Section 4. This monograph does not delve into multi-period optimization and stochastic optimization D-OPF formulations in order to keep the discussion contained and focused.

3.2 Notations

In addition to the notations defined in Section 2.2.1, we define additional notations required for D-OPF formulation here. Let, $v_i = \text{diag}(V_i \times V_i^H)$. $(\cdot)^H$ represents the complex-conjugate, $(\cdot)^T$ denotes matrix transpose, and $\mathbf{j} = \sqrt{-1}$.

3.3 Basics D-OPF Problem

D-OPF problems are formulated as constrained optimization problems consisting of an objective function and a set of system-level and operational constraints. A typical representation of the D-OPF is given by (3).

$$\min / \max f(x, u) \quad (3.1)$$

Subject to:

$$g(x, u) = 0 \quad (3.2)$$

$$h(x, u) \leq 0 \quad (3.3)$$

where, x is the set of state variables representing power flow quantities; u is the set of decision variables that can be continuous or integer depending upon the control parameter, $f(x, u)$ represents problem objective, $g(x, u)$ is set of power flow equations modeled as equality constraints, $h(x, u)$ represents operating constraints specifying limits on state and decision variables.

3.3.1 Problem Objectives

The problem objective, $f(x, u)$, is formulated as a function of state and decision variables. In DOPF, different objective functions could be formulated depending on the desired goals to be achieved for optimal dispatch of the DERs as appropriate [142]. A few example formulations are detailed below.

- Minimize the total power loss: $\min f(x)$, where,

$$f(x, u) = \sum_{(ij) \in \mathcal{E}} \text{real}(I_{ij}^H Z_{ij} I_{ij}).$$
- Maximize the PV hosting capacity: $\max f(x)$, where,

$$f(x, u) = \sum_{(i) \in \mathcal{N}_{DG}} \sum_{\psi \in \Phi_i} \text{real}(s_{DG,i}^\psi).$$
- Minimize the voltage deviations with respect to the setpoint voltage: $\min f(x)$, where, $f(x, u) = \sum_{(i) \in \mathcal{N}} \sum_{\psi \in \Phi_i} |v_i^\psi - v_{set}^\psi|$.
This is a non-convex function and can be reformulated as a convex function as the following: $f(x, u) = \sum_{i \in \mathcal{N}} \sum_{\psi \in \Phi_i} \Delta v_i^\psi$, with the inclusion of the following additional constraints, $v_i^\psi - v_{set}^\psi \leq \Delta v_i$, and $v_{set}^\psi - v_i^\psi \leq \Delta v_i$.

As an example, we also introduce an objective function for coordinating PVs and BESS. The goal is to minimize net load demand by scheduling BESS charging ($p_{i,\text{CHA}}^{\psi,t}$) and discharging ($p_{i,\text{DIS}}^{\psi,t}$) for $t \in \mathcal{T}$ and coordinating active power generation from PVs ($p_{i,DG}^{\psi,t}$). This objective could be associated with energy cost reduction for the customer using DERs. The problem objective is to minimize the net load demand for $t \in \mathcal{T}$: $\min f(x)$, where,

$$\begin{aligned} f(x, u) = & \sum_{i \in \mathcal{N}_L} \sum_{\psi \in \Psi_i} \sum_{t \in \mathcal{T}} p_{i,L}^{\psi,t} - \sum_{i \in \mathcal{N}_{DG}} \sum_{\psi \in \Psi_i} \sum_{t \in \mathcal{T}} p_{i,DG}^{\psi,t} \\ & + \sum_{i \in \mathcal{N}_{BESS}} \sum_{\psi \in \Psi_i} \sum_{t \in \mathcal{T}} p_{i,\text{CHA}}^{\psi,t} - \sum_{i \in \mathcal{N}_{BESS}} \sum_{\psi \in \Psi_i} \sum_{t \in \mathcal{T}} p_{i,\text{DIS}}^{\psi,t}. \end{aligned}$$

3.3.2 Problem Constraints

The problem constraints include a set of equations defining power flow model and operating constraints for network variables such as bus voltages, branch currents, DG power limits, etc.

- Power flow constraints: The power flow constraints are binding nonlinear equality constraints, represented by $g(x, u) = 0$. Depending upon the power flow model, we obtain different formulations for D-OPF.
- Node voltage limit: The node voltages need to be maintained within the pre-specified upper and lower limits, V_{min} and V_{max} , where $|V_{min}| = 0.95$ p.u. and $|V_{max}| = 1.05$ p.u.
- Thermal Limit: The thermal loading for each branch should be maintained within the pre-specified rating designated by (I_{ij}^{rated}) for branch (ij) .
- DG operating limits: The operating points for DG, both $p_{DG,j}$ and $q_{DG,j}$, need to be constrained depending upon the problem formulation. Typically, for loss minimization and voltage deviation minimization, we constrain reactive power generation based on the apparent power rating of the DG, $s_{DG,j}^{rated}$, and measured/forecasted value of active power generation, $p_{DG,j}$. For the PV hosting maximization problem, we assume the DGs are operating at unity power factor and we constrain individual DGs power by their maximum active power generation, $p_{DG,j}^{max}$. If both $p_{DG,j}$ and $q_{DG,j}$ are controllable variables, the apparent power need to be constrained as per the apparent power rating of the DG, $s_{DG,j}^{rated}$.

3.3.3 Decision variables

The decision variables model the controllable parameters in the distribution system. Mathematically, these can be represented as continuous or integer variables depending upon the controlled device. Based on the device models detailed in Section 2.2, here we define decision variables for most common controllable devices: voltage regulators, capacitor banks and grid-following DGs (with smart inverters).

- Voltage Regulator: A 32-step voltage regulator is controlled by selecting the tap position. We model the tap selection as an integer variable. For each regulator step (per-phase), we define a binary variables, $u_{tap,i}^{\psi} \in \{0, 1\}$, where $u_{tap,i}^{\psi} = 1$ indicates that the

regulator is at the i^{th} tap position. Note that additional constraints are needed to define the decision variable in a meaningful way in the D-OPF problem formulation.

- Capacitor Bank: A capacitor bank in an on/off control device. We model connectivity status of capacitor banks as a binary variable, $u_{cap,i}^{\psi} = \{0, 1\}$, where, $u_{cap,i}^{\psi} = 1$ indicates that the capacitor bank is connected to the system. Note that additional constraints are needed to appropriately represent the local control settings for the switched capacitor banks in a D-OPF problem.
- Distributed generators (DGs): Here, we model only grid-following inverters (with DGs) with controllable active and reactive power. Thus, the control parameters are active and/or reactive power dispatch from the DGs modeled as continuous variables, $p_{DG,i}^{\psi}$ and $q_{DG,i}^{\psi}$, respectively. Additional constraints are needed to appropriately model the operating limits for DGs and inverters.

3.4 Distribution Nonlinear Optimal Power Flow Models

In this section, we describe different formulations for D-OPF problem based on nonlinear models for distribution power flow detailed in Section 2. Specifically, we define the following two D-OPF formulations: Nonlinear Bus-injection Model (NLP-BIM) and Nonlinear Branch-flow Model (NLP-BFM).

3.4.1 D-OPF using Bus-injection Power Flow Model (NLP-BIM)

The current-voltage D-OPF (IV-DOPF) [26] expresses the power flow equations in terms of the current-voltage (IV) relationship. Linear network flows can be obtained in terms of the current injection method. The load models at each phase are expressed in terms of bilinear terms ($V_i^{\psi,re} I_i^{\psi,re}, V_i^{\psi,im} I_i^{\psi,im}, V_i^{\psi,im} I_i^{\psi,re}, V_i^{\psi,re} I_i^{\psi,im}$). Note that the IV-DOPF formulation has the nonlinearities in the bilinear terms which couple variables associated with a single bus; this makes it scale better compared to other power flow formulations that have nonlinearities which couple variables associated with different buses [67].

The D-OPF formulation is as follows, where, state variables, $x = (V_i^{\psi,re}, I_i^{\psi,re}, V_i^{\psi,im}, I_i^{\psi,im})$ and decision variables, $u = (p_{DG,i}^\psi, q_{DG,i}^\psi)$.

$$\min / \max f(x, u) \quad (3.4)$$

Subject to:

Power flow constraints $g(x, u)$:

$$0 = V_i^{\psi,re} I_i^{\psi,re} + V_i^{\psi,im} I_i^{\psi,im} + p_{L,i}^\psi - p_{DG,i}^\psi \quad (3.5)$$

$$0 = V_i^{\psi,im} I_i^{\psi,re} - V_i^{\psi,re} I_i^{\psi,im} + q_{L,i}^\psi - q_{DG,i}^\psi - q_{cap,i}^\psi \quad (3.6)$$

$$I_i^{\psi,re} = \sum_{j: ij \in E, \phi \in \{a,b,c\}} V_j^{\phi,re} G_{ij}^{\psi\phi} - V_j^{\phi,im} B_{ij}^{\psi\phi} \quad (3.7)$$

$$I_i^{\psi,im} = \sum_{j: ij \in E, \phi \in \{a,b,c\}} V_j^{\phi,re} B_{ij}^{\psi\phi} + V_j^{\phi,im} G_{ij}^{\psi\phi} \quad (3.8)$$

Operating Constraints, $h(x, u)$:

$$(V_{min})^2 \leq (V_i^{\psi,re})^2 + (V_i^{\psi,im})^2 \leq (V_{max})^2 \quad (3.9)$$

$$(I_{ij}^{\psi,re})^2 + (I_{ij}^{\psi,im})^2 \leq (I_{ij}^{\psi,rated})^2 \quad (3.10)$$

where

$$I_{ij}^{\psi,re} = -G_{ij}^{\psi\psi} V_i^{\psi,re} + B_{ij}^{\psi\psi} V_i^{\psi,im} + G_{ij}^{\psi\psi} V_j^{\psi,re} - B_{ij}^{\psi\psi} V_j^{\psi,im} \quad (3.11)$$

$$I_{ij}^{\psi,im} = -G_{ij}^{\psi\psi} V_i^{\psi,im} + B_{ij}^{\psi\psi} V_i^{\psi,re} + B_{ij}^{\psi\psi} V_j^{\psi,re} + G_{ij}^{\psi\psi} V_j^{\psi,im} \quad (3.12)$$

Operating constraints specific to loss and voltage deviation minimization (assuming reactive power control):

$$-\sqrt{(s_{DG,j}^{\psi,rated})^2 - (p_{DG,j}^\psi)^2} \leq q_{DG,j}^\psi \leq \sqrt{(s_{DG,j}^{\psi,rated})^2 - (p_{DG,j}^\psi)^2} \quad (3.13)$$

Operating constraints specific to PV hosting maximization (assuming active power control):

$$0 \leq p_{DG,j}^\psi \leq p_{DG,j}^{\psi,max} \text{ and } q_{DG,j}^\psi = 0 \quad \forall j \in \mathcal{N}_{DG} \quad (3.14)$$

3.4.2 D-OPF using Branch-flow Power Flow Model (NLP-BFM)

The NLP-BFM formulation for D-OPF problem is detailed below, where power flow constraints are modeled using non-linear branch flow model (BFM).

$$\min / \max f(x) \quad (3.15)$$

Subject to:

Power flow constraints:

$$V_j = V_i - Z_{ij}I_{ij} \quad (3.16)$$

$$\text{diag}(S_{ij} - z_{ij}l_{ij}) = \sum_{k:j \rightarrow k} \text{diag}(S_{jk}) + s_{L,j} \quad (3.17)$$

$$S_{ij} = V_i I_{ij}^H \quad (3.18)$$

Operating Constraints, $h(x, u)$:

$$\begin{aligned} V_{min}^2 &\leq (V_i^{\psi,re})^2 + (V_i^{\psi,im})^2 \leq V_{max}^2 \\ (I_{ij}^{\psi\psi,re})^2 + (I_{ij}^{\psi\psi,im})^2 &\leq (I_{ij}^{rated})^2 \end{aligned} \quad (3.19)$$

Operating constraints specific to loss and voltage deviation minimization (assuming reactive power control):

$$-\sqrt{(s_{DG,j}^{\psi,rated})^2 - (p_{DG,j}^{\psi})^2} \leq q_{DG,j}^{\psi} \leq \sqrt{(s_{DG,j}^{\psi,rated})^2 - (p_{DG,j}^{\psi})^2} \quad (3.20)$$

Operating constraints specific to PV hosting maximization (assuming active power control):

$$0 \leq p_{DG,j}^{\psi} \leq p_{DG,max}^{\psi} \quad \text{and} \quad q_{DG,j}^{\psi} = 0 \quad \forall j \in \mathcal{N}_{DG} \quad (3.21)$$

3.5 Approximation and Relaxation Techniques

The nonlinear relationship between power flow variables makes the OPF problem non-convex. NLP models for unbalanced D-OPF often converge to infeasible or sub-optimal operating points, especially for large or mid-sized feeders. Recent research in this domain actively looked into scalable algorithms for unbalanced D-OPF that result in a feasible and optimal solution. To this end, there is extensive literature on relaxation and approximation techniques applied to unbalanced D-OPF problem [18], [50], [58], [146].

The relaxation-based approaches attempt to relax the nonlinear power flow equations as convex inequalities, resulting in a convex optimization problem for D-OPF, which solves within a reasonable time for large-scale distribution systems [50], [160]. The existing methods

either relax a BIM based D-OPF as a semi-definite program (SDP) [7], or a BFM based D-OPF as a second-order cone program (SOCP) [65] or SDP [50]. The relaxations, however, may lead to infeasible power flow solutions. The approximation-based approaches, approximate the non-linear power flow equations into linear equations. The approximation accuracy depends upon the linearization approach and the system conditions.

In what follows, we discuss some common approximation and relaxation techniques applied to D-OPF problems. It should be noted that D-OPF problems also encounter other types of nonlinearities due to decision variables and objective functions. However, here we focus on only power flow-related nonlinearities.

3.5.1 Conic Relaxation – Semidefinite programming

Conic relaxation leads to a convex problem formulation for an original non-convex model. This is achieved by relaxing nonlinear equality constraint into a convex inequality constraint. Below, we describe a conic relaxation for branch flow model. First, the branch flow equations are lifted to a new variable space by multiplying both sides of the voltage drop constraint by its hermitian conjugate. This results in the following power flow equations.

$$v_i = v_j + (S_{ij}z_{ij}^H + z_{ij}S_{ij}^H) - z_{ij}l_{ij}z_{ij}^H \quad (3.22)$$

$$\text{diag}(S_{ij} - z_{ij}l_{ij}) - s_{L,j} + s_{DG,i} = \sum_{k:j \rightarrow k} \text{diag}(S_{jk}) \quad (3.23)$$

$$\begin{bmatrix} v_i & S_{ij} \\ S_{ij}^H & l_{ij} \end{bmatrix} = \begin{bmatrix} V_i \\ I_{ij} \end{bmatrix} \begin{bmatrix} V_i \\ I_{ij} \end{bmatrix}^H \quad (3.24)$$

Now the power flow equations are described in lifted variable space, (v_{ij} and l_{ij}) by representing (3.24) as the following two equations.

$$\begin{bmatrix} v_i & S_{ij} \\ S_{ij}^H & l_{ij} \end{bmatrix} \geq 0 \quad (3.25)$$

$$\text{rank} \begin{bmatrix} v_i & S_{ij} \\ S_{ij}^H & l_{ij} \end{bmatrix} = 1 \quad (3.26)$$

Note that the rank constraint defined in (3.26) is a non-convex constraint. The following relaxation simply drops the rank constraints resulting in the following semidefinite programming (SDP) formulation:

$$\min / \max f(x) \quad (3.27)$$

Subject to:

Power flow constraints:

$$v_i = v_j + (S_{ij}z_{ij}^H + z_{ij}S_{ij}^H) - z_{ij}l_{ij}z_{ij}^H \quad (3.28)$$

$$\text{diag}(S_{ij} - z_{ij}l_{ij}) = \sum_{k:j \rightarrow k} \text{diag}(S_{jk}) + s_{L,j} - s_{DG,j} \quad (3.29)$$

$$\begin{bmatrix} v_i & S_{ij} \\ S_{ij}^H & l_{ij} \end{bmatrix} \succeq 0 \quad (3.30)$$

Operating Constraints, $h(x, u)$:

$$\begin{aligned} V_{\min}^2 \leq \text{diag}(v_i) \leq V_{\max}^2 \\ \text{diag}(l_{ij}) \leq (I_{ij}^{\text{rated}})^2 \end{aligned} \quad (3.31)$$

Operating constraints specific to loss and voltage deviation minimization:

$$-\sqrt{(s_{DG,j}^{\psi, \text{rated}})^2 - (p_{DG,j}^{\psi})^2} \leq q_{DG,j}^{\psi} \leq \sqrt{(s_{DG,j}^{\psi, \text{rated}})^2 - (p_{DG,j}^{\psi})^2} \quad (3.32)$$

Operating constraints specific to PV hosting maximization:

$$0 \leq p_{DG,j}^{\psi} \leq p_{DG,max}^{\psi} \text{ and } q_{DG,j}^{\psi} = 0 \quad \forall j \in \mathcal{N}_{DG} \quad (3.33)$$

Note that for solutions to be meaningful, the optimal solution obtained using the relaxed model must satisfy the rank constraint (3.26). Only then the optimal solution is AC-feasible and meaningful for the real-world distribution operations.

3.5.2 Linear Approximation - Three-phase LinDistFlow

The linearized three-phase model is obtained using lifted branch flow equations. This model involves two major approximations:

- *Ignoring Power Losses:* The effects of power losses are ignored in power flow equations.

- *Approximating Nodal Voltage Phase Angle:* For a given node, it is assumed that the nodal voltage phase angles are separated by 120° and the degree of unbalance in voltage magnitudes is not large. This assumption allows us to represent off diagonal elements $S_{ij}^{\psi\phi}$ as a function of the diagonal elements, $S_{ij}^{\psi\psi}$, in S_{ij} .

$$\min / \max f(x) \quad (3.34)$$

Subject to:

Power flow constraints:

$$v_j^\psi = v_i^\psi - \sum_{\phi \in \phi_j} 2 \left(\text{real} \left(\gamma^{\psi\phi} S_{ij}^{\phi\phi} (z_{ij}^{\psi\phi})^T \right) \right) \quad (3.35)$$

$$P_{ij}^{\psi\psi} = \sum_{k:j \rightarrow k} P_{jk}^{\psi\psi} + p_{L,j} - p_{DG,j} \quad (3.36)$$

$$Q_{ij}^{\psi\psi} = \sum_{k:j \rightarrow k} Q_{jk}^{\psi\psi} + q_{L,j} - q_{DG,j} \quad (3.37)$$

where,

$$\gamma = \begin{bmatrix} 1 & \alpha & \alpha^2 \\ \alpha^2 & 1 & \alpha \\ \alpha & \alpha^2 & 1 \end{bmatrix} \quad (3.38)$$

Operating Constraints, $h(x, u)$: The bus voltages are constrained by the allowed limits for minimum and maximum voltages.

$$V_{min}^2 \leq v_i^\psi \leq V_{max}^2 \quad (3.39)$$

An approximation is needed to include the line thermal limit constraint in linear power flow model. There are multiple ways to approximate the line currents. Here we present one such approach using the polygon-based linearization proposed in [2]. The set of linear constraints for line thermal limit are defined in (3.40).

$$\begin{aligned} -\sqrt{3} (\mathbf{P}_{ij} + \mathbf{S}_{ij}) &\leq \mathbf{Q}_{ij} \leq -\sqrt{3} (\mathbf{P}_{ij} - \mathbf{S}_{ij}) \\ -\sqrt{3}/2 \mathbf{S}_{ij} &\leq \mathbf{Q}_{ij} \leq \sqrt{3}/2 \mathbf{S}_{ij} \\ \sqrt{3} (\mathbf{P}_{ij} - \mathbf{S}_{ij}) &\leq \mathbf{Q}_{ij} \leq \sqrt{3} (\mathbf{P}_{ij} + \mathbf{S}_{ij}) \end{aligned} \quad (3.40)$$

where, $\mathbf{S}_{ij} = \mathbf{S}_{ij}^{rated} \sqrt{(2\pi/n)/\sin(2\pi/n)}$ and $n = 6$.

Operating constraints specific to loss and voltage deviation minimization:

$$-\sqrt{(s_{DG,j}^{\psi, \text{rated}})^2 - (p_{DG,j}^{\psi})^2} \leq q_{DG,j}^{\psi} \leq \sqrt{(s_{DG,j}^{\psi, \text{rated}})^2 - (p_{DG,j}^{\psi})^2} \quad (3.41)$$

Operating constraints specific to PV hosting maximization:

$$0 \leq p_{DG,j}^{\psi} \leq p_{DG,max}^{\psi} \text{ and } q_{DG,j}^{\psi} = 0 \quad \forall j \in \mathcal{N}_{DG} \quad (3.42)$$

Although the errors introduced due to linearization are typically small, it has been shown in the existing literature that the accuracy of the linearization reduces under stressed system conditions such as during high loading conditions.

3.5.3 Hybrid model - Second-order cone programming

The hybrid model detailed here incorporates elements of both approximation and relaxation techniques. The approximation includes ignoring the mutual coupling in three phase lines. This results in three single-phase branch flow equations written separately for each phase. The resulting nonlinear power flow equations are then relaxed to obtain a second-order cone programming model.

Specifically, the approximation is detailed as below:

$$Z_{ij} = \begin{bmatrix} Z_{ij}^{aa} & Z_{ij}^{ab} & Z_{ij}^{ac} \\ Z_{ij}^{ba} & Z_{ij}^{bb} & Z_{ij}^{bc} \\ Z_{ij}^{ca} & Z_{ij}^{cb} & Z_{ij}^{cc} \end{bmatrix} \approx \begin{bmatrix} Z_{ij}^{aa} & 0 & 0 \\ 0 & Z_{ij}^{bb} & 0 \\ 0 & 0 & Z_{ij}^{cc} \end{bmatrix} \quad (3.43)$$

The resulting power flow model is as following:

$$v_i^{\psi} = v_j^{\psi} + (S_{ij}^{\psi\psi}(z_{ij}^{\psi\psi})^H + (S_{ij}^{\psi\psi})^H(z_{ij}^{\psi\psi})) - z_{ij}^{\psi\psi} l_{ij}^{\psi\psi} (z_{ij}^{\psi\psi})^H \quad (3.44)$$

$$S_{ij}^{\psi\psi} - z_{ij}^{\psi\psi} l_{ij}^{\psi\psi} = \sum_{k:j \rightarrow k} S_{jk}^{\psi\psi} + s_{L,j}^{\psi} - s_{DG,j}^{\psi} \quad (3.45)$$

$$(S_{ij}^{\psi\psi})^2 = v_i^{\psi} l_{ij}^{\psi\psi} \quad (3.46)$$

Note that (3.46) is a nonlinear equality constraint. The convex relaxation involves relaxing (3.46) to a conic constraint defined below.

$$(P_{ij}^{\psi\psi})^2 + (Q_{ij}^{\psi\psi})^2 \leq v_i^{\psi} l_{ij}^{\psi\psi} \quad (3.47)$$

The relaxed constrained shown by inequality (3.47) is a second-order cone and can be written as the following.

$$\begin{array}{c} \left\| \begin{array}{c} 2P_{ij} \\ 2Q_{ij} \\ l_{ij} - v_i \end{array} \right\| \leq l_{ij} + v_i \end{array} \quad (3.48)$$

The hybrid model for the D-OPF problem as second-order conic programming problem is detailed below.

$$\min / \max f(x) \quad (3.49)$$

Subject to:

Power flow constraints:

$$v_i^\psi = v_j^\psi + 2(P_{ij}^{\psi\psi} R_{ij}^{\psi\psi} + Q_{ij}^{\psi\psi} X_{ij}^{\psi\psi}) - l_{ij}^{\psi\psi} (z_{ij}^{\psi\psi})^2 \quad (3.50)$$

$$P_{ij}^{\psi\psi} - R_{ij}^{\psi\psi} l_{ij}^{\psi\psi} = \sum_{k:j \rightarrow k} P_{jk}^{\psi\psi} + p_{L,j}^\psi - p_{DG,j}^\psi \quad (3.51)$$

$$Q_{ij}^{\psi\psi} - X_{ij}^{\psi\psi} l_{ij}^{\psi\psi} = \sum_{k:j \rightarrow k} Q_{jk}^{\psi\psi} + q_{L,j}^\psi - q_{DG,j}^\psi \quad (3.52)$$

$$(P_{ij}^{\psi\psi})^2 + (Q_{ij}^{\psi\psi})^2 \leq v_i^\psi l_{ij}^{\psi\psi} \quad (3.53)$$

Operating Constraints, $h(x, u)$:

$$V_{min}^2 \leq v_i^\psi \leq V_{max}^2 \quad (3.54)$$

$$l_{ij}^{\psi\psi} \leq (I_{ij}^{rated})^2 \quad (3.55)$$

Operating constraints specific to loss and voltage deviation minimization:

$$-\sqrt{(s_{DG,j}^{\psi,rated})^2 - (p_{DG,j}^\psi)^2} \leq q_{DG,j}^\psi \leq \sqrt{(s_{DG,j}^{\psi,rated})^2 - (p_{DG,j}^\psi)^2} \quad (3.56)$$

Operating constraints specific to PV hosting maximization:

$$0 \leq p_{DG,j}^\psi \leq p_{DG,max}^\psi \text{ and } q_{DG,j}^\psi = 0 \quad \forall j \in \mathcal{N}_{DG} \quad (3.57)$$

Recall that in this model we are approximating power equations first by ignoring the mutual coupling and second by relaxing the voltage, current, power relationship equation. Thus, this model is a poor approximation if the distribution system under study has significant mutual coupling. Likewise, it is important to check the AC feasibility of the solutions obtained from the relaxed D-OPF model. In this

model, the OPF solutions are AC-feasible if they satisfy the equality $(P_{ij}^{\psi\psi})^2 + (Q_{ij}^{\psi\psi})^2 = v_i^\psi l_{ij}^{\psi\psi}$, although the relaxed D-OPF model solves for inequality. If the OPF solutions do not satisfy this equality, they are AC-infeasible and meaningless.

3.6 Multi-period Optimization: D-OPF problems

The D-OPF problem formulation may require consideration of multiple time periods in a single optimization model. Specifically, device models including battery energy storage or OLTC daily switching limits require inter-temporal constraints to be included on the D-OPF formulation that links multiple time periods and necessitates the development of multi-period D-OPF formulation. On the other hand, some D-OPF problems could be of time-series nature but not without inter-temporal constraints (e.g., running D-OPF for daily/yearly PV generation profiles). For such problems, the D-OPF model with multi-period time consideration may not be required as such D-OPF problems can be easily decoupled into multiple single period D-OPF problems and solved effectively.

3.7 Illustrated Example

In this section, we detail the D-OPF formulations using a 5-bus example that was introduced in Section 2 (see Figure 3.1). The feeder consists of unbalanced lines and loads and the following controllable devices: a voltage regulator, a capacitor bank, and two DGs with smart inverters. The variable definitions follow from those defined in Section 2. Here, we define the decision variables for the 5-bus system.

- Optimum step for the voltage regulator at branch 12, $x_{m,12} = [x_{m,12}^a, x_{m,12}^b, x_{m,12}^c]$, where, $x_{m,12}^\psi \in \{0, 1\}$, and m defines the step.
- Decision on on/off status of capacitor bank at bus 3, $u_{c,3} = [u_{c,3}^a, u_{c,3}^b, u_{c,3}^c]$, where, $u_{c,3}^\psi \in \{0, 1\}$.
- Reactive power dispatch from DG smart inverters connected at buses 4 and 5 are $\{q_{DG,4}^a, q_{DG,4}^b, q_{DG,5}^c\}$.

Next, we formulate the D-OPF formulation for the 5-bus test system using the models introduced in this section including NLP-BIM, NLP-

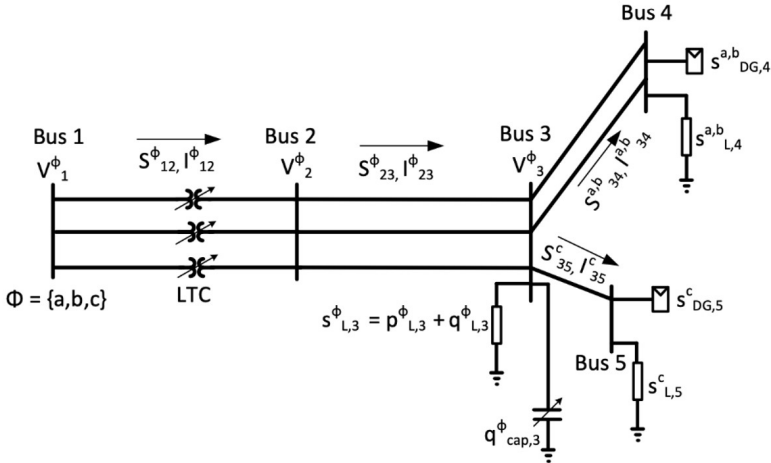


Figure 3.1: An example 5-bus test system.

BFM, SDP, SOCP, and LinDistFlow. The goal of the OPF problem to minimize the feeder losses by controlling all voltage control devices in the 5-bus test system.

Note that in all the cases, the discrete decision variables will lead to a mixed-integer problem formulation. In order to formulate an optimization problem with only continuous variables, one can freeze the set-points of discrete control devices (i.e. voltage regulator and capacitor bank) and optimize only for the continuous decision variables.

3.7.1 D-OPF using Bus-injection Power Flow Model (NLP-BIM)

Power flow constraints $g(x, u)$:

$$0 = V_2^{a,re} I_2^{a,re} + V_2^{a,im} I_2^{a,im} \quad (3.58)$$

$$0 = V_2^{a,im} I_2^{a,re} - V_2^{a,re} I_2^{a,im} \quad (3.59)$$

$$0 = V_2^{b,re} I_2^{b,re} + V_2^{b,im} I_2^{b,im} \quad (3.60)$$

$$0 = V_2^{b,im} I_2^{b,re} - V_2^{b,re} I_2^{b,im} \quad (3.61)$$

$$0 = V_2^{c,re} I_2^{c,re} + V_2^{c,im} I_2^{c,im} \quad (3.62)$$

$$0 = V_2^{c,im} I_2^{c,re} - V_2^{c,re} I_2^{c,im} \quad (3.63)$$

$$0 = V_3^{a,re} I_3^{a,re} + V_3^{a,im} I_3^{a,im} + p_{L,3}^a \quad (3.64)$$

$$0 = V_3^{a,im} I_3^{a,re} - V_3^{a,re} I_3^{a,im} + q_{L,3}^a - q_{cap,3}^a \quad (3.65)$$

$$0 = V_3^{b,re} I_3^{b,re} + V_3^{b,im} I_3^{b,im} + p_{L,3}^b \quad (3.66)$$

$$0 = V_3^{b,im} I_3^{b,re} - V_3^{b,re} I_3^{b,im} + q_{L,3}^b - q_{cap,3}^b \quad (3.67)$$

$$0 = V_3^{c,re} I_3^{c,re} + V_3^{c,im} I_3^{c,im} + p_{L,3}^c \quad (3.68)$$

$$0 = V_3^{c,im} I_3^{c,re} - V_3^{c,re} I_3^{c,im} + q_{L,3}^c - q_{cap,3}^c \quad (3.69)$$

$$0 = V_4^{a,re} I_4^{a,re} + V_4^{a,im} I_4^{a,im} + p_{L,4}^a - p_{DG,4}^a \quad (3.70)$$

$$0 = V_4^{a,im} I_4^{a,re} - V_4^{a,re} I_4^{a,im} + q_{L,4}^a - q_{DG,4}^a \quad (3.71)$$

$$0 = V_4^{b,re} I_4^{b,re} + V_4^{b,im} I_4^{b,im} + p_{L,4}^b - p_{DG,4}^b \quad (3.72)$$

$$0 = V_4^{b,im} I_4^{b,re} - V_4^{b,re} I_4^{b,im} + q_{L,4}^b - q_{DG,4}^b \quad (3.73)$$

$$0 = V_5^{c,re} I_5^{c,re} + V_5^{c,im} I_5^{c,im} + p_{L,5}^c - p_{DG,5}^c \quad (3.74)$$

$$0 = V_5^{c,im} I_5^{c,re} - V_5^{c,re} I_5^{c,im} + q_{L,5}^c - q_{DG,5}^c \quad (3.75)$$

$$I_2^{a,re} = \sum_{j \in \{1,2,3,4,5\}, \psi \in \{a,b,c\}} V_j^{\psi,re} G_{2j}^{a\psi} - V_j^{\psi,im} B_{2j}^{a\psi} \quad (3.76)$$

$$I_2^{a,im} = \sum_{j \in \{1,2,3,4,5\}, \psi \in \{a,b,c\}} V_j^{\psi,re} B_{2j}^{a\psi} + V_j^{\psi,im} G_{2j}^{a\psi} \quad (3.77)$$

$$I_2^{b,re} = \sum_{j \in \{1,2,3,4,5\}, \psi \in \{a,b,c\}} V_j^{\psi,re} G_{2j}^{b\psi} - V_j^{\psi,im} B_{2j}^{b\psi} \quad (3.78)$$

$$I_2^{b,im} = \sum_{j \in \{1,2,3,4,5\}, \psi \in \{a,b,c\}} V_j^{\psi,re} B_{2j}^{b\psi} + V_j^{\psi,im} G_{2j}^{b\psi} \quad (3.79)$$

$$I_2^{c,re} = \sum_{j \in \{1,2,3,4,5\}, \psi \in \{a,b,c\}} V_j^{\psi,re} G_{2j}^{c\psi} - V_j^{\psi,im} B_{2j}^{c\psi} \quad (3.80)$$

$$I_2^{c,im} = \sum_{j \in \{1,2,3,4,5\}, \psi \in \{a,b,c\}} V_j^{\psi,re} B_{2j}^{c\psi} + V_j^{\psi,im} G_{2j}^{c\psi} \quad (3.81)$$

$$I_3^{a,re} = \sum_{j \in \{1,2,3,4,5\}, \psi \in \{a,b,c\}} V_j^{\psi,re} G_{3j}^{a\psi} - V_j^{\psi,im} B_{3j}^{a\psi} \quad (3.82)$$

$$I_3^{a,im} = \sum_{j \in \{1,2,3,4,5\}, \psi \in \{a,b,c\}} V_j^{\psi,re} B_{3j}^{a\psi} + V_j^{\psi,im} G_{3j}^{a\psi} \quad (3.83)$$

$$I_3^{b,re} = \sum_{j \in \{1,2,3,4,5\}, \psi \in \{a,b,c\}} V_j^{\psi,re} G_{3j}^{b\psi} - V_j^{\psi,im} B_{3j}^{b\psi} \quad (3.84)$$

$$I_3^{b,im} = \sum_{j \in \{1,2,3,4,5\}, \psi \in \{a,b,c\}} V_j^{\psi,re} B_{3j}^{b\psi} + V_j^{\psi,im} G_{3j}^{b\psi} \quad (3.85)$$

$$I_3^{c,re} = \sum_{j \in \{1,2,3,4,5\}, \psi \in \{a,b,c\}} V_j^{\psi,re} G_{3j}^{c\psi} - V_j^{\psi,im} B_{3j}^{c\psi} \quad (3.86)$$

$$I_3^{c,im} = \sum_{j \in \{1,2,3,4,5\}, \psi \in \{a,b,c\}} V_j^{\psi,re} B_{3j}^{c\psi} + V_j^{\psi,im} G_{3j}^{c\psi} \quad (3.87)$$

$$I_4^{a,re} = \sum_{j \in \{1,2,3,4,5\}, \psi \in \{a,b,c\}} V_j^{\psi,re} G_{4j}^{a\psi} - V_j^{\psi,im} B_{4j}^{a\psi} \quad (3.88)$$

$$I_4^{a,im} = \sum_{j \in \{1,2,3,4,5\}, \psi \in \{a,b,c\}} V_j^{\psi,re} B_{4j}^{a\psi} + V_j^{\psi,im} G_{4j}^{a\psi} \quad (3.89)$$

$$I_4^{b,re} = \sum_{j \in \{1,2,3,4,5\}, \psi \in \{a,b,c\}} V_j^{\psi,re} G_{4j}^{b\psi} - V_j^{\psi,im} B_{4j}^{b\psi} \quad (3.90)$$

$$I_4^{b,im} = \sum_{j \in \{1,2,3,4,5\}, \psi \in \{a,b,c\}} V_j^{\psi,re} B_{4j}^{b\psi} + V_j^{\psi,im} G_{4j}^{b\psi} \quad (3.91)$$

$$I_5^{c,re} = \sum_{j \in \{1,2,3,4,5\}, \psi \in \{a,b,c\}} V_j^{\psi,re} G_{5j}^{c\psi} - V_j^{\psi,im} B_{5j}^{c\psi} \quad (3.92)$$

$$I_5^{c,im} = \sum_{j \in \{1,2,3,4,5\}, \psi \in \{a,b,c\}} V_j^{\psi,re} B_{5j}^{c\psi} + V_j^{\psi,im} G_{5j}^{c\psi} \quad (3.93)$$

Operating Constraints, $h(x, u)$:

$$0.95^2 \leq (V_2^{a,re})^2 + (V_2^{a,im})^2 \leq 1.05^2 \quad (3.94)$$

$$0.95^2 \leq (V_2^{b,re})^2 + (V_2^{b,im})^2 \leq 1.05^2 \quad (3.95)$$

$$0.95^2 \leq (V_2^{c,re})^2 + (V_2^{c,im})^2 \leq 1.05^2 \quad (3.96)$$

$$0.95^2 \leq (V_3^{a,re})^2 + (V_3^{a,im})^2 \leq 1.05^2 \quad (3.97)$$

$$0.95^2 \leq (V_3^{b,re})^2 + (V_3^{b,im})^2 \leq 1.05^2 \quad (3.98)$$

$$0.95^2 \leq (V_3^{c,re})^2 + (V_3^{c,im})^2 \leq 1.05^2 \quad (3.99)$$

$$0.95^2 \leq (V_4^{a,re})^2 + (V_4^{a,im})^2 \leq 1.05^2 \quad (3.100)$$

$$0.95^2 \leq (V_4^{b,re})^2 + (V_4^{b,im})^2 \leq 1.05^2 \quad (3.101)$$

$$0.95^2 \leq (V_5^{c,re})^2 + (V_5^{c,im})^2 \leq 1.05^2 \quad (3.102)$$

$$(I_{12}^{a,re})^2 + (I_{12}^{a,im})^2 \leq \left(I_{12}^{a,rated} \right)^2 \quad (3.103)$$

$$(I_{12}^{b,re})^2 + (I_{12}^{b,im})^2 \leq \left(I_{12}^{b,rated} \right)^2 \quad (3.104)$$

$$(I_{12}^{c,re})^2 + (I_{12}^{c,im})^2 \leq \left(I_{12}^{c,rated} \right)^2 \quad (3.105)$$

$$(I_{23}^{a,re})^2 + (I_{23}^{a,im})^2 \leq \left(I_{23}^{a,rated} \right)^2 \quad (3.106)$$

$$(I_{23}^{b,re})^2 + (I_{23}^{b,im})^2 \leq \left(I_{23}^{b,rated} \right)^2 \quad (3.107)$$

$$(I_{23}^{c,re})^2 + (I_{23}^{c,im})^2 \leq \left(I_{23}^{c,rated} \right)^2 \quad (3.108)$$

$$(I_{34}^{a,re})^2 + (I_{34}^{a,im})^2 \leq \left(I_{34}^{a,rated} \right)^2 \quad (3.109)$$

$$(I_{34}^{b,re})^2 + (I_{34}^{b,im})^2 \leq \left(I_{34}^{b,rated} \right)^2 \quad (3.110)$$

$$(I_{45}^{c,re})^2 + (I_{45}^{c,im})^2 \leq \left(I_{45}^{c,rated} \right)^2 \quad (3.111)$$

where

$$I_{12}^{a,re} = -G_{12}^{aa}V_1^{a,re} + B_{12}^{aa}V_1^{a,im} + G_{12}^{aa}V_2^{a,re} - B_{12}^{aa}V_2^{a,im} \quad (3.112)$$

$$I_{12}^{a,im} = -G_{12}^{aa}V_1^{a,im} + B_{12}^{aa}V_1^{a,re} + B_{12}^{aa}V_2^{a,re} + G_{12}^{aa}V_2^{a,im} \quad (3.113)$$

$$I_{12}^{b,re} = -G_{12}^{bb}V_1^{b,re} + B_{12}^{bb}V_1^{b,im} + G_{12}^{bb}V_2^{b,re} - B_{12}^{bb}V_2^{b,im} \quad (3.114)$$

$$I_{12}^{b,im} = -G_{12}^{bb}V_1^{b,im} + B_{12}^{bb}V_1^{b,re} + B_{12}^{bb}V_2^{b,re} + G_{12}^{bb}V_2^{b,im} \quad (3.115)$$

$$I_{12}^{c,re} = -G_{12}^{cc}V_1^{c,re} + B_{12}^{cc}V_1^{c,im} + G_{12}^{cc}V_2^{c,re} - B_{12}^{cc}V_2^{c,im} \quad (3.116)$$

$$I_{12}^{c,im} = -G_{12}^{cc}V_1^{c,im} + B_{12}^{cc}V_1^{c,re} + B_{12}^{cc}V_2^{c,re} + G_{12}^{cc}V_2^{c,im} \quad (3.117)$$

$$I_{23}^{a,re} = -G_{23}^{aa}V_2^{a,re} + B_{23}^{aa}V_2^{a,im} + G_{23}^{aa}V_3^{a,re} - B_{23}^{aa}V_3^{a,im} \quad (3.118)$$

$$I_{23}^{a,im} = -G_{23}^{aa}V_2^{a,im} + B_{23}^{aa}V_2^{a,re} + B_{23}^{aa}V_3^{a,re} + G_{23}^{aa}V_3^{a,im} \quad (3.119)$$

$$I_{23}^{b,re} = -G_{23}^{bb}V_2^{b,re} + B_{23}^{bb}V_2^{b,im} + G_{23}^{bb}V_3^{b,re} - B_{23}^{bb}V_3^{b,im} \quad (3.120)$$

$$I_{23}^{b,im} = -G_{23}^{bb}V_2^{b,im} + B_{23}^{bb}V_2^{b,re} + B_{23}^{bb}V_3^{b,re} + G_{23}^{bb}V_3^{b,im} \quad (3.121)$$

$$I_{23}^{c,re} = -G_{23}^{cc}V_2^{c,re} + B_{23}^{cc}V_2^{c,im} + G_{23}^{cc}V_3^{c,re} - B_{23}^{cc}V_3^{c,im} \quad (3.122)$$

$$I_{23}^{c,im} = -G_{23}^{cc}V_2^{c,im} + B_{23}^{cc}V_2^{c,re} + B_{23}^{cc}V_3^{c,re} + G_{23}^{cc}V_3^{c,im} \quad (3.123)$$

$$I_{34}^{a,re} = -G_{34}^{\phi\phi}V_3^{a,re} + B_{34}^{aa}V_3^{a,im} + G_{34}^{aa}V_4^{a,re} - B_{34}^{aa}V_4^{a,im} \quad (3.124)$$

$$I_{34}^{a,im} = -G_{34}^{\phi\phi}V_3^{a,im} + B_{34}^{aa}V_3^{a,re} + B_{34}^{aa}V_4^{a,re} + G_{34}^{aa}V_4^{a,im} \quad (3.125)$$

$$I_{34}^{b,re} = -G_{34}^{\phi\phi}V_3^{b,re} + B_{34}^{bb}V_3^{b,im} + G_{34}^{bb}V_4^{b,re} - B_{34}^{bb}V_4^{b,im} \quad (3.126)$$

$$I_{34}^{b,im} = -G_{34}^{\phi\phi}V_3^{b,im} + B_{34}^{bb}V_3^{b,re} + B_{34}^{bb}V_4^{b,re} + G_{34}^{bb}V_4^{b,im} \quad (3.127)$$

$$I_{35}^{c,re} = -G_{35}^{\phi\phi}V_3^{c,re} + B_{35}^{cc}V_3^{c,im} + G_{35}^{cc}V_5^{c,re} - B_{35}^{cc}V_5^{c,im} \quad (3.128)$$

$$I_{35}^{c,im} = -G_{35}^{cc}V_3^{c,im} + B_{35}^{cc}V_3^{c,re} + B_{35}^{cc}V_5^{c,re} + G_{35}^{cc}V_5^{c,im} \quad (3.129)$$

Operating constraints specific to loss and voltage deviation minimization:

$$-\sqrt{\left(s_{DG,4}^{a,rated}\right)^2 - \left(p_{DG,4}^a\right)^2} \leq q_{DG,4}^a \leq \sqrt{\left(s_{DG,4}^{a,rated}\right)^2 - \left(p_{DG,4}^a\right)^2} \quad (3.130)$$

$$-\sqrt{\left(s_{DG,4}^{b,rated}\right)^2 - \left(p_{DG,4}^b\right)^2} \leq q_{DG,4}^b \leq \sqrt{\left(s_{DG,4}^{b,rated}\right)^2 - \left(p_{DG,4}^b\right)^2} \quad (3.131)$$

$$-\sqrt{\left(s_{DG,5}^{c,rated}\right)^2 - \left(p_{DG,5}^c\right)^2} \leq q_{DG,5}^c \leq \sqrt{\left(s_{DG,5}^{c,rated}\right)^2 - \left(p_{DG,5}^c\right)^2} \quad (3.132)$$

Operating constraints specific to PV hosting maximization:

$$0 \leq p_{DG,4}^a \leq p_{DG,4}^{a,max} \quad (3.133)$$

$$0 \leq p_{DG,4}^b \leq p_{DG,4}^{b,max} \quad (3.134)$$

$$0 \leq p_{DG,5}^c \leq p_{DG,5}^{c,max} \quad (3.135)$$

$$q_{DG,4}^a = 0 \quad (3.136)$$

$$q_{DG,4}^b = 0 \quad (3.137)$$

$$q_{DG,5}^c = 0 \quad (3.138)$$

$$(3.139)$$

3.7.2 D-OPF using Branch Power Flow Model (NLP-BFM)

Problem Objective, $f(x, u)$: Loss minimization. Total power loss is defined as,

$$f(x, u) = P_{loss}^{total} = \text{real}(I_{23}^H Z_{23} I_{23}) + \text{real}(I_{34}^H Z_{34} I_{34}) + \text{real}(I_{35}^H Z_{35} I_{35}) \quad (3.140)$$

Subject to:

Equality constraints (Branch flow model), $g(x, u) = 0$

$$V_2 = a_{12} V_1 \quad (3.141)$$

$$V_3 = V_2 - Z_{23} I_{23} \quad (3.142)$$

$$V_4 = V_3 - Z_{34} I_{34} \quad (3.143)$$

$$V_5 = V_3 - Z_{35} I_{35} \quad (3.144)$$

$$I_{12} = a_{12} I_{23} \quad (3.145)$$

$$\begin{aligned} \text{diag}(S_{23} - Z_{23} I_{23} {I_{23}}^H) &= \text{diag}(S_{34}) + \text{diag}(S_{35}) + \\ &\quad s_{L,3} - s_{DG,3} - u_{c,3} q_{c,3} \end{aligned} \quad (3.146)$$

$$\text{diag}(S_{34} - Z_{34} I_{34} {I_{34}}^H) = s_{L,4} - s_{DG,4} \quad (3.147)$$

$$\text{diag}(S_{35} - Z_{35} I_{35} {I_{35}}^H) = s_{L,5} - s_{DG,5} \quad (3.148)$$

$$S_{23} = V_2 I_{23}^H \quad (3.149)$$

$$S_{34} = V_3 I_{34}^H \quad (3.150)$$

$$S_{35} = V_3 I_{35}^H \quad (3.151)$$

Voltage regulator model

$$a_{12}^\psi = \sum_{m=1}^{32} (b_m x_{m,12}^\psi) \quad (3.152)$$

$$\sum_{m=1}^{32} x_{m,12}^\psi = 1 \quad (3.153)$$

Operating constraints (inequalities, $h(x,u) < 0$):

Voltage limit

$$0.95 \leq |V_2^\psi| \leq 1.05 \quad (3.154)$$

$$0.95 \leq |V_3^\psi| \leq 1.05 \quad (3.155)$$

$$0.95 \leq |V_4^\psi| \leq 1.05 \quad (3.156)$$

$$0.95 \leq |V_5^\psi| \leq 1.05 \quad (3.157)$$

Thermal limit:

$$|I_{23}^\psi| \leq I_{23}^{rated} \quad (3.158)$$

$$|I_{34}^\psi| \leq I_{34}^{rated} \quad (3.159)$$

$$|I_{35}^\psi| \leq I_{35}^{rated} \quad (3.160)$$

Smart Inverter Rating

$$|q_{DG,3}^\psi| \leq \sqrt{(s_{DG,3}^{\psi,rated})^2 - (p_{DG,3}^\psi)^2} \quad (3.161)$$

$$|q_{DG,4}^\psi| \leq \sqrt{(s_{DG,4}^{\psi,rated})^2 - (p_{DG,4}^\psi)^2} \quad (3.162)$$

$$|q_{DG,5}^\psi| \leq \sqrt{(s_{DG,5}^{\psi,rated})^2 - (p_{DG,5}^\psi)^2} \quad (3.163)$$

$$(3.164)$$

3.7.3 D-OPF using SDP Relaxation for Power Flow Model

Problem Objective, $f(x, u)$: Loss minimization. Total power loss is defined as,

$$f(x, u) = P_{loss}^{total} = \text{real}(Z_{23}l_{23}) + \text{real}(Z_{34}l_{34}) + \text{real}(Z_{35}I_{35}) \quad (3.165)$$

Subject to:

Equality constraints (Branch flow model), $g(x, u) = 0$

$$v_2 = A_{12}v_1 \quad (3.166)$$

$$v_3 = v_2 - (S_{23}Z_{23}^H + Z_{23}S_{23}^H) + Z_{23}l_{23}Z_{23}^H \quad (3.167)$$

$$v_4 = v_3 - (S_{34}Z_{34}^H + Z_{34}S_{34}^H) + Z_{34}l_{34}Z_{34}^H \quad (3.168)$$

$$v_5 = v_4 - (S_{35}Z_{35}^H + Z_{35}S_{35}^H) + Z_{35}l_{35}Z_{35}^H \quad (3.169)$$

$$l_{12} = A_{12}l_{23} \quad (3.170)$$

$$\text{diag}(S_{23} - Z_{23}l_{23}) = \text{diag}(S_{34}) + s_{L,3} - u_{c,3}q_{c,3} \quad (3.171)$$

$$\text{diag}(S_{34} - Z_{34}l_{34}) = s_{L,4} - s_{DG,4} \quad (3.172)$$

$$\text{diag}(S_{35} - Z_{35}l_{35}) = s_{L,5} - s_{DG,5} \quad (3.173)$$

SDP relaxation (Rank constraint is relaxed to obtain a convex programming model)

$$\begin{bmatrix} v_2 & S_{23} \\ S_{23}^H & l_{23} \end{bmatrix} \succeq 0 \quad (3.174)$$

$$\begin{bmatrix} v_3 & S_{34} \\ S_{34}^H & l_{34} \end{bmatrix} \succeq 0 \quad (3.175)$$

$$\begin{bmatrix} v_3 & S_{35} \\ S_{35}^H & l_{35} \end{bmatrix} \succeq 0 \quad (3.176)$$

Voltage regulator model

$$A_{12} = \begin{bmatrix} \sum_{m=1}^{32} (b_m x_{m,12}^a) & 0 & 0 \\ 0 & \sum_{m=1}^{32} (b_m x_{m,12}^b) & 0 \\ 0 & 0 & \sum_{m=1}^{32} (b_m x_{m,12}^c) \end{bmatrix} \quad (3.177)$$

$$\sum_{m=1}^{32} x_{m,12}^\psi = 1 \quad \forall \{\psi \in a, b, c\} \quad (3.178)$$

Operating constraints (inequalities, $h(x,u) < 0$):

Voltage limits:

$$0.95 \leq \text{diag}(v_2) \leq 1.05 \quad (3.179)$$

$$0.95 \leq \text{diag}(v_3) \leq 1.05 \quad (3.180)$$

$$0.95 \leq \text{diag}(v_4) \leq 1.05 \quad (3.181)$$

$$0.95 \leq \text{diag}(v_5) \leq 1.05 \quad (3.182)$$

Thermal limit:

$$\text{diag}(l_{23}) \leq I_{23}^{\text{rated}} \quad (3.183)$$

$$\text{diag}(l_{34}) \leq I_{34}^{\text{rated}} \quad (3.184)$$

$$\text{diag}(l_{35}) \leq I_{35}^{\text{rated}} \quad (3.185)$$

Smart Inverter Rating

$$|q_{DG,3}^\psi| \leq \sqrt{(s_{DG,3}^{\psi,\text{rated}})^2 - (p_{DG,3}^\psi)^2} \quad (3.186)$$

$$|q_{DG,4}^\psi| \leq \sqrt{(s_{DG,4}^{\psi,\text{rated}})^2 - (p_{DG,4}^\psi)^2} \quad (3.187)$$

$$|q_{DG,5}^\psi| \leq \sqrt{(s_{DG,5}^{\psi,\text{rated}})^2 - (p_{DG,5}^\psi)^2} \quad (3.188)$$

3.7.4 D-OPF using LinDistFlow Power Flow Model

Problem Objective, $f(x, u)$: Loss minimization. Total power loss is a function of branch current. Since the LinDistFlow model does not directly include the branch currents in power flow formulation, we present an alternate and approximate formulation for the loss function.

The per-phase branch current is defined as the following.

$$(I_{ij}^{\psi\psi})^2 = \frac{(P_{ij}^{\psi\psi})^2 + (Q_{ij}^{\psi\psi})^2}{(V_i^\psi)^2} \quad (3.189)$$

Assuming, $|V_i^\psi| \approx 1$, The per-phase branch current can be approximated as a function of branch active and reactive power flow as shown below.

$$(\tilde{I}_{ij}^{\psi\psi})^2 = (P_{ij}^{\psi\psi})^2 + (Q_{ij}^{\psi\psi})^2 \quad (3.190)$$

Then, loss minimization objective function is expressed using approximated branch current.

$$f(x, u) = P_{loss}^{total} = \sum_{\psi \in \{abc\}} (\tilde{I}_{23}^{\psi\psi})^2 r_{23}^{\psi\psi} + \sum_{\psi \in \{ab\}} (\tilde{I}_{34}^{\psi\psi})^2 r_{34}^{\psi\psi} + \sum_{\psi \in \{c\}} (\tilde{I}_{35}^{\psi\psi})^2 r_{35}^{\psi\psi} \quad (3.191)$$

Subject to:

Equality constraints (Branch flow model), $g(x, u) = 0$

$$v_2^\psi = a_{12}^\psi v_1^\psi \quad (3.192)$$

$$v_3^\psi = v_2^\psi - \sum_{\phi \in \Phi_2} 2 \left(\text{real} \left(\gamma^{\psi\phi} S_{23}^{\phi\phi} (Z_{23}^{\psi\phi})^H \right) \right) \quad (3.193)$$

$$v_4^\psi = v_3^\psi - \sum_{\phi \in \Phi_3} 2 \left(\text{real} \left(\gamma^{\psi\phi} S_{34}^{\phi\phi} (Z_{34}^{\psi\phi})^H \right) \right) \quad (3.194)$$

$$v_5^\psi = v_3^\psi - \sum_{\phi \in \Phi_3} 2 \left(\text{real} \left(\gamma^{\psi\phi} S_{35}^{\phi\phi} (Z_{35}^{\psi\phi})^H \right) \right) \quad (3.195)$$

$$S_{12}^{\psi\psi} = S_{23}^{\psi\psi} \quad (3.196)$$

$$S_{23}^{\psi\psi} = S_{34}^{\psi\psi} + S_{35}^{\psi\psi} + s_{L,3}^\psi - u_{c,3}^\psi q_{c,3}^\psi \quad (3.197)$$

$$S_{34}^{\psi\psi} = s_{L,4}^\psi - s_{DG,4}^\psi \quad (3.198)$$

$$S_{35}^{\psi\psi} = s_{L,5}^\psi - s_{DG,5}^\psi \quad (3.199)$$

Voltage regulator model

$$a_{12}^\psi = \sum_{m=1}^{32} (b_m x_{m,12}^\psi) \quad (3.200)$$

$$\sum_{m=1}^{32} x_{m,12}^\psi = 1 \quad (3.201)$$

Operating constraints (inequalities, $h(x, u) < 0$): Voltage limits:

$$0.95 \leq |V_2^\psi| \leq 1.05 \quad (3.202)$$

$$0.95 \leq |V_3^\psi| \leq 1.05 \quad (3.203)$$

$$0.95 \leq |V_4^\psi| \leq 1.05 \quad (3.204)$$

$$0.95 \leq |V_5^\psi| \leq 1.05 \quad (3.205)$$

Thermal limit constraints are difficult to define in LinDistFlow formulation. One can use linearization techniques such as the one using

polygon-based approximation as defined in previous sections (Section 3.5.2).

Smart Inverter Ratings:

$$|q_{DG,3}^\psi| \leq \sqrt{(s_{DG,3}^{\psi,rated})^2 - (p_{DG,3}^\psi)^2} \quad (3.206)$$

$$|q_{DG,4}^\psi| \leq \sqrt{(s_{DG,4}^{\psi,rated})^2 - (p_{DG,4}^\psi)^2} \quad (3.207)$$

$$|q_{DG,5}^\psi| \leq \sqrt{(s_{DG,5}^{\psi,rated})^2 - (p_{DG,5}^\psi)^2} \quad (3.208)$$

3.7.5 D-OPF using SOCP Relaxation for Power Flow Model

Problem Objective, $f(x, u)$: Loss minimization. Total power loss is defined as,

$$f(x, u) = P_{loss}^{total} = \text{real}(Z_{23}l_{23}) + \text{real}(Z_{34}l_{34}) + \text{real}(Z_{35}l_{35}) \quad (3.209)$$

Subject to:

Equality constraints (Branch flow model), $g(x, u) = 0$

$$v_2^\psi = a_{12}^\psi v_1^\psi \quad (3.210)$$

$$v_3^\psi = v_2^\psi + 2(P_{23}^{\psi\psi} R_{23}^{\psi\psi} + Q_{23}^{\psi\psi} X_{23}^{\psi\psi}) - l_{23}^{\psi\psi} (z_{23}^{\psi\psi})^2 \quad (3.211)$$

$$v_4^\psi = v_3^\psi + 2(P_{34}^{\psi\psi} R_{34}^{\psi\psi} + Q_{34}^{\psi\psi} X_{34}^{\psi\psi}) - l_{34}^{\psi\psi} (z_{34}^{\psi\psi})^2 \quad (3.212)$$

$$v_5^\psi = v_3^\psi + 2(P_{35}^{\psi\psi} R_{35}^{\psi\psi} + Q_{35}^{\psi\psi} X_{35}^{\psi\psi}) - l_{35}^{\psi\psi} (z_{35}^{\psi\psi})^2 \quad (3.213)$$

$$P_{12}^{\psi\psi} = P_{23}^{\psi\psi} \quad (3.214)$$

$$Q_{12}^{\psi\psi} = Q_{23}^{\psi\psi} \quad (3.215)$$

$$P_{23}^{\psi\psi} - R_{23}^{\psi\psi} l_{23}^{\psi\psi} = P_{34}^{\psi\psi} + P_{35}^{\psi\psi} + p_{L,3}^\psi \quad (3.216)$$

$$Q_{23}^{\psi\psi} - X_{23}^{\psi\psi} l_{23}^{\psi\psi} = Q_{34}^{\psi\psi} + Q_{35}^{\psi\psi} + q_{L,3}^\psi - u_{c,3}^\psi q_{c,3}^\psi \quad (3.217)$$

$$P_{34}^{\psi\psi} - R_{34}^{\psi\psi} l_{34}^{\psi\psi} = p_{L,4}^\psi - p_{DG,4}^\psi \quad (3.218)$$

$$Q_{34}^{\psi\psi} - X_{34}^{\psi\psi} l_{34}^{\psi\psi} = q_{L,4}^\psi - q_{DG,4}^\psi \quad (3.219)$$

$$P_{35}^{\psi\psi} - R_{35}^{\psi\psi} l_{35}^{\psi\psi} = p_{L,5}^\psi - p_{DG,5}^\psi \quad (3.220)$$

$$Q_{35}^{\psi\psi} - X_{35}^{\psi\psi} l_{35}^{\psi\psi} = q_{L,5}^\psi - q_{DG,5}^\psi \quad (3.221)$$

$$l_{12}^{\psi\psi} = a_{12}^\psi l_{23}^{\psi\psi} \quad (3.222)$$

$$(P_{23}^{\psi\psi})^2 + (Q_{23}^{\psi\psi})^2 \leq v_2^\psi l_{23}^{\psi\psi} \quad (3.223)$$

$$(P_{34}^{\psi\psi})^2 + (Q_{34}^{\psi\psi})^2 \leq v_3^\psi l_{34}^{\psi\psi} \quad (3.224)$$

$$(P_{35}^{\psi\psi})^2 + (Q_{35}^{\psi\psi})^2 \leq v_3^\psi l_{35}^{\psi\psi} \quad (3.225)$$

Voltage regulator model

$$a_{12}^\psi = \sum_{m=1}^{32} (b_m x_{m,12}^\psi) \quad (3.226)$$

$$\sum_{m=1}^{32} x_{m,12}^\psi = 1 \quad (3.227)$$

Operating constraints (inequalities, $h(x,u) < 0$):

Voltage limits:

$$0.95 \leq |V_2^\psi| \leq 1.05 \quad (3.228)$$

$$0.95 \leq |V_3^\psi| \leq 1.05 \quad (3.229)$$

$$0.95 \leq |V_4^\psi| \leq 1.05 \quad (3.230)$$

$$0.95 \leq |V_5^\psi| \leq 1.05 \quad (3.231)$$

Thermal limit constraints:

$$l_{23}^{\psi\psi} \leq I_{23}^{rated} \quad (3.232)$$

$$l_{34}^{\psi\psi} \leq I_{34}^{rated} \quad (3.233)$$

$$l_{35}^{\psi\psi} \leq I_{35}^{rated} \quad (3.234)$$

Smart Inverter Ratings:

$$|q_{DG,3}^\psi| \leq \sqrt{(s_{DG,3}^{\psi,rated})^2 - (p_{DG,3}^\psi)^2} \quad (3.235)$$

$$|q_{DG,4}^\psi| \leq \sqrt{(s_{DG,4}^{\psi,rated})^2 - (p_{DG,4}^\psi)^2} \quad (3.236)$$

$$|q_{DG,5}^\psi| \leq \sqrt{(s_{DG,5}^{\psi,rated})^2 - (p_{DG,5}^\psi)^2} \quad (3.237)$$

3.8 Modeling Tools and Solvers

This section briefly summarizes the modeling tools and solvers commonly used to solve D-OPF problems.

3.8.1 MATLAB

MATLAB, a programming and numeric computing platform, has been extensively used to model and solve optimization problems. MATLAB, designed to operate on matrices and arrays, have provided structure to model linear, nonlinear, convex, and mixed-integer programming problems. Moreover, MATLAB's Optimization Toolbox can solve LP, MILP, QP, and NLP problems. For example, fmincon and intlinprog are MATLAB's function for solving NLP and MILP problems, respectively. The toolbox includes multiple algorithms for each class of the optimization problems. More details can be found here (<https://www.mathworks.com/products/optimization.html>). MATLAB can also call external optimization solvers such as: CPLEX, Knitro, Gurobi, SDPT3, SeDuMi, Mosek and GLPK solvers.

Dedicated MATLAB-based software packages have also been developed to model and solve optimization problems. These packages have been extensively used in D-OPF problems.

- **CVX:** CVX is a MATLAB based software designed to model and solve convex optimization problems (<http://cvxr.com/cvx/>). It doesn't support modeling of general nonlinear and mixed-integer optimization problems, but a newer version supports mixed-integer disciplined convex programming (MIDCP) problems. CVX already includes SDPT3, SeDuMi solvers and supports external solvers including Gurobi, Mosek and GLPK (see <http://web.cvxr.com/cvx/doc/solver.html>).
- **YALMIP:** This is another MATLAB toolbox for modeling optimization problems. YALMIP supports efficient modeling of several classes of optimization problems including LP, MILP, SOCP, SDP, QP, MIQP, NLP (<https://yalmip.github.io/>). YALMIP relies on external solvers to solve the optimization problems. It supports the integration of many open-source and commercial optimization solver (<https://yalmip.github.io/allsolvers/>).

3.8.2 Python

Python is a high-level, general-purpose programming language, that has been extensively used for scientific computing and optimization. Multiple Python-based and open-source optimization modeling platforms have been developed that readily support many external optimization solvers.

- **CVXOPT:** CVXOPT is a Python-based free software package for modeling and solving convex optimization problems (<https://cvxopt.org/>). It interfaces to the linear programming solver in GLPK, the semidefinite programming solver in DSDP5, and the linear, quadratic and second-order cone programming solvers in MOSEK.
- **Pyomo:** Pyomo is a Python-based open-source software package that supports modeling of multiple classes of optimization problems (<http://www.pyomo.org/about>). Pyomo also supports a wide variety of solvers with specialized interfaces such as BARON, CBC, CPLEX, and Gurobi. It also has generic interfaces that support calling any solver that can read AMPL “.nl” and write “.sol” files and the ability to generate GAMS-format models and retrieve the results.
- **PuLP:** PuLP is a linear programming (LP) modeler written in Python. PuLP can generate MPS or LP files and call GLPK, COIN-OR CLP/CBC, CPLEX, GUROBI, MOSEK, XPRESS, CHOCO, MIPCL, SCIP to solve linear problems (<https://pypi.org/project/PuLP/>).
- **SciPy:** SciPy is a free and open-source Python library used for scientific computing and technical computing (<https://scipy.org/>). SciPy optimizer provides a modeling interface to define optimization problem. It includes solvers for nonlinear problems, linear programming, constrained and nonlinear least-squares, root finding, and curve fitting (<https://docs.scipy.org/doc/scipy/reference/optimize.html>).
- **gurobipy:** gurobipy is a Python interface to Gurobi and provides access to the Gurobi Optimizer, which is a mathematical optimization software library for solving mixed-integer linear and quadratic optimization problems (<https://pypi.org/project/gurobipy/>).

3.8.3 Julia and JuMP

Julia is a flexible dynamic language extensively used by the scientific and numerical computing community (<https://julialang.org/>). One can employ JuMP modeling language to model and solve optimization problems in Julia (<https://jump.dev/JuMP.jl/stable/>). JuMP currently supports multiple open-source and commercial solvers for a variety of problem classes, including linear, mixed-integer, second-order conic, semidefinite, and nonlinear programming.

3.9 Summary and Discussions

In this section, we introduced mathematical modeling of different D-OPF formulations based on nonlinear power flow models (both bus-injection and branch flow) and introduced different relaxation and approximation techniques. We also described the detailed D-OPF formulations using 5-bus test system. Note that a practically viable D-OPF algorithm should be able to obtain an optimal and feasible solution faster than the changes in distribution systems operating conditions. The added nonlinearities due to phase unbalance, mutual coupling among distribution lines, heterogeneous decision variables, and nonlinear load models make solving the D-OPF problems especially challenging.

Linear approximations scale well for large systems [18], [22], [155]; but they either ignore power losses, or assume balanced system conditions, or assume node voltages to be close to their nominal values (1 pu). These assumptions may not valid for unbalanced power distribution systems that typically under high loading conditions observe significant power losses and voltage drops [37]. Furthermore, the solutions of linearized D-OPF models are typically not feasible for the original nonlinear programming (NLP) OPF problem. One approach is to employ successive linear programming (SLP) methods where the basic idea is to solve the NLP OPF as multiple iterations of approximate linear programming (LP) problems. This simultaneously leads to a feasible and optimal solution. This approach has been explored to solve OPF for the bulk power grid [30], [151]. However, the existence of mutual coupling among the phases and the requirement for solving OPF on the

full three-phase model makes it challenging to apply the SLP algorithm in distribution OPF. It is to be noted that while the exact linearization of three-phase power flow equations, as proposed in [17], may be used to develop SLP problems, the resulting linearized power models may pose computational challenges for large feeders.

Likewise, although the proposed SDP and SOCP relaxations lead to a convex problem of reduced complexity, they may result in solutions that are infeasible for the original nonlinear power flow model. Consequently, several researchers have attempted to derive conditions that ensure the exactness of the relaxed OPF problems [47], [65], [89]. While convex relaxations for single-phase distribution systems have been found to be exact for a certain choice of objective functions and under specific conditions on the distribution system, no such guarantees exist for a three-phase unbalanced system [146]. For example, SDP relaxation has been applied to three-phase D-OPF problems [34], [50]. However, it has been reported that for three-phase distribution systems, SDP relaxation may lead to numerical stability issues [50], [149], and infeasible power flow solutions depending upon the choice of system parameters and objective functions [66], [146], [156]. More generally, the algorithms based on relaxation do not render exact solutions for the cases when the overall OPF cost function is not strictly increasing in the power injections [156]; minimizing PV curtailment is one such example [66].

As most of the relaxed problems for unbalanced D-OPF were found to be ac-infeasible, several iterative algorithms have also been proposed to obtain ac-feasible solutions [23], [58], [68], [156]. These algorithms still make use of convex optimization techniques that are computationally attractive but can simultaneously result in feasible power flow solutions. For example, in [146] the authors proposed a convex iteration technique to solve SDP relaxation for the D-OPF model that leads to a feasible and optimal solution. However, the approach does not scale well for large systems and requires additional heuristics. In [156], the authors proposed an iterative approach that starts with a feasible operating point for power flow and solves multiple iterates of convex programming problems to reach to the optimal solution. In [66], [68], the authors proposed an iterative approach where a feasible OPF solution is obtained by solving multiple iterations of relaxed-OPF problems. Scaling D-OPF

for large systems and multiple and diverse control variables in an open research problem as further outlined in Section 7.

4

Mixed-Integer D-OPF Model

4.1 Introduction

The inclusion of legacy Volt/VAr control devices (e.g., OLTC, cap banks) and network switches render the D-OPF problem mixed-integer in nature as these control devices can only take discrete (integer) states, e.g., binary ON/OFF (cap banks) or integer states, e.g., $-16, -15, \dots, 16$ (OLTCs). Since legacy controllers on distribution can only be controlled in discrete integer steps, this turns continuous D-OPF problem into a mixed-integer program (MIP). When a base non-linear power flow model is used along with the discrete control, the D-OPF becomes mixed-integer non-linear programming (MINLP) in nature. Oftentimes, the mixed-integer model of OLTCs and Cap banks are combined with linear or SOCP-based power grid model that render the D-OPF as mixed-integer linear program (MILP or MIP) or mixed-integer SOCP model (MISOCP). This section intends to provide basic modeling approaches for developing MISOCP [129] and MILP versions of the D-OPF problems.

4.2 Mixed-Integer Non-Linear Formulation

The mathematical model of the D-OPF can be concisely stated as an objective function, followed by several linear and non-linear constraints. For an arbitrary distribution network, let the nodes in that network be indexed by i and j . y_{ij} is complex admittance, for the branch between node i and node j . Shunt admittance at arbitrary node j is represented by g_j . For every line segment between node i and node j , the real power flowing from i to j be denoted by P_{ij} and reactive power by Q_{ij} , $S_{ij} = P_{ij} + \mathbf{i} Q_{ij}$. p_i and q_i denote real and reactive injections at node i . Voltage at each node is given by V_i . \underline{V}_i and \overline{V}_i are the lower and upper voltage limits on the i^{th} node. Similarly, the limits on real power are given by \underline{P}_i and \overline{P}_i , and the reactive powers are constrained by the lower limit \underline{Q}_i and upper limit \overline{Q}_i . The MINLP version of D-OPF can mathematically be stated as,

$$\underset{V, p, q}{\operatorname{argmin}} \quad f(V, p, q) \quad (4.1a)$$

$$\text{subject to : } S_{ij} = V_i (V_i^* - V_j^*) \mathbf{y}_{ij}^* \quad (4.1b)$$

$$\sum_{j:i \rightarrow j} P_{ij} = p_i \quad (4.1c)$$

$$\sum_{j:i \rightarrow j} Q_{ij} = q_i + b_i q_i^{cap} \quad (4.1d)$$

$$\underline{P}_i \leq p_i \leq \overline{P}_i \quad (4.1e)$$

$$\underline{Q}_i \leq q_i \leq \overline{Q}_i \quad (4.1f)$$

$$Q_{ij}^2 + P_{ij}^2 \leq S_{ij}^2 \quad (4.1g)$$

$$\underline{V}_i \leq |V_i| \leq \overline{V}_i \quad (4.1h)$$

$$\mathbf{y}_{ij} = f(y_{ij}, tap_{ij}) \quad (4.1i)$$

4.3 Mixed-Integer Convex Formulation

4.3.1 Modeling of Legacy Grid Devices

Branch Flow Model (BFM) [10] based SOCP formulation is adopted as the base DOPF model [46]. However, integrating the following LTC model, as shown in Figure 4.1, voltage relation (4.2) of LTCs renders the problem non-convex.

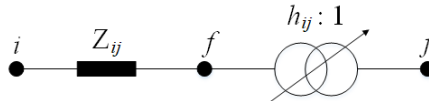


Figure 4.1: LTC model with an impedance branch and ideal LTC branch [153].

$$v_f = h_{ij}^2 v_j \quad (4.2)$$

where i, j indicate nodes on the feeder. f is fictitious node on a LTC connected between nodes i and j . v_j is squared node voltage, i.e., $v_j = |V_j|^2$. v_f is squared of voltage at the fictitious node of a LTC. $h_{ij} \in [h_{ij}^{\min}, h_{ij}^{\max}]$ represents the turn ratio. Note that LTC is modelled as an ideal LTC section with series impedance, where the series impedance of LTC is modelled similar to a feeder section in the SOCP formulation.

The relation between tap position and turns ratio can be modelled as,

$$h_{ij} = h_{ij}^{\min} + \Delta h_{ij} \text{Tap}_{ij} \quad (4.3)$$

where $\text{Tap}_{ij} \in \{0, 1, 2, \dots, D_{ij}\}$ denotes the integer tap position. D_{ij} is the total number of tap positions. Δh_{ij} is the change in turns ratio for one step change in tap position. For tap settings of -16 to +16, we represent as $\text{Tap}_{ij} \in \{0, 1, 2, \dots, 32\}$ in (4.3).

Utilizing binary expansion scheme, linear LTC model can be obtained and readily incorporated to the SOCP model [153]. Applying binary expansion to Tap_{ij} as,

$$h_{ij} = h_{ij}^{\min} + \Delta h_{ij} \sum_{n=0}^{N_{ij}} 2^n \lambda_{ij,n} \quad (4.4)$$

$$\sum_{n=0}^{N_{ij}} 2^n \lambda_{ij,n} \leq D_{ij} \quad (4.5)$$

where $\lambda_{ij,n}$ represents binary digit to represent integer tap position. Multiplying both sides of (4.4) by v_j , and replacing the bi-linear terms $v_j h_{ij} = m_{ij}$ and $\lambda_{ij,n} v_j = x_{ij,n}$ we obtain,

$$m_{ij} = h_{ij}^{\min} v_j + \Delta h_{ij} \sum_{n=0}^{N_{ij}} 2^n x_{ij,n} \quad (4.6)$$

The bi-linear term $\lambda_{ij,n} v_j = x_{ij,n}$ can be linearized using McCormick relaxation as in [134], which would require iterative bound tightening

techniques. Instead, we eliminate the need for McCormick relaxation by adopting an exact mixed-integer linear reformulation of the bi-linear term (product of a binary and a continuous variable) as,

$$0 \leq v_j - x_{ij,n} \leq (1 - \lambda_{ij,n}) M \quad (4.7)$$

$$0 \leq x_{ij,n} \leq \lambda_{ij,n} M \quad (4.8)$$

Substituting (4.4) and (4.6) in (4.2), using the bi-linear term $\lambda_{ij,n} m_{ij} = y_{ij,n}$ we obtain,

$$v_f = h_{ij}^{\min} m_{ij} + \Delta h_{ij} \sum_{n=0}^{N_{ij}} 2^n y_{ij,n} \quad (4.9)$$

similarly, using big-M the bi-linear term $\lambda_{ij,n} m_{ij} = y_{ij,n}$ can be represented using mixed-integer linear form as,

$$0 \leq m_{ij} - y_{ij,n} \leq (1 - \lambda_{ij,n}) M \quad (4.10)$$

$$0 \leq y_{ij,n} \leq \lambda_{ij,n} M \quad (4.11)$$

Integer-linear LTC model is represented by (4.6)-(4.11) utilizing auxiliary variables $m_{ij}, \lambda_{ij,n}, x_{ij,n}, y_{ij,n}$.

Switched capacitors are another legacy devices, which can be modelled in mixed-integer linear form as,

$$u_j C_j = q_j^c \quad (4.12)$$

where C_j represents VAr rating of each capacitor, whose switching operation is modelled by binary variable u_j . q_j^c denotes the reactive power injection of the capacitor.

4.3.2 Objective Functions

We have considered three objective functions that provide choices to the operator as each feeder could be operated with a different objective. The first objective function J_1 refers to total active power losses given as,

$$J_1 = \sum_{t \in \mathcal{T}, (i,j) \in \mathcal{E}} r_{ij} \ell_{ij}^t \quad (4.13)$$

where r_{ij} is line resistance, ℓ_{ij} represents the square of branch current, \mathcal{E} represents the set of all branches, and $t(\in \mathcal{T})$ denotes the time index.

We consider a multi-objective function J_2 as the combination of total active power losses and voltage deviations from the nominal values. Multi-objective function J_2 is motivated by the fact that the underlying SOCP model may be inexact for voltage deviation objective alone, and it is a common practice in SOCP formulation to combine the two terms as this improves the tightness [85].

$$J_2 = J_1 + \sum_{t \in \mathcal{T}, i \in \mathcal{N}} \Delta V_i^t \quad (4.14)$$

where $\Delta V_i^t := (v_i^t - v_i^{nom})^2$, is defined as the squared voltage deviations from the nominal value at each bus in the node set \mathcal{N} .

Since the operators may want to limit the number of LTC operations per day to reduce wear and tear, we consider a third multi-objective function J_3 which includes inter-temporal representation of the number of tap operations per day.

$$J_3 = J_2 + \sum_{t \in \mathcal{T}, (i,j) \in \mathcal{H}} \Delta X_{ij}^t \quad (4.15)$$

where $\Delta X_{ij}^t := |Tap_{ij}^t - Tap_{ij}^{t-1}|$ defines the absolute value of the tap position deviations between two consecutive time intervals for each LTC branch. \mathcal{H} is the set of LTC branches.

4.3.3 MISOCOP DOPF Model

S Three different MISOCOP DOPF models are developed based on the choice of the objective function.

Min : J_1

Subject to :

$$\text{LTC Constraints } (4.6) - (4.11) \quad \forall (i, j) \in \mathcal{H}, \forall t \in \mathcal{T} \quad (4.16)$$

$$\text{Capacitor Constraints } (11) \quad \forall j \in \mathcal{N}, \forall t \in \mathcal{T} \quad (4.17)$$

$$p_j^{q,t} - p_j^{d,t} = \sum_{k:(j,k) \in \mathcal{E}} P_{jk}^t - \sum_{i:(i,j) \in \mathcal{E}} (P_{ij}^t - r_{ij} \ell_{ij}^t) \quad \forall j \in \mathcal{N}, \forall t \in \mathcal{T} \quad (4.18)$$

$$q_j^{g,t} + q_j^{c,t} - q_j^{d,t} = \sum_{k:(j,k) \in \mathcal{E}} Q_{jk}^t - \sum_{i:(i,j) \in \mathcal{E}} (Q_{ij}^t - x_{ij}\ell_{ij}^t) \quad \forall j \in \mathcal{N}, \forall t \in \mathcal{T} \quad (4.19)$$

$$v_j^t = v_i^t - 2(r_{ij}P_{ij}^t + x_{ij}Q_{ij}^t) + ((r_{ij})^2 + (x_{ij})^2)\ell_{ij}^t \quad \forall (i,j) \in \mathcal{E} \setminus \mathcal{H}, \forall t \in \mathcal{T} \quad (4.20)$$

$$v_j^t = v_f^t - 2(r_{ij}P_{ij}^t + x_{ij}Q_{ij}^t) + ((r_{ij})^2 + (x_{ij})^2)\ell_{ij}^t \quad \forall (i,j) \in \mathcal{H}, \forall t \in \mathcal{T} \quad (4.21)$$

$$\left\| \begin{array}{l} 2P_{ij}^t \\ 2Q_{ij}^t \\ \ell_{ij}^t - v_i^t \end{array} \right\|_2 \leq \ell_{ij}^t + v_i^t \quad \forall (i,j) \in \mathcal{E}, \forall t \in \mathcal{T} \quad (4.22)$$

$$p_j^{g,t} \in [\underline{p}_j^{g,t}, \overline{p}_j^{g,t}], \quad v_j^t \in [\underline{v}_j^t, \overline{v}_j^t] \quad \forall j \in \mathcal{N}', t \in \mathcal{T} \quad (4.23)$$

$$u_i^t \in \{0, 1\}, \lambda_{ij,n}^t \in \{0, 1\} \quad \forall i \in \mathcal{N}, t \in \mathcal{T} \quad (4.24)$$

where $p_j^{g,t}$ ($q_j^{g,t}$) and $p_j^{d,t}$ ($q_j^{d,t}$) are the real (reactive) power generation and demand respectively at bus j . P_{ij}^t and Q_{ij}^t represent the sending-end real and reactive power flowing on the line (i, j) at time t . \mathcal{N}' is the set of nodes excluding the substation node. In the formulation, (4.15) represents LTC model, (4.16) represents switched capacitor constraint, real and reactive power balance equations are given by (4.17) and (4.18), voltage drop equations for line segments and LTC branches are given by (4.19) and (4.20), respectively. Second-order cone constraint are given by (4.21), which relates the node voltage and branch current with branch power flow variables. Variable bounds and integrality constraints are provided by (4.22)-(4.23).

OPF model with objective function J_2 is obtained by modifying the quadratic deviation term as second order cone constraint (4.24) as,

$$\text{Min : } J_2$$

Subject to :

Constraints (4.15) – (4.23)

$$\left\| \begin{array}{l} 2(v_i^t - v_i^{\text{nom}}) \\ \Delta \mathcal{V}_i^t - 1 \end{array} \right\|_2 \leq \Delta \mathcal{V}_i^t + 1, \quad \forall i \in \mathcal{N}', \forall t \in \mathcal{T} \quad (4.25)$$

The absolute value function of tap deviations in J_3 is modified to linear formulation using valid inequalities (4.25)-(4.27) as,

$$\text{Min : } J_3$$

Subject to :

Constraints (4.15) – (4.24)

$$\Delta \mathcal{X}_{ij}^t \geq Tap_{ij}^t - Tap_{ij}^{t-1} \quad \forall (i,j) \in \mathcal{H}, \forall t \in \mathcal{T} \quad (4.26)$$

$$\Delta \mathcal{X}_{ij}^t \geq Tap_{ij}^{t-1} - Tap_{ij}^t \quad \forall (i,j) \in \mathcal{H}, \forall t \in \mathcal{T} \quad (4.27)$$

$$\Delta \mathcal{X}_{ij}^t \geq 0, \quad \forall (i,j) \in \mathcal{H}, \forall t \in \mathcal{T} \quad (4.28)$$

4.3.4 Mixed-Integer Linear Formulation

DOPF formulation using *LinDist3FLow* model is given by (4.29)-(4.37), where the objective function is defined as total generation minimization.

$$\text{Min : } \sum_{t \in \mathcal{T}} \sum_{i \in \mathcal{N}} \sum_{\phi \in \Phi_i} p_{g,i}^\phi \quad (4.29)$$

Subject to :

$$p_{g,j}^{\phi,t} - p_{d,j}^{\phi,t} = \sum_{k:(j,k) \in \mathcal{E}} P_{jk}^{\phi,t} - \sum_{i:(i,j) \in \mathcal{E}} P_{ij}^{\phi,t}, \quad \forall j \in \mathcal{N}, \forall \phi \in \Phi_j, \forall t \in \mathcal{T} \quad (4.30)$$

$$q_{g,j}^{\phi,t} + q_{c,j}^{\phi,t} - q_{d,j}^{\phi,t} = \sum_{k:(j,k) \in \mathcal{E}} Q_{jk}^{\phi,t} - \sum_{i:(i,j) \in \mathcal{E}} Q_{ij}^{\phi,t}, \quad \forall j \in \mathcal{N}, \forall \phi \in \Phi_j, \forall t \in \mathcal{T} \quad (4.31)$$

$$v_j^{\phi,t} = v_i^{\phi,t} - \sum_{\gamma \in \Phi_{ij}} \mathbb{H}_{ij}^P(\phi, \gamma) P_{ij}^{\gamma,t} - \sum_{\gamma \in \Phi_{ij}} \mathbb{H}_{ij}^Q(\phi, \gamma) Q_{ij}^{\gamma,t}, \\ \forall (i,j) \in \mathcal{E} \setminus \mathcal{H}, \forall \phi \in \Phi_{ij}, \forall t \in \mathcal{T} \quad (4.32)$$

$$v_{f_{ij}}^{\phi,t} = v_i^{\phi,t} - \sum_{\gamma \in \Phi_{ij}} \mathbb{H}_{ij}^P(\phi, \gamma) P_{ij}^{\gamma,t} - \sum_{\gamma \in \Phi_{ij}} \mathbb{H}_{ij}^Q(\phi, \gamma) Q_{ij}^{\gamma,t}, \\ \forall (i,j) \in \mathcal{H}, \forall \phi \in \Phi_{ij}, \forall t \in \mathcal{T} \quad (4.33)$$

$$\text{LTC Model}(i, j, \phi, t), \quad \forall (i,j) \in \mathcal{H}, \forall \phi \in \Phi_{ij}, \forall t \in \mathcal{T} \quad (4.34)$$

$$0 \leq p_{g,j}^{\phi,t} \leq \overline{p}_{g,j}^{\phi,t}, \quad \forall j \in \mathcal{N}_{\text{PV}}, \forall \phi \in \Phi_j, \forall t \in \mathcal{T} \quad (4.35)$$

$$\underline{q}_{g,j}^{\phi,t} \leq p_{g,j}^{\phi,t} \leq \overline{q}_{g,j}^{\phi,t}, \quad \forall j \in \mathcal{N}_{\text{PV}}, \forall \phi \in \Phi_j, \forall t \in \mathcal{T} \quad (4.36)$$

$$p_{g,j}^{\phi,t} \in [\underline{p}_{g,j}^{\phi,t}, \bar{p}_{g,j}^{\phi,t}], q_{g,j}^{\phi,t} \in [\underline{q}_{g,j}^{\phi,t}, \bar{q}_{g,j}^{\phi,t}], v_j^{\phi,t} \in [\underline{v}_j^t, \bar{v}_j^{\phi,t}], \\ \forall j \in \mathcal{N}', \forall \phi \in \Phi_j, t \in \mathcal{T} \quad (4.37)$$

4.4 Performance of MISOCP DOPF Formulation

Simulations are carried out using one phase of the IEEE 123-node feeder. Loads are modelled as constant power loads, shunt capacitors on the original network are considered to have on/off capability, and 15 PV generators are added to the network as shown in Figure 4.2, which operate at unity power factor mode. Delta connected loads are converted to wye type for modeling convenience. We used 6-bit of binary representation for 33 tap positions. A Macintosh machine with core-i5 2.9 GHz processor and 8 GB of RAM is used, and Gurobi is chosen as an optimization solver. Simulations are run with 15-minute time intervals for an entire day, hence, 96 intervals in total. LTC settings, Cap bank settings, and active power dispatch of PV are used as decision variables.

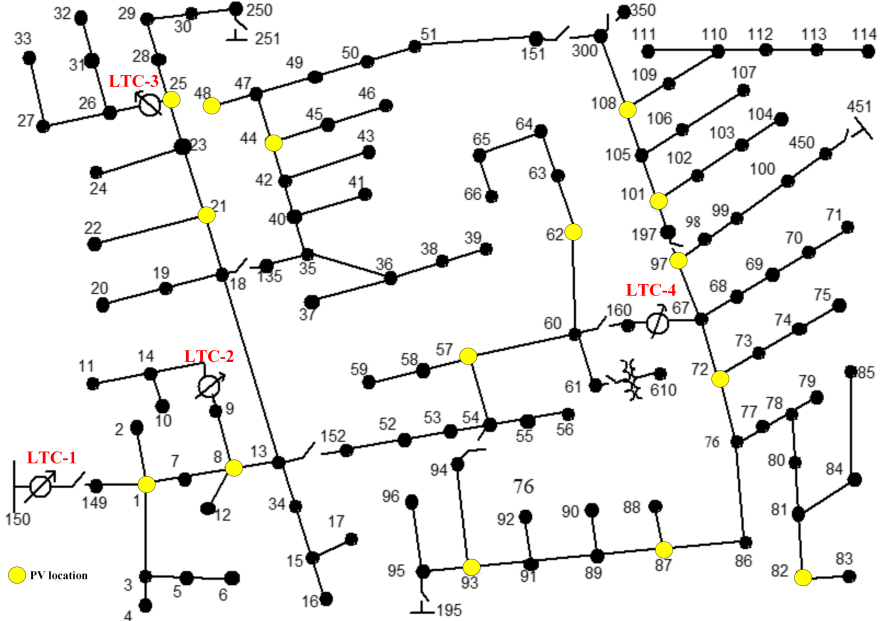


Figure 4.2: Single-line diagram of the modified IEEE 123-node feeder.

Objective functions J_1 and J_2 are tested for the single period operation with an optimality gap of 0.01%, and setting M to 10^{10} . As intuitively expected, J_1 yields lower active power losses compared to multi-objective function J_2 as shown in Figure 4.3. However, as can be seen from Figure 4.4, the distribution of node voltages with J_1 has larger standard deviation (0.01 p.u.) compared to that of J_2 (0.0053 p.u.); thus, J_2 can provide narrower min. and max. distribution of nodal voltages and is better suited for voltage positioning applications without degrading loss reduction impact.

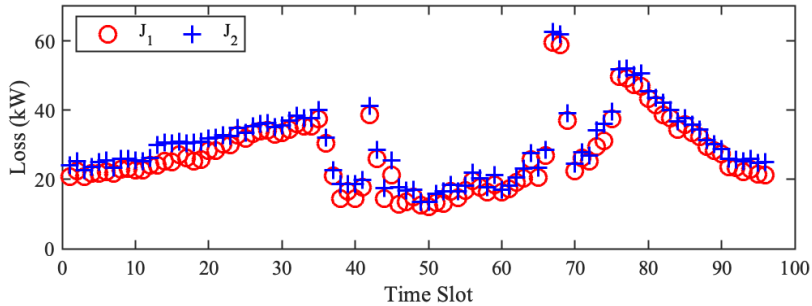


Figure 4.3: Active power losses with J_1 and J_2 for 24 hours (15-min res.).

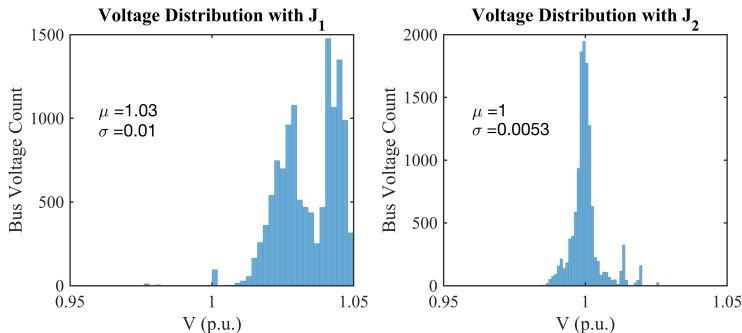


Figure 4.4: Voltage histograms for objective functions J_1 and J_2 .

Figure 4.5 shows the daily power supplied by the grid and PV generators. It can be observed that J_2 leads to 4.8% more PV energy curtailment compared to J_1 . Note that the energy curtailment with objective J_2 depends on the weight of each objective terms.

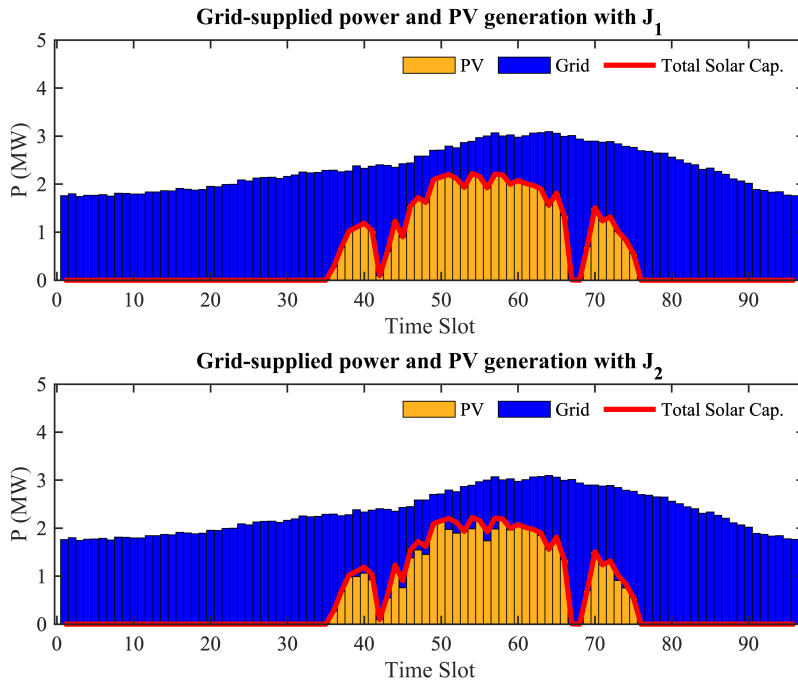


Figure 4.5: Grid and PV power with J_1 and J_2 for 24 hours (15-min res.).

Table 4.1 summarizes the total number of tap operations per day with J_1 and J_2 as an objective. The number of tap operations are calculated using $\sum |Tap^t - Tap^{t-1}|$ for each LTC over the daily operation window based on sequential run of single-period DOPF models. J_2 results in 60 total number of tap operations, while J_1 results in 259 tap operations. The average computation times (wall-clock) over 96-time intervals are 0.87 s. and 1.75 s for J_1 and J_2 , respectively, which are very efficient for single-period optimization.

Table 4.1: Number of tap changes for different objective functions

Obj	LTC-1	LTC-2	LTC-3	LTC-4	Total Tap Changes
J_1	0	72	125	62	259
J_2	10	12	14	24	60

4.5 Performance of MILP DOPF Formulation

The MILP DOPF formulation is tested on a 2500-node three-phase distribution feeder (see Figure 4.6), which is obtained by modifying the original IEEE 8500-node test feeder. Five OLTCs are added as the controllable assets, which are controlled in discrete steps (thus modeled as integer variables). The MILP model was successfully solved using off-the-shelf Gurobi solver for the large scale test feeder. Figure 4.7 shows the optimal tap settings of the OLTCs obtained at 15 minute intervals for an entire day of simulation. Figure 4.8 shows the voltage profile on each phase of the feeder. The solve time of DOPF for each interval was less than 1 minute.

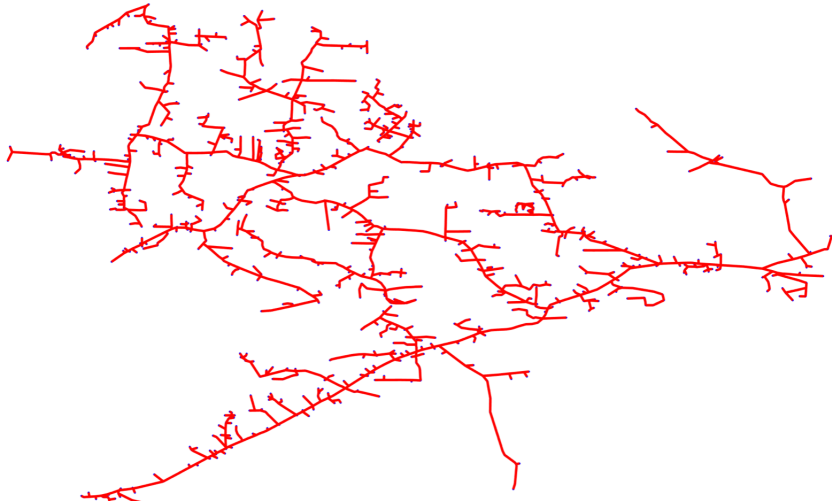


Figure 4.6: A 2522-node test system obtained by modifying the IEEE 8500-node test system.

4.6 Summary and Discussion

As seen in the problem formulation in this section, the discrete control makes the D-OPF mixed-integer in nature. This is the most difficult class of D-OPF problem to solve. Depending on the choice of base grid model, and with the inclusion of mixed-integer constraints for OLTC,

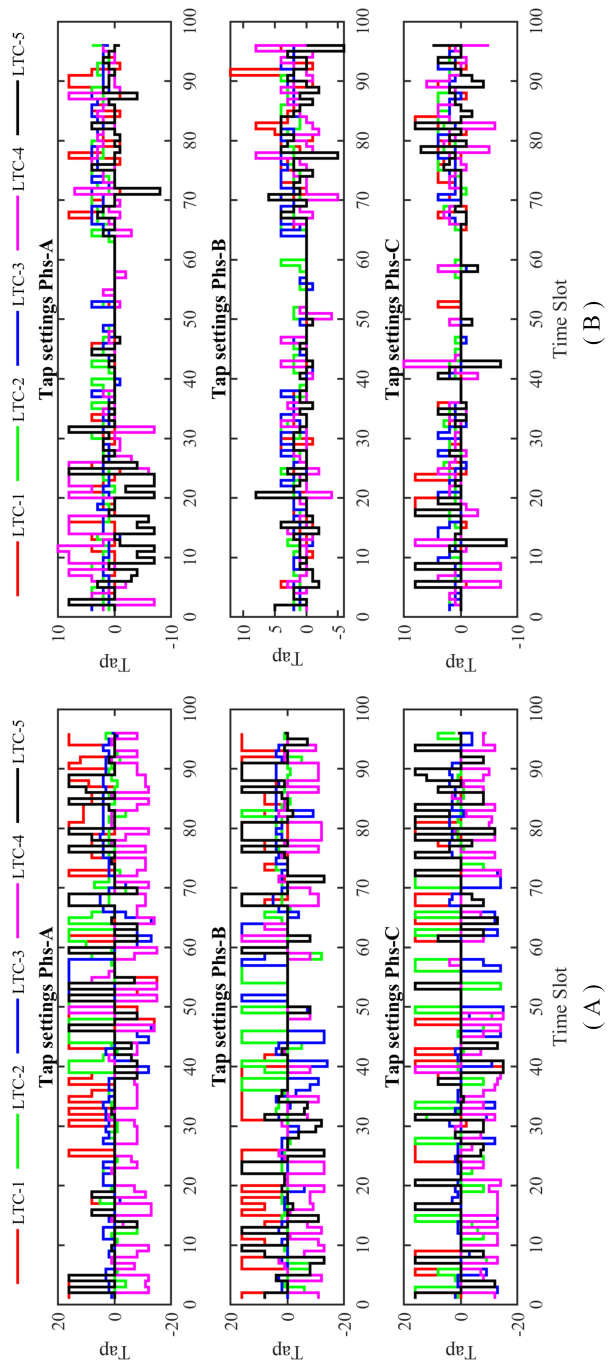


Figure 4.7: Change of five LTC taps A) with J_1 as an objective, and B) with J_2 as an objective.

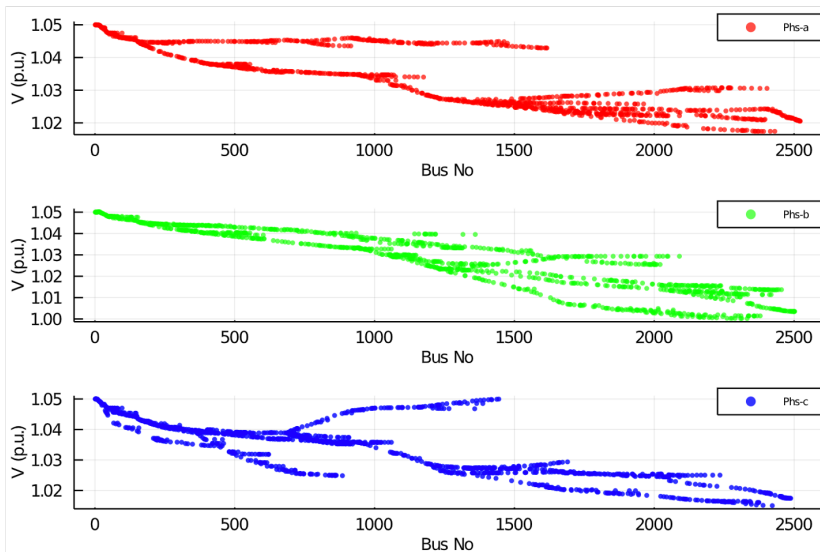


Figure 4.8: Feeder voltage profile with obtained from SOCP model.

cap bank, and network switches, the D-OPF could lead to MINLP, MILP, MISOCP, and MISDP problems. Among these, MINLP is the most accurate but most difficult to solve. However, their applications are unavoidable in distribution grid volt/var management and reconfiguration problems. The performance and accuracy of these models on the large-scale distribution grids depends on the choice of underlying grid models used in those methods, state-of-the-art methods in solving mixed integer problems, and the implementation of such methods in the off-the-shelf mixed-integer solvers. MILP solvers being mature technology, the MILP models are better tractable.

To gain the computational tractability for mixed-integer D-OPF problem, integer variables are often relaxed in [15], [36], [108], [123] and rounding heuristics are used in [36], [108]. A linear grid model is used in [99] to reduce computational complexity, which renders the D-OPF as a MILP problem. In [84], [134], [153], computational efficiency of second-order cone programming (SOCP) is leveraged. Similarly, in [3] integer LTC variables are added to a Semi-definite Programming (SDP) OPF which makes the resulting problem mixed-integer SDP (MISDP).

5

Distribution Voltage Control: Conservation Voltage Reduction

Most of the operational problems at the distribution system level require coordination of the grid's voltage control devices (voltage regulators, capacitor banks, smart inverters, etc.) to meet a specific system-level objective. In this section, we select a specific operational problem for the power distribution system, namely conservation voltage reduction (CVR) that uses Volt/VAR optimization (VVO) methods to reduce customer power consumption. The benefits of voltage control to energy savings are realized due to the sensitivity of customer loads to service voltages where decreasing the voltage helps to reduce the demand [49]. A study by PNNL shows that implementing conservation voltage reduction in all the distribution feeder in the US will cause a total reduction in energy consumption by 3% [132]. Traditionally, CVR is accomplished by controlling the feeder's legacy voltage control devices such as capacitor banks, load tap changers, and voltage regulators using Volt-VAR control (VVC) techniques. The feeder is operated at a lower service voltage range while still maintaining the service voltages within the recommended ANSI voltage limits (0.95 - 1.05 pu). Since most DERs are equipped with smart inverters that can absorb and supply reactive power, they can be used to control feeder voltages locally that can help

achieve additional CVR benefits [21]. This section introduces a D-OPF formulation to optimally manage the grid's all voltage control devices, including legacy devices (capacitor banks, voltage regulators) and new devices (smart inverters), can help achieve higher CVR benefits.

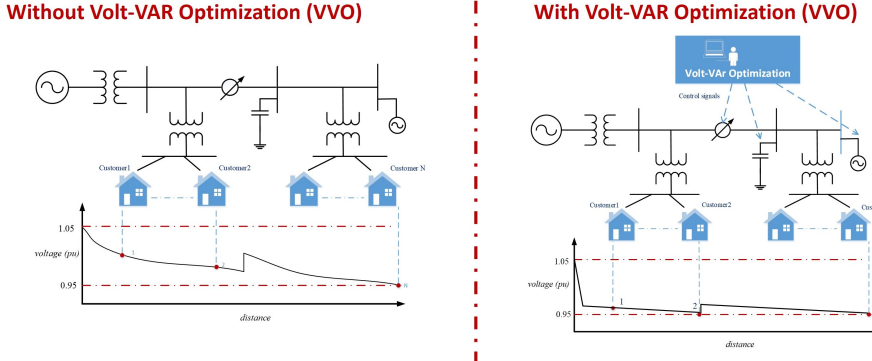


Figure 5.1: Feeder voltage profile with and without Volt-VAR Optimization for Conservation Voltage Reduction (CVR).

In literature, several Volt-VAR Control (VVC) methods have been proposed: 1) by employing autonomous or rule-based approach, 2) using end-of-line measurements, and 3) using integrated Volt/VAR control (IVVC) based on real-time measurements [12], [59], [103]. Several commercial VVC products are also available that perform IVVC function mostly using heuristic [55]. They primarily optimize the operation of legacy control devices. Several researchers have worked on optimizing the reactive power dispatch from DERs and have proposed methods for smart inverter control using: 1) autonomous control, 2) distributed control, and 3) centralized control [35], [47], [71], [122], [135], [161]. Maximizing CVR benefits require methods that can coordinate the system's legacy devices that introduce discrete decision variables, along with the new devices with continuous control set-points in a computationally tractable manner for an unbalanced distribution system. In this section, we discuss the use of optimization methods to help orchestrate the feeder-level voltage control devices, both legacy and new devices, to maximize the CVR benefits.

5.1 Optimization Problem Formulation

The problem objective is to minimize the substation power flow subject to network operating constraints. The variable notations are stated below. A radial distribution system can be represented as a directed graph $\mathcal{G} = (\mathcal{N}, \mathcal{E})$ where \mathcal{N} denotes set of buses and \mathcal{E} denotes set of edges. An edge (i, j) joins two adjacent nodes i and j where i is the parent node for node j . The three phase $\{a, b, c\}$ for a node i in the distribution system is denoted by $\Phi_i \subseteq \{a, b, c\}$. For each bus $i \in \mathcal{N}$ and phase ψ , let V_i^ψ , $s_{L,i}^\psi$, and $s_{DG,i}^\psi$ be complex voltage, complex power demand and complex DG power generation, respectively. Let, $V_i := [V_i^\psi]_{\psi \in \Phi_i}$, $s_{L,i} := [s_{L,i}^\psi]_{\psi \in \Phi_i}$ and $s_{DG,i} := [s_{DG,i}^\psi]_{\psi \in \Phi_i}$. For each line, let ψ phase current be I_{ij}^ψ and define, $I_{ij} := [I_{ij}^\psi]_{\psi \in (\Phi_i \cap \Phi_j)}$. Let z_{ij} be the phase impedance matrix.

5.1.1 Problem Objective

The objective is to reduce power demand for the feeder. This can be simply achieved by minimizing the power flow from the substation, as defined in (5.1).

$$\min \sum_{\psi \in \{a,b,c\}} \text{real}(S_{12}^\psi) \quad (5.1)$$

5.1.2 Problem Constraints

The problem constraints include power flow model, device models, and system and device operating constraints.

Power Flow Constraints

We employ branch power flow model to describe power flow constraints. Both nonlinear and three-phase lindistflow models are detailed below.

Branch-flow Nonlinear Model

$$V_j = V_i - Z_{ij} I_{ij} \quad (5.2)$$

$$\text{diag}(S_{ij} - z_{ij} I_{ij}) = \sum_{k:j \rightarrow k} \text{diag}(S_{jk}) + s_{L,j} - s_{DG,j} \quad (5.3)$$

$$S_{ij} = V_i I_{ij}^H \quad (5.4)$$

Three-phase LinDistFlow Model

$$v_i^\psi = v_j^\psi + \sum_{\phi \in \Phi_j} 2R \left(\gamma^{\psi\phi} S_{ij}^{\phi\phi} (z_{ij}^{\psi\phi})^T \right) \quad \forall \psi \in \Phi_i \quad (5.5)$$

$$P_{ij}^{\psi\psi} = \sum_{k:j \rightarrow k} P_{jk}^{\psi\psi} + p_{L,j} - p_{DG,j} \quad \forall \psi \in (\Phi_i \cap \Phi_j) \quad (5.6)$$

$$Q_{ij}^{\psi\psi} = \sum_{k:j \rightarrow k} Q_{jk}^{\psi\psi} + q_{L,j} - q_{DG,j} \quad \forall \psi \in (\Phi_i \cap \Phi_j) \quad (5.7)$$

$$\gamma = \begin{bmatrix} 1 & \alpha & \alpha^2 \\ \alpha^2 & 1 & \alpha \\ \alpha & \alpha^2 & 1 \end{bmatrix} \quad (5.8)$$

Voltage-dependent Load Model

The most widely used load model is the ZIP model which is a combination of constant impedance (Z), constant current (I) and constant power (P) characteristics of the load [20]. The mathematical representation of the ZIP model for the load connected at phase ψ of bus i is given by (5.9)-(5.10). The ZIP load model represented in (5.9)-(5.10) is a function of both V_i^ψ and $v_i^\psi = (V_i^\psi)^2$.

$$p_{L,i}^\psi = p_{i,0}^\psi \left[k_{p,1} \left(\frac{V_i^\psi}{V_0} \right)^2 + k_{p,2} \left(\frac{V_i^\psi}{V_0} \right) + k_{p,3} \right] \quad (5.9)$$

$$q_{L,i}^\psi = q_{i,0}^\psi \left[k_{q,1} \left(\frac{V_i^\psi}{V_0} \right)^2 + k_{q,2} \left(\frac{V_i^\psi}{V_0} \right) + k_{q,3} \right] \quad (5.10)$$

where, $k_{p,1} + k_{p,2} + k_{p,3} = 1$, $k_{q,1} + k_{q,2} + k_{q,3} = 1$, $p_{i,0}^\psi$ and $q_{i,0}^\psi$ are per-phase load consumption at nominal voltage, V_0 .

Here we introduce an equivalent load model for voltage-dependent loads using the definition of CVR factors. We also detail an equivalence between the ZIP parameters and the CVR factors. This model is linear in v_i^ψ and hence can be easily used with LinDistFlow power flow model [69].

CVR factor is defined as the ratio of percentage reduction in active or reactive power to the percentage reduction in bus voltage. Let CVR

factor for active and reactive power reduction be CVR_p , and CVR_q , respectively defined in (5.11).

$$CVR_p = \frac{dp_{L,i}^\psi}{p_{i,0}^\psi} \frac{V_0}{dV_i^\psi} \text{ and } CVR_q = \frac{dq_{L,i}^\psi}{q_{i,0}^\psi} \frac{V_0}{dV_i^\psi} \quad (5.11)$$

where, $p_{L,i}^\psi = p_{i,0}^\psi + dp_i^\psi$ and $q_{L,i}^\psi = q_{i,0}^\psi + dq_i^\psi$. Furthermore, $v_i^\psi = (V_i^\psi)^2$. Therefore, $dv_i^\psi = 2V_i^\psi dV_i^\psi$. Assuming $V_i^\psi \approx V_0$ and $dv_i^\psi = v_i^\psi - (V_0)^2$, we obtain:

$$p_{L,i}^\psi = p_{i,0}^\psi + CVR_p \frac{p_{i,0}^\psi}{2} \left(\frac{v_i^\psi}{V_0^2} - 1 \right) \quad (5.12)$$

$$q_{L,i}^\psi = q_{i,0}^\psi + CVR_q \frac{q_{i,0}^\psi}{2} \left(\frac{v_i^\psi}{V_0^2} - 1 \right) \quad (5.13)$$

Note that the CVR based load model detailed in (5.12) and (5.13) is linear in v_i^ψ , thus can be easily included in approximate power flow equations. The CVR factors, CVR_p and CVR_q are estimated from the ZIP coefficients of the load. On differentiating the ZIP model detailed and assuming $V_0 = 1$ p.u., we obtain:

$$\frac{dp_{L,i}^\psi}{dV_i^\psi} = p_{i,0}^\psi \left(2k_{p,1}V_i^\psi + k_{p,2} \right) \quad (5.14)$$

$$\frac{dq_{L,i}^\psi}{dV_i^\psi} = q_{i,0}^\psi \left(2k_{q,1}V_i^\psi + k_{q,2} \right) \quad (5.15)$$

Using (5.11), (5.14), (5.15) and assuming $V_i^\psi \approx V_0$, we obtain (5.16). Using (5.16), the CVR factors for customer loads can be obtained from the ZIP coefficients.

$$CVR_p = 2k_{p,1} + k_{p,2} \text{ and } CVR_q = 2k_{q,1} + k_{q,2} \quad (5.16)$$

Voltage Regulator and Capacitor Banks Models

A 32-step voltage regulator with a voltage regulation range of $\pm 10\%$ is assumed. The series and shunt impedance of the voltage regulator are ignored as these have very small value [72]. Let, a^ψ be the turn

ratio for the voltage regulator connected to phase ψ of line (i, j) . Then a^ψ can take values between 0.9 to 1.1 with each step resulting in a change of 0.00625 pu. An additional node i' is introduced to model the current equations. The control for regulator is defined using binary variables. Let, for $u_{tap,i}^\psi \in \{0, 1\}$ be a binary variable defined for each regulator step position i.e. $i \in (1, 2, \dots, 32)$. Also, define a vector $b_i \in \{0.9, 0.90625, \dots, 1.1\}$. Then V_i^ψ , V_j^ψ , $I_{ii'}^\psi$, and $I_{i'j}^\psi$ where $\psi \in \Phi_i \cap \Phi_j$ are given as follows:

$$V_j^\psi = V_{i'}^\psi = a^\psi V_i^\psi \text{ and } I_{ii'}^\psi = a^\psi I_{i'j}^\psi \quad (5.17)$$

$$\text{where, } a^\psi = \sum_{i=1}^{32} b_i u_{tap,i}^\psi \text{ and } \sum_{i=1}^{32} u_{tap,i}^\psi = 1.$$

We also express (5.17) as a function of $v_i^\psi = (V_i^\psi)^2$, $v_j^\psi = (V_j^\psi)^2$, $l_{ii'}^{\psi\psi} = (I_{ii'}^\psi)^2$, and $l_{i'j}^{\psi\psi} = (I_{i'j}^\psi)^2$. Take square of (5.17) and define $a_p^2 = A_p$ and $b_i^2 = B_i$. Further realizing that $(u_{tap,i}^\psi)^2 = u_{tap,i}^\psi$, (5.17) can be reformulated as (5.18).

$$v_j^\psi = A^\psi \times v_i^\psi \text{ and } l_{ii'}^{\psi\psi} = A^\psi l_{i'j}^{\psi\psi} \quad (5.18)$$

Next, we detail the per-phase model for capacitor banks. The reactive power generated by capacitor bank, $q_{cap,i}^\psi$, is defined as a function of binary control variable $u_{cap,i}^\psi \in \{0, 1\}$ indicating the status (ON/OFF) of the capacitor bank, its rated per-phase reactive power $q_{cap,i}^{rated,\psi}$, and the square of the bus voltage at bus i for phase ψ , v_i^ψ .

$$q_{cap,i}^\psi = u_{cap,i}^\psi q_{cap,i}^{rated,\psi} v_i^\psi \quad (5.19)$$

The capacitor bank model is assumed to be voltage dependent and provides reactive power as a function of v_i^ψ when connected, i.e. $u_{cap,i} = 1$. For a three-phase capacitor bank, a common control variable, $u_{cap,i}^\psi$, is assumed for each phase.

Distributed Generation with Smart Inverters

A per-phase model for reactive power support from smart inverter connected to DGs is developed. The DGs are modeled as negative loads with a known active power generation equal to the forecasted value.

The reactive power support from DG depend upon the rating of the smart inverter. Let, the rated per-phase apparent power capacity for smart inverter connected to i^{th} DG be $s_{DG,i}^{rated,\psi}$ and the forecasted active power generation be $p_{DG,i}^\psi$. The available reactive power, $q_{DG,i}^\psi$ from the smart inverter is given by (5.20) which is a box constraint.

$$-\sqrt{(s_{DG,i}^{rated,\psi})^2 - (p_{DG,i}^\psi)^2} \leq q_{DG,i}^\psi \leq \sqrt{(s_{DG,i}^{rated,\psi})^2 - (p_{DG,i}^\psi)^2} \quad (5.20)$$

Network Operating Constraints

For Nonlinear OPF problem:

$$V_{min}^2 \leq (V_i^{re})^2 + (V_i^{im})^2 \leq V_{max}^2 \quad (5.21)$$

$$(I_{ij}^{re})^2 + (I_{ij}^{im})^2 \leq (I_{ij}^{rated})^2 \quad (5.22)$$

For LinDistFFlow OPF problem: we define voltage limits using square of the per-phase voltages.

$$V_{min}^2 \leq v_i^\psi \leq V_{max}^2 \quad (5.23)$$

We use the polygon-based linearization approach proposed in [2] to linearize line thermal limit constraint as a set of linear constraints defined in (6.10).

$$\begin{aligned} -\sqrt{3} (\mathbf{P}_{ij} + \mathbf{S}_{ij}) &\leq \mathbf{Q}_{ij} \leq -\sqrt{3} (\mathbf{P}_{ij} - \mathbf{S}_{ij}) \\ -\sqrt{3}/2 \mathbf{S}_{ij} &\leq \mathbf{Q}_{ij} \leq \sqrt{3}/2 \mathbf{S}_{ij} \\ \sqrt{3} (\mathbf{P}_{ij} - \mathbf{S}_{ij}) &\leq \mathbf{Q}_{ij} \leq \sqrt{3} (\mathbf{P}_{ij} + \mathbf{S}_{ij}) \end{aligned} \quad (5.24)$$

where, $\mathbf{S}_{ij} = \mathbf{S}_{ij}^{rated} \sqrt{(2\pi/n)/\sin(2\pi/n)}$ and $n = 6$.

5.1.3 Overall Problem

The overall CVR optimization problem is defined as the following:

Status of voltage control devices

Minimize: $\sum_{\psi \in \{a,b,c\}} real(S_{12}^{\psi})$

Subject to: (5.2) - (5.4), (5.9), (5.10), (5.17), (5.19), (5.20)-(5.22).

Note that the resulting optimization problem is a Mixed-Integer Nonlinear Programming problem (MINLP). The MINLP problems are hard to solve and do not scale well for larger systems (as also discussed in Section 4). Commercial solvers have been demonstrated to solve small-scale feeder (≈ 100 nodes) with few OLTC devices. Therefore, to reduce the complexity and ensure scalability, we use a two-stage approach by decomposing the problem into MILP (Stage 1) and NLP (Stage 2). Another approach could be to convexify the “continuous part” of the problem to obtain MI convex models (e.g., MISCOP, MISDP). These models scale better compared to their MINLP counterparts. However, additional feasibility evaluations are needed to ensure that the relaxed solutions are power flow feasible (see additional discussions in Section 4).

5.2 Solution Approach

We decompose the original MINLP problem into two relatively simpler problems: MILP and NLP, see [69] for additional details.

1. Stage 1 (MILP Formulation): Develops a 5-min/15-min schedule for legacy devices and smart inverter reactive power demand set-points with the objective of minimizing active power consumption for the feeder based on a MILP formulation. This is a coarse timescale operation and is employed to dispatch discrete control assets (voltage regulator and capacitor banks).

Status of voltage regulator ($u_{tap,i}^\psi$) and capacitor bank ($u_{cap,i}^\psi$)

Minimize: $\sum_{\psi \in \{a,b,c\}} real(S_{12}^\psi)$

Subject to: (5.5) - (5.8), (5.12), (5.13), (5.18), (5.19), (5.20), (5.23), (5.24).

2. Stage 2 (NLP Formulation): Develops a revised fine time-scale schedule for smart inverter control using a NLP formulation. It also corrects any errors due to Stage-1 approximations. Stage-1 uses a linear three-phase power flow model that approximates the losses. The solutions although feasible for linear power flow formulation, may violate the critical operating constraints of the feeder. The objective of this stage is to adjust the set-points of smart inverter control variables in order to obtain an optimal and feasible three-phase nonlinear power flow solution. The discrete control variables, $u_{tap,i}^\psi$, $u_{cap,i}^\psi$, are assumed to be fixed as obtained in Stage-1. The optimal control set points for reactive power dispatch from smart inverters are obtained by solving the NLP problem (with linear objective and quadratic constraints) defined below.

Optimal DG reactive power dispatch, q_{DG}^ψ .

Fix voltage regulator ($u_{tap,i}^\psi$) and capacitor bank ($u_{cap,i}^\psi$) positions based on Stage-1 solutions.

Minimize: $\sum_{\psi \in \{a,b,c\}} real(S_{12}^\psi)$

Subject to: (5.2) - (5.4), (5.9), (5.10), (5.17), (5.19), (5.20)-(5.22).

5.3 Large-feeder Simulation Results

In what follows, we demonstrate the proposed VVO approach using standard test feeders: IEEE 123-bus [131], and PNNL R3-12.47-2 test feeder [133]. All simulations are done on MATLAB platform. Stage-1 problem, modeled as MILP, is solved using CPLEX 12.7 and Stage-2 problem, modeled as NLP, is solved using fmincon function in MATLAB optimization toolbox. A computer with core i7 3.41 GHz processor with 16 GB of RAM is used for the simulations. The results obtained from MATLAB are validated against OpenDSS. For additional discussions, also refer to [69].

IEEE-123 bus feeder is a standard test feeder used for OPF analysis for unbalanced loading conditions. It includes several single-phase lines and loads with voltage drop problems making it a good candidate for demonstration of VVO application. There are four voltage regulators and four capacitor banks deployed along the feeder as shown in Figure 5.2. The feeder is modified to include three DGs of capacity 345 kVA, 345 kVA, and 690 kVA at nodes 35, 52, and 97 respectively (see Figure 5.2). The R3-12.47-2 test feeder is used to demonstrate the scalability of the proposed approach. Notice that R3-12.47-2 feeder includes 329 physical nodes and a total of 860 single-phase nodes. Compared to the state-of-art, this is a significantly large test system to demonstrate the coordinated control of all voltage control devices. The feeder includes one voltage regulator, one 600 kVAr three-phase capacitor bank, three 100 kVAr single-phase capacitor banks, and three DGs of capacity 23kVA, 57.5kVA and 115kVA (see Figure 5.3).

Customer loads are assumed to have a CVR factor of 0.6 for active power and 3 for reactive power [49]. Note that the CVR values are arbitrary and can be easily adjusted based on the parameters for ZIP model of the load, if available, as detailed in the previous section. To demonstrate the applicability of the proposed approach for different load mix, additional cases are simulated using a combination of residential and small and large commercial loads. The daily load and generation profiles are simulated in 15-min intervals and are based on example profiles provided in OpenDSS (see Figure 5.4).

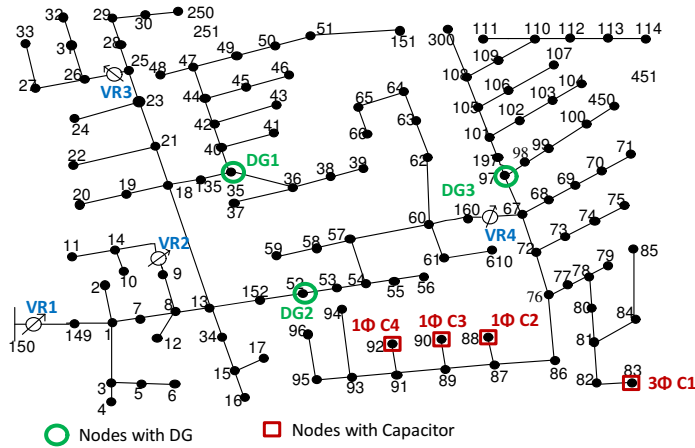


Figure 5.2: IEEE 123-bus distribution test feeder.

Device	Node	Size
C-1	178	600 kVar
C-2	140	100 kVar
C-3	12	100 kVar
C-4	183	100 kVar
DG-1	111	23kW
DG-2	35	57.5kW
DG-3	24	115kW

○ Node with DG
□ Node with Capacitor

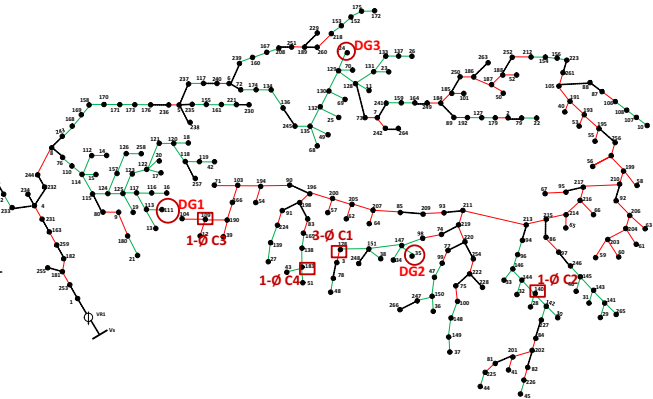


Figure 5.3: Modified R3-12.47-2 feeder.

5.3.1 Validation of CVR-based Load Model

The CVR-based voltage dependent load model introduced in this section in equations (5.12)-(5.13) is validated against an equivalent ZIP load model detailed in equations (5.9)-(5.10). The CVR-based load model should incur the same power demand as the equivalent ZIP load model for the acceptable range of operating voltages (0.95-1.05 pu). To validate the load models, the active and reactive power consumption for CVR-based load models are compared against the power consumption for

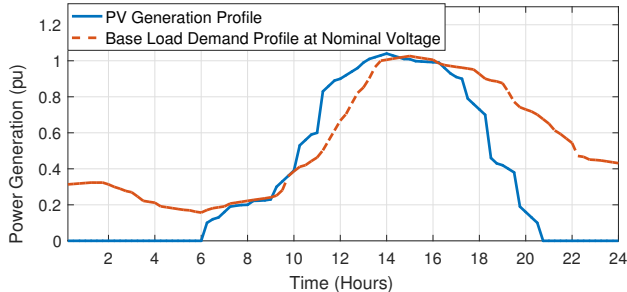


Figure 5.4: Load demand and PV generation in 15-min interval.

ZIP load model for varying node voltages. ZIP models for residential, small commercial, and large commercial loads are used for validation. The ZIP coefficients for the different class of loads are obtained from [20] and converted to CVR-based load model using (5.16) (see Table 5.1).

Table 5.1: ZIP coefficients for different class of loads.

Load Class	Z_p	I_p	P_p	Z_q	I_q	Q_q	CVR_p	CVR_q
Residential	0.96	-1.17	1.21	6.28	-10.16	4.88	0.75	2.4
Small Commercial	0.77	-0.84	1.07	8.09	-13.65	6.56	0.7	2.53
Large Commercial	0.4	-0.41	1.01	4.43	-7.99	4.56	0.39	0.87

The simulation details are included here. For each load class, the base active $p_{i,0}$ and $q_{i,0}$ reactive power are assumed to be 100 kW and 100 kVAr, respectively at voltage of 1 pu. The voltage at the load node is then varied from 0.95 to 1.05 pu. The active and reactive power demand for the three load classes are shown in Figure 5.5. It can be observed that for different load classes, the variation in power demand, both active and reactive, due to change in bus voltage are similar for both CVR-based load model and equivalent ZIP load model. This validates that CVR-based load models are reasonably accurate when modeling voltage dependent loads.

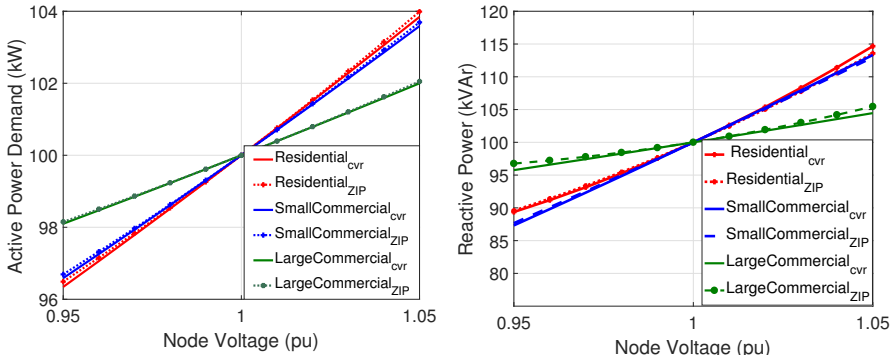


Figure 5.5: Comparison of proposed load model with ZIP model: (a) Active power demand, (b) Reactive power demand [69].

IEEE 123-bus test system

The two-stage approach detailed in Section 5.2 is validated using the IEEE 123-node system. The VVO control is run for 1 day at 15-min time intervals. The results are shown Tables 5.2 and 5.3. The optimal statuses for all voltage regulation devices per the optimization program for both minimum and maximum loading conditions are detailed in Table 5.2. The voltage regulator 1, located at the substation (see Figure 5.2), has the following optimal setting: –13 tap at minimum load and –8 tap at maximum load conditions. The voltage regulator 4 is always at tap 0. Voltage regulators 2 and 3 are single and two-phase devices, respectively, and their tap settings vary as per the loading conditions. Cap1 is a three-phase device and is OFF during minimum loading and ON at maximum loading conditions. Cap2, Cap3, and Cap4 are single-phase devices and their ON/OFF statuses vary as per the variation in loading conditions. The DGs are located at three-phase nodes (see Figure 5.2). The reactive power demand or generation for DG1 does not change significantly for either loading condition. DG3, on the other hand, absorbs reactive power in Phase B during the maximum load condition; it has a similar pattern for phases A and C for either loading condition. Since Reg3 does not change the tap position, Phase B of DG3 adjusts the set points to account for the increase in load. Similarly, since there is no other VVC device between Reg1 and DG2, there is

a significant change in optimal dispatch for DG2 for the two loading conditions. The feeder voltage characteristics are also shown in Table 5.3. On average, the feeder operates close to the minimum voltage limit for both load conditions.

Table 5.2: VVO for IEEE 123-bus ($CVR_p = 0.6$ and $CVR_q = 3$) [69]

IEEE-123 Phase	Minimum Load			Maximum Load		
	A	B	C	A	B	C
OPF solution from BFM						
Reg1 Tap	-13	-13	-13	-8	-8	-8
Reg2 Tap	0	—	—	-2	—	—
Reg3 Tap	1	—	1	7	—	2
Reg4 Tap	0	0	0	0	0	0
Cap1 Status	OFF	OFF	OFF	ON	ON	ON
Cap2 Status	OFF	—	—	ON	—	—
Cap3 Status	—	OFF	—	—	OFF	—
Cap4 Status	—	—	OFF	—	—	OFF
DG1 q_{DG}^p (MVAR)	-0.03	0.045	0.012	-0.028	0.03	0.04
DG2 q_{DG}^p (MVAR)	0.04	-0.03	0.03	-0.025	0.039	-0.01
DG3 q_{DG}^p (MVAR)	-0.08	-0.02	-0.08	-0.09	0.045	-0.09

Table 5.3: OpenDSS Validation for IEEE-123 Node System [69]

IEEE-123 Phase	Minimum Load			Maximum Load		
	A	B	C	A	B	C
Optimal substation power flow and voltages using MATLAB						
Load (MW)	0.20	0.13	0.18	0.99	0.78	1.02
Min. Voltage (pu)	0.955	0.955	0.955	0.951	0.953	0.951
Max. Voltage (pu)	0.965	0.965	0.965	0.995	0.995	0.995
Avg. Voltage (pu)	0.957	0.957	0.958	0.963	0.965	0.966
Validation of substation power flow and voltages using OpenDSS						
Load (MW)	0.205	0.134	0.183	1.00	0.79	1.024
Min. Voltage (pu)	0.954	0.954	0.954	0.95	0.95	0.95
Max. Voltage (pu)	0.965	0.965	0.965	0.995	0.995	0.995
Avg. Voltage (pu)	0.956	0.956	0.956	0.96	0.961	0.963

The results obtained using the two-stage VVO approach are validated using OpenDSS – a distribution system simulation platform. The optimal statuses of the capacitor banks, voltage regulator taps, and reactive power reference to the DGs obtained from the optimization model are implemented in the OpenDSS model for the test system. The

substation power demand and feeder voltage characteristics obtained using optimization program validated against OpenDSS (see Table 5.3). It can be observed that system parameters obtained from BFM closely match those obtained from OpenDSS.

Finally, the CVR benefits obtained using the proposed approach are reported. The total three-phase substation load demand is compared to the case when VVO control is not enabled as shown in Figure 5.6. On average, a reduction of around 150 kW is reported in net feeder active power demand. As expected the largest savings are reported during the minimum load conditions.

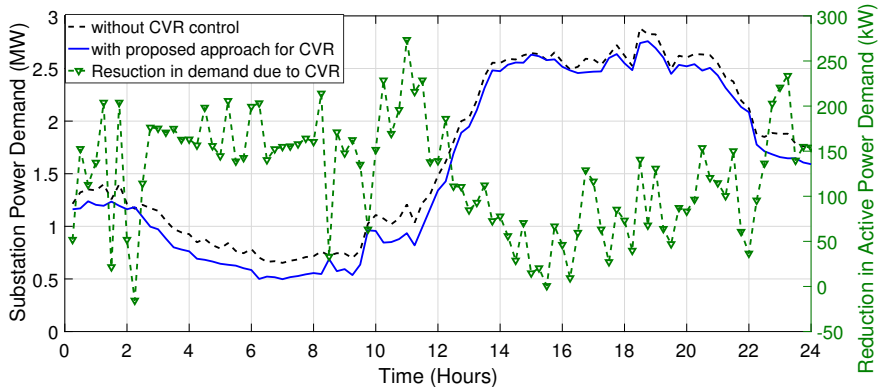


Figure 5.6: IEEE-123 CVR Benefits Observed using the Proposed Approach ($CVR_p = 0.6$ and $CVR_q = 3$) [69].

The proposed approach is further validated using ZIP load models for residential, commercial and large commercial loads. The ZIP coefficients detailed in Table 5.4 are used to obtain CVR factors for each case with different load mix. The total feeder load demand for the minimum and maximum load condition are reported in Table 5.4. As anticipated, loads with higher voltage sensitivity show larger CVR benefits.

Computational Complexity: On average, on a dual-core i7 3.41 GHz processor with 16 GB of RAM, the Stage-1 solutions are obtained in less than 5 sec for the IEEE 123-bus system. The Stage-2 problem for the 123-bus system takes an average of 2 minutes to solve. The longest time taken to solve the Stage-2 problem for the 123-bus system is 4 min. The solution times for Stages 1 and 2 are within the 15-minute control

Table 5.4: CVR for IEEE 123-Bus Feeder, R-Residential, SC-Small Commercial, LC-Large Commercial [69].

Load Composition	Minimum Load		Maximum Load	
	CVR	No CVR	CVR	No CVR
100% R	0.588	0.777	2.726	2.842
70% R, 30% SC	0.588	0.776	2.727	2.846
50% R, 30% SC, 20% LC	0.589	0.748	2.728	2.859

interval. It should be noted that the 123-bus test feeder is a practical mid-size primary distribution circuit. The test feeder consists of 123 buses and 267 single-phase nodes.

It should be noted that the Stage-1 formulation scales well for larger feeders. This is due to the fact that Stage-1 solves a MILP, which is relatively easier to solve even with a large set of constraints. The Stage-2 NLP problem, on the other hand, is more difficult to scale for a large distribution system. In such cases, network reduction techniques are required to represent the system with fewer equations.

R3-12.47-2 Test Feeder

The selected PNNL taxonomy feeder includes 329 buses, where, the number of nodes for phases A, B and C are 288, 298 and 274, respectively (total 860 single-phase nodes) (see Figure 5.3). The proposed two-stage approach is implemented on 329-bus system. It is observed that Stage-1 problem (MILP) takes on an average 20-sec. to solve, however, Stage-2 problem (NLP) takes on an average 20-mins. Note that Stage-2, for R3-12.47-2 system, solves for 4233 variables. In order to scale the Stage-2 problem and to obtain a solution within 15-min interval, the R3-12.47-2 test feeders is reduced using a simple network reduction technique. To reduce the network, we used the property of radial distribution feeders; the nodes that do not include branches, loads, or voltage control devices are combined using the equations for the series system for the corresponding branches. Using this method, the R3-12.47-2 system is reduced to a 184-bus system where, the number of nodes in phase A , B and C are 163, 171 and 156, respectively. After network reduction, the total number of variables for the Stage-2 problem are reduced to 2415.

Since network reduction is exact both models result in the same power flow quantities. The maximum computation time required to solve the Stage-2 problem for the reduced network model is 9 mins.

Table 5.5: VVO Results for R3-12.47-2 Test Feeder [69].

IEEE-329	Minimum Load			Maximum Load		
	Phase	A	B	C	A	B
OPF solution from BFM						
Reg1 Tap	-6	-6	-6	1	1	1
Cap1 Status	OFF	OFF	OFF	ON	ON	ON
Cap2 Status	OFF	—	—	OFF	—	—
Cap3 Status	—	OFF	—	—	OFF	—
Cap4 Status	—	—	OFF	—	—	OFF
DG1 q_{DG}^P (MVAR)	0.02	0.02	0.02	0.01	0.01	0.01
DG2 q_{DG}^P (MVAR)	-0.06	-0.06	-0.06	-0.03	-0.03	-0.03
DG3 q_{DG}^P (MVAR)	-0.11	-0.11	-0.08	0.055	0.035	0.022

Table 5.6: OpenDSS Validation for R3-12.47-2 feeder [69].

IEEE-329	Minimum Load			Maximum Load		
	Phase	A	B	C	A	B
Optimal substation power flow and voltages using BFM						
Load (MW)	0.444	0.459	0.434	2.86	2.97	2.775
Min. Voltage (pu)	0.958	0.958	0.958	0.955	0.955	0.955
Max. Voltage (pu)	0.962	0.962	0.962	1.0063	1.0063	1.0063
Avg. Voltage (pu)	0.959	0.959	0.959	0.974	0.972	0.976
Validation of substation power flow and voltages using OpenDSS						
Load (MW)	0.445	0.462	0.438	2.87	2.98	2.79
Min. Voltage (pu)	0.958	0.958	0.958	0.954	0.953	0.954
Max. Voltage (pu)	0.962	0.962	0.962	1.0063	1.0063	1.0063
Avg. Voltage (pu)	0.959	0.959	0.959	0.971	0.97	0.973

The CVR results obtained for maximum and minimum load conditions are shown in Tables 5.5 and 5.6. Note that the Stage-1 problem is implemented using full R3-12.47-2 test feeder and the Stage-2 problem is implemented using reduced 184-bus feeder. As the load is closely balanced, the behavior of each phase is almost similar. The voltage regulator at the substation is at -6 tap for the minimum load and at 1 tap position for the maximum load condition. At minimum load, the

three-phase as well as single-phase capacitor banks are OFF. However, at the maximum load condition, the three-phase capacitor is ON and single-phase capacitor banks are OFF. The reactive power support from DG1 is the same for all phases for both maximum and minimum load conditions. The minimum voltage for all the phases is at 0.958 pu at minimum load condition and at 0.955 pu at maximum load. The average voltage along the feeder is 0.959 and 0.972 at minimum and maximum load conditions, respectively. The substation power demand and feeder voltage characteristics obtained using MATLAB are validated against OpenDSS (see Table 5.6). The system parameters obtained from MATLAB closely match to those obtained from OpenDSS, validating the proposed VVO model.

The CVR benefits obtained using the proposed approach for 24-hour duration are reported in Figure 5.7. The total three-phase substation load demand is compared to the case when VVO control is not enabled. On average, a reduction of around 200kW is reported in the net feeder active power demand.

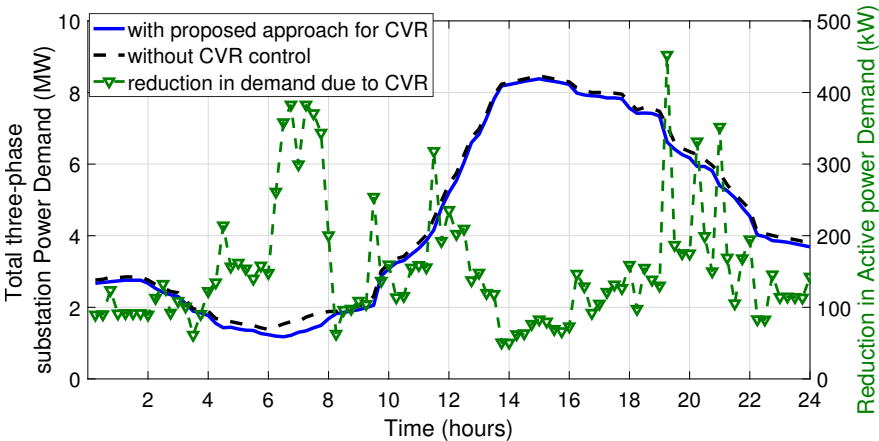


Figure 5.7: R3-12.47-2 test feeders CVR Benefits Observed using the Proposed Approach ($CVR_p = 0.6$ and $CVR_q = 3$) [69].

5.4 Summary and Discussions

Optimal voltage control of distribution system is one of the most fundamental applications of the optimal power flow algorithms. In this section, we presented an application of distribution optimal power flow models (D-OPF) for distribution-level voltage control to achieve conservation voltage reduction (CVR). CVR leverages the load's sensitivity to nodal voltages to help reduce the customer power demand by operating the system toward its lower operating limit. We described how a CVR optimization problem could be formulated as an OPF problem. The resulting optimization formulation is a MINLP problem that is extremely difficult to solve and scale for large systems. We describe a two-stage algorithm to efficiently handle the discrete and continuous control variables simultaneously by separating the MINLP into simpler problems: Stage 1 solves a MILP problem, and Stage 2 solves an NLP problem. The approach is thoroughly validated using test feeders. The results demonstrate that the proposed approach successfully coordinates the operation of legacy and new devices for CVR benefits.

The growing complexity with grid-edge integration requires computationally efficient approaches to manage the real-time operational requirements of voltage control applications. Significant efforts have been made to employ optimal power flow (OPF) algorithms to optimize the grid-edge resources [96]. However, power grid optimization is computationally challenging due to multiple sources of nonlinearities, a combination of continuous and discrete decisions, decision-making under uncertainties, and the sheer scale of the problem. Moreover, the problem complexity grows significantly when attempting to optimize millions of grid-edge controllable nodes with the integration of roof-top PVs, battery storage units, transportation electrification, grid-interactive buildings, data centers. Scalable algorithms are called for to manage massive penetration of grid-edge resources. Existing methods manage the computational challenges using convex relaxation or linear approximation techniques. Methods based on both approximation and relaxation techniques use a centralized paradigm that leads to scalability challenges as the problem size increases; Figure 5.8 shows how poorly the central nonlinear OPF model scales with the network size (all cases

are solved using a commercial NLP solver). Alternatively, distributed optimization techniques can be used to scale OPF for large networks. These methods decompose the large-scale optimization problem into several smaller sub-problems that are solved parallelly at distributed computing nodes and use message-passing protocols to enforce network-level consensus. Please refer to the following articles for additional discussions [95], [125].

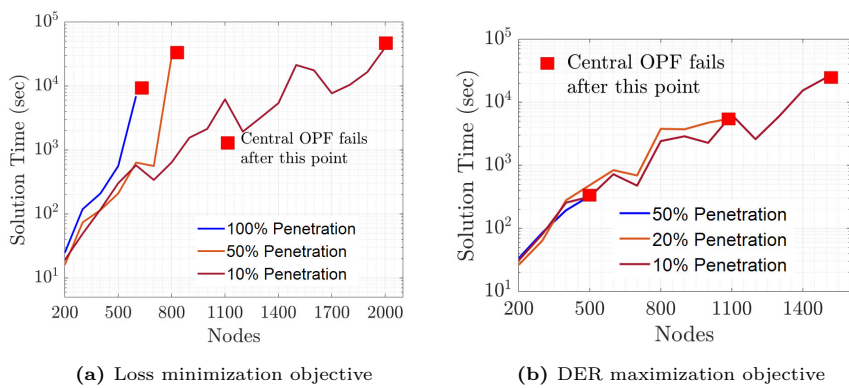


Figure 5.8: Solution time for central OPF problems for different objective functions

6

Resilient Distribution Systems Operations

Electric power grids face severe threats from extreme weather events leading to extended outages and adversely affecting community well-being. In the aftermath of an outage/disruption, restoring the power supply to critical loads as quickly as possible is crucial to minimize economic loss and ensure reliability. While utility companies might be well-equipped to manage normal outages, extreme events are much more challenging. Extreme events lead to drastic changes in the system's operational conditions requiring new mechanisms for system recovery and restoration. Usually, an outage caused by extreme events takes several days and sometimes even weeks and months to restore the normal power supply. After extreme weather events, distribution networks may not be able to connect with the bulk power system. Multiple distribution system facilities may also be damaged, making the feeder and service restoration even more challenging. The staggering cost of power outages and their impacts on the grid demands expedited incorporation of resilience in aging and stressed power distribution systems towards these high-impact, low-probability (HILP) events [98]. Fortunately, recent advances in distribution systems, including the integration of DGs and distribution automation capabilities, provide potential means to improve system resilience if applied in a purposeful and methodical manner.

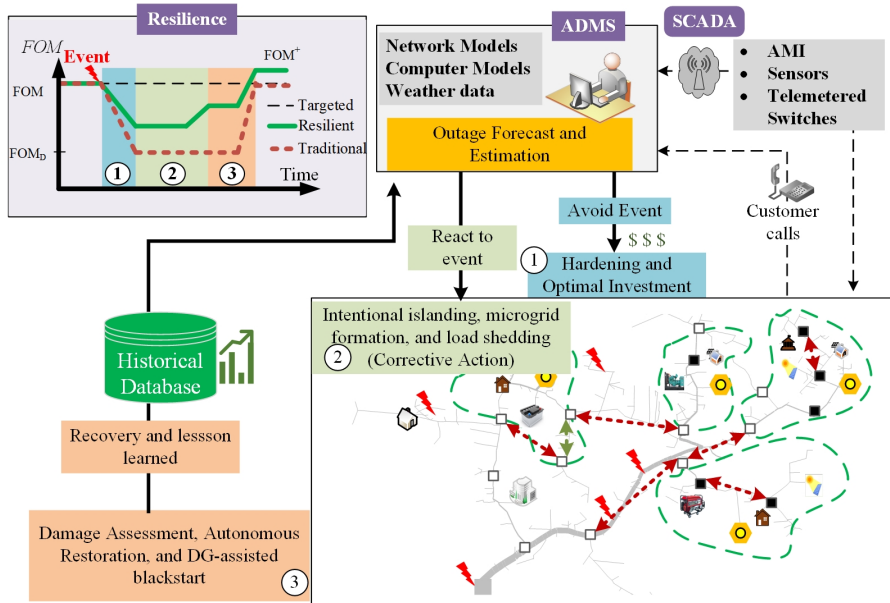


Figure 6.1: Framework to enable resilient operations in power distribution systems.

Figure 6.1 describes a potential framework for enabling resilience-driven operations in power distribution systems to enhance community resilience. The top left portion of Figure 1 illustrates a notional system performance curve when impacted by an extreme weather event; the figure of merit (FOM) quantifies the system's overall resilience. The FOM drops immediately after the system is impacted by an extreme weather event; this drop in FOM can be reduced via deploying appropriate infrastructure planning and hardening measures such as microgrids, grid forming DGs for emergency support, etc. (see curve with green line). The resilience can be further improved by enabling resilient operations such as intentional islanding using DGs to support community loads [118]. Enabling such advanced operations requires (1) infrastructure planning that is driven by the cost of system upgrades and the outage risk posed by extreme weather events, and (2) appropriate mechanisms for communication and controls to enable resilient operations.

This section focuses on the use of optimization methods to ensure resilience grid operations. To this end, we focus on distribution system restoration problems using all available resources including grid-forming DGs and microgrids. The problem objective is to maximize the load restored using the minimum number of switching operations while allowing for the formation of intentional islands to support the system's critical loads. The resulting application is termed as "DG-assisted Resilient restoration". In what follows, we provide a description of the problem, define problem objectives and constraints, and provide a demonstration using large-scale test feeders. For additional details, kindly refer to [119] and [116].

6.1 DG-assisted Distribution System Restoration

Distribution companies employ a fault location, isolation, and service restoration (FLISR) system for distribution system restoration (DSR) during outages. Algorithmically, DSR solves a feeder reconfiguration problem which is typically a combinatorial optimization problem. The growing complexity of distribution grids due to numerous sectionalizing switches, tie switches, and DERs available for restoration significantly increases the complexity of the inherent combinatorial DSR problem. Earlier methods for DSR focused on designing expert systems and heuristic search methods to avoid solving the combinatorial problem [87], [94]. Soft computing algorithms, including genetic algorithm, particle swarm optimization, simulated annealing, and fuzzy set approaches, have also been proposed [81], [86]. To manage the growing computational complexity, several optimization-based methods for DSR have been explored [74], [83], [150]. For an unbalanced power distribution system, the DSR problem is typically formulated as a mixed-integer nonlinear program (MINLP). Though accurate, MINLP formulations are computationally unattractive as they do not scale well, i.e., the simulation time increases significantly with the increase in the complexity of the restoration problem. This led to use of scalable linearized formulations with mixed-integer decision variables to model DSR problem. Mathematically, the problem remains nonlinear due to integer/binary decision

variables. However, recent advances in solvers for mixed-integer linear programming (MILP) problems aids in scaling the resulting formulation.

In what follows, we describe the use of D-OPF models to formulate the DSR problem for a three-phase unbalanced distribution system [119]. The presented DSR formulation is developed at Washington State University (WSU) and integrated into Pacific Northwest National Laboratory's (PNNL) GridAPPS-D platform – an open-source platform for hosting advanced distribution system applications [120]. The proposed DSR application determines feeder restoration and reconfiguration using all available resources: backup feeders, microgrids, and DGs. Intentional islanding methods are employed to ensure resilience to extreme events using DGs and remotely-controlled smart switches that may help restore critical loads during emergency conditions, especially when the upstream subtransmission/transmission system is outaged.

6.2 Optimization Problem Formulation

Fault detection and isolation routines autonomously isolate the parts of the distribution system downstream from the affected protection devices due to a fault. While repairing the root cause and impacts of fault is time-consuming, one can employ available switches to reconfigure the system to serve the customers connected to healthy feeders. This feeder reconfiguration problem can be formulated as a D-OPF problem. Specifically, given the post-fault status of the network, the D-OPF problem obtains an optimal restored network topology that minimizes the impacts of the outages while complying with the system's operational constraints. The restoration plan includes the possibility of intentional DG-supplied islands (with the grid-forming capability) to restore additional loads. For computational advantages, a linear power flow model is used in the optimization formulation. Given discrete decision variables, the resulting formulation an MILP, where the problem objective is to maximize the restored loads subject to network operational and topological constraints. The decision variables are switch (line/load) statuses and the statuses of grid-forming DGs.

6.2.1 Defining Problem Variables

We represent the distribution system comprised of multiple feeders and DGs using a connected graph, $\mathcal{G}(\mathcal{V}, \mathcal{E})$, where nodes represent buses and edges represent physical line sections including switches. An edge, $e \in \mathcal{E}$, is defined by its incident nodes (i, j) with $(i, j) \in \mathcal{V}$.

The normal operating tree of a well-planned distribution network is given as $\mathcal{T}_o = (\mathcal{V}_o, \mathcal{E}_o)$ where all tie-switches are open, all grid-forming DGs are disconnected, and all sectionalizing-switches are closed. Once a fault occurs on a normal operating tree, the proposed DSR algorithm identifies a desired tree or subtrees (if intentional islanding is needed) within the original graph, \mathcal{G} , that maximizes the given objective function of restoring loads subject to various connectivity and operating constraints. After the suitable switching scheme is implemented, the new operating tree is defined as $\mathcal{T} = (\hat{\mathcal{V}}, \hat{\mathcal{E}})$ where $\hat{\mathcal{E}} \subseteq \mathcal{E}$ and $\hat{\mathcal{V}} \subseteq \mathcal{V}$. We describe a mathematical programming formulation to obtain the optimal restored operational topology.

The following define the binary variables associated with the proposed DSR algorithm.

- *Bus Energization Variable:* A binary variable $v_i = \{0, 1\}$ is assigned to each bus, where $v_i = 1$ implies that bus i is energized, while $v_i = 0$ implies bus i is not energized during the restoration
- *Load Energization Variable:* Each load bus is assigned a binary variable $s_i = \{0, 1\}$ that represents the switch status of the load connected to the particular bus. This variable helps in the case when only a few critical loads are to be restored without restoring all the loads in the path. Note that for a load to be restored, both s_i and v_i must be 1.
- *Switch Status Variable:* A binary variable $\{\delta_e\}_{e \in \mathcal{E}_S} \in \{0, 1\}^{|\mathcal{E}_S|}$ is associated with each switch, where $\delta_e = 1$ implies that switch connecting buses i and j is closed, while $\delta_e = 0$ implies that the switch is open. The decision on the line/switch binary variable helps maintain a radial configuration for the restored network. The line variable will be used to formulate power flow constraints and connectivity constraints for the distribution system.

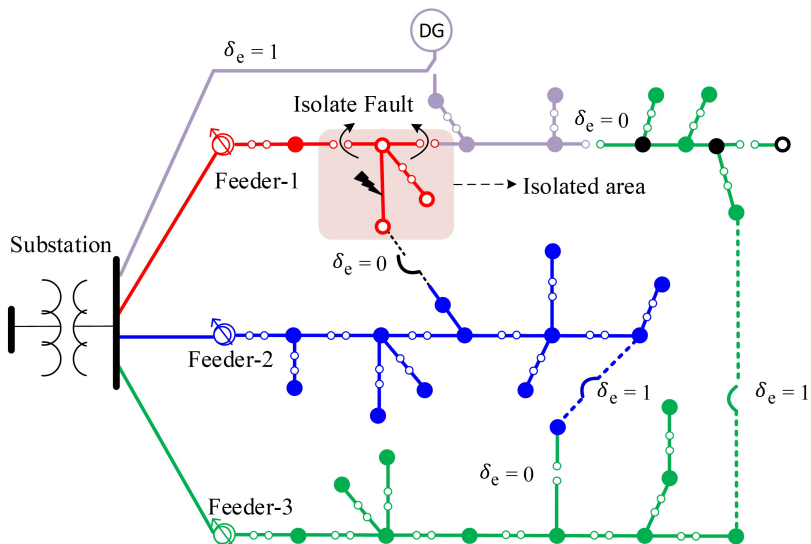


Figure 6.2: An example restoration scenario. The colors indicate energized feeder sections and binary variables define the topology.

- *DG Islanding Variable:* The complexity of the restoration problem in the distribution system increases significantly in the presence of grid-forming DGs that can intentionally island to restore additional loads. To formulate a unified DSR problem that enables restoration using both DG islands and other feeders, a virtual edge, δ_e , is added between the sub-transmission bus and each grid-forming DG as shown in Figure 6.2. The state of this edge determines whether the DG is in isolation mode (OFF) or an island is formed.

6.2.2 Problem Objective

The problem objective is to maximize the restored load and minimize the number of switching operations subject to the feeder's operational and connectivity constraints. The first objective is to maximize the amount of load restored while considering different weight factors for each load (w_i) that indicate load priority. The objective is defined as the following.

$$\text{Maximize} \sum_{i \in \mathcal{V}_S} \sum_{\phi \in \{a,b,c\}} w_i s_i P_{Li}^\phi. \quad (6.1)$$

The number of switching operation determines the performance of the restoration plan as it closely relates to the time taken to execute the restoration plan. Also, frequently operating switches adds additional maintenance cost. Therefore, it is desirable to minimize the number of switching operations so that the restoration plan can be executed in an efficient and timely manner. Thus, the second objective is to minimize the total number of switching operations defined in (6.2).

$$\text{Minimize} \left(\sum_{e \in \mathcal{E}_S^s} (1 - \delta_e) + \sum_{e \in \mathcal{E}_S^t} \delta_e + \sum_{e \in \mathcal{E}_S^v} \delta_e \right). \quad (6.2)$$

We define a multi-objective restoration problem using a weighted combination of the two previously defined objective functions in (6.3).

$$\text{Maximize} \left(\alpha \sum_{i \in \mathcal{V}_S} \sum_{\phi \in \{a,b,c\}} w_i s_i P_{Li}^\phi - \beta \left(\sum_{e \in \mathcal{E}_S^s} (1 - \delta_e) - \sum_{e \in \mathcal{E}_S^t} \delta_e \right) - \gamma \sum_{e \in \mathcal{E}_S^v} \delta_e \right). \quad (6.3)$$

The maximization of the restored load is defined as the primary objective and is always given a higher preference. The minimization of the total number of switching operations is defined as the secondary objective. The weights, α , β , and γ are defined such that the primary objective is always prioritized. Since the secondary objective is a sum of binary variables only, making $\beta < 1$, $\gamma < 1$, and assigning α a large number ensures that the problem first restores the maximum weighted loads and then minimizes the switching operations. Also, gamma is made at least $2|\mathcal{E}_S^t|$ times higher than β (i.e, $\gamma \geq 2|\mathcal{E}_S^t|\beta$) to account for switch operations needed to get a radial topology.

6.2.3 Problem Constraints:

The several constraints associated with the service restoration problem are described below.

Connectivity Constraints

This section defines the set of constraints required to ensure proper network connectivity and radial topology for the restored network/s.

- Constraint (6.4a) ascertains that a load with a switch can be picked up if and only if it is connected to a bus that is energized in the restored network by one of the feeders or DGs. Constraint (6.4b) ensures that a non-switchable load will be energized depending upon the associated bus energization variable. Thus, a non-switchable load is always picked up if the corresponding bus is energized.

$$s_i \leq v_i, \quad \forall i \in V^R \quad (6.4a)$$

$$s_i = v_i, \quad \forall i \in V \setminus V^R \quad (6.4b)$$

- Next, we describe the constraints for line energization variable, (δ_{ij}) in (6.5a-6.5d). The set of equations indicates the relationship among line energization variable corresponding buses and their energization statuses. Equation (6.5a) ensures that if a line with a switch is energized, the buses connecting the line must be energized. Equation (6.5b) ensures that a line without a switch must be energized if any of the buses connecting it is energized. The faults and the open switches in the distribution network are modeled using constraint (6.5c). For a disaster case, a substation fault is included using (6.5d), which implies all the feeders are disconnected from the main supply.

$$\delta_{ij} \leq v_i, \quad \delta_{ij} \leq v_j, \quad \forall (i \rightarrow j) \in E^R \setminus E^F \quad (6.5a)$$

$$\delta_{ij} = v_i = v_j, \quad \forall (i \rightarrow j) \in E \setminus (E^R \cup E^F) \quad (6.5b)$$

$$\delta_{ij} = 0, \quad \forall (i \rightarrow j) \in E^F \quad (6.5c)$$

$$\delta_{ij} = 0, \quad \forall (i \rightarrow j) \in E_T \quad (6.5d)$$

- A radial topology for restored network/s is ensured using constraint (6.6) that enforces at least one switch in any cycle to be open. All possible cycles in a distribution network are enumerated using iterative loop counting algorithm [77]. Then, (6.6) is written for each cycle. The number of cycles in a graph increases with the

increase in the number of tie switches. Despite that, G is usually sparse for a distribution network where the total number of cycles is much less than $2^{|V|}$. Note that the cycle enumeration is done offline using as-built topology of the power distribution system.

$$\sum_{(i \rightarrow j) \in E^c} \delta_{ij} \leq |E^c| - 1, \quad \forall (i \rightarrow j) \in E^c \quad (6.6)$$

Power Flow Constraints

We use three-phase LinDistFlow model for the unbalanced distribution system [50]. The linearized model is sufficiently accurate and applicable for restoration problems. The linearized model for the 1096-bus test system incurs the largest errors of 2.56%, and 0.002 pu in apparent power flow and bus voltages, respectively compared to the actual power flow solution obtained using OpenDSS. The restoration problem requires the decision upon which lines are energized while accounting for network operating constraints. The power flow along a line is only valid if the line is energized. Therefore, to appropriately represent the restoration problem the branch flow equations are coupled with line and bus decision variables.

- Constraints (6.7a-6.7c) represent three-phase unbalanced linearized power flow equations coupled with line decision variable δ_{ij} and load pick-up variable s_i . Note that $\delta_{ij} = 1$, if $(i \rightarrow j) \in E \setminus (E^R \cup E^F)$. Constraint (6.7a) defines voltage equations where if two buses i and j are connected without a remotely switchable line or if the line is energized, the voltage difference of the branch is then constrained by the branch power flow. Similarly, constraints (6.7b) and (6.7c) define active and reactive power flow constraints that must be satisfied for each energized line. Note that constraints (6.7a)-(6.7c) are non-convex as they involve product of variables. These constraints are linearized by defining an auxiliary variable and using big-M method [152].

$$\delta_{ij} (\mathbf{U}_i - \mathbf{U}_j) = 2(\tilde{\mathbf{r}}_{ij} \mathbf{P}_{ij} + \tilde{\mathbf{x}}_{ij} \mathbf{Q}_{ij}), \quad \forall (i, j) \in V \quad (6.7a)$$

$$\sum_{(i \rightarrow j) \in E} \delta_{ij} \mathbf{P}_{ij} = s_j \mathbf{P}_{Lj} + \sum_{\substack{(j \rightarrow c) \in E \\ i \neq c}} \delta_{jc} \mathbf{P}_{jc}, \quad \forall (i, j) \in V \quad (6.7b)$$

$$\sum_{(i \rightarrow j) \in E} \delta_{ij} \mathbf{Q}_{ij} = s_j \mathbf{Q}_{Lj} + \sum_{\substack{(j \rightarrow c) \in E \\ i \neq c}} \delta_{jc} \mathbf{Q}_{jc}, \quad \forall (i, j) \in V \quad (6.7c)$$

where, $\tilde{\mathbf{r}}_{ij} = \text{Real}\{\alpha\alpha^H\} \otimes \mathbf{r}_{ij} + \text{Im}\{\alpha\alpha^H\} \otimes \mathbf{x}_{ij}$, $\tilde{\mathbf{x}}_{ij} = \text{Real}\{\alpha\alpha^H\} \otimes \mathbf{x}_{ij} + \text{Im}\{\alpha\alpha^H\} \otimes \mathbf{r}_{ij}$, $\alpha = [1 \ e^{-j2\pi/3} \ e^{j2\pi/3}]^T$

Network Operating Constraints

This section defines nodal voltage limit constraints and thermal limit constraints for lines and transformers.

- The voltage of each bus should be within the limit as specified in ANSI C84.1 and is ensured by equation (6.8). \mathbf{U}^{min} and \mathbf{U}^{max} are set to $(0.95)^2$ and $(1.05)^2$, respectively for each phase of the bus.

$$v_i \mathbf{U}^{min} \leq \mathbf{U}_i \leq v_i \mathbf{U}^{max}, \quad \forall i \in V \quad (6.8)$$

- The loading on the lines and transformers must not exceed the rated kVA capacity. The rated kVA capacity is specified for the transformers. The thermal limit for the lines is, however, specified in terms of their ampacity. We use a nominal feeder voltage of 1 p.u. to convert line ampacity rating to their rated kVA capacity. The actual thermal limit constraint is specified using the quadratic equation in (6.9). We use the polygon-based linearization approach proposed in [2] to linearize (6.9) by a set of linear constraints defined in (6.10). We use (6.10) instead of (6.9) in MILP model.

$$(\mathbf{P}_{ij})^2 + (\mathbf{Q}_{ij})^2 \leq \left(\mathbf{S}_{ij}^{rated}\right)^2 \quad \forall (i \rightarrow j) \in E \quad (6.9)$$

$$\begin{aligned} -\sqrt{3} (\mathbf{P}_{ij} + \mathbf{S}_{ij}) &\leq \mathbf{Q}_{ij} \leq -\sqrt{3} (\mathbf{P}_{ij} - \mathbf{S}_{ij}) \\ -\sqrt{3}/2 \mathbf{S}_{ij} &\leq \mathbf{Q}_{ij} \leq \sqrt{3}/2 \mathbf{S}_{ij} \end{aligned} \quad (6.10)$$

$$\sqrt{3} (\mathbf{P}_{ij} - \mathbf{S}_{ij}) \leq \mathbf{Q}_{ij} \leq \sqrt{3} (\mathbf{P}_{ij} + \mathbf{S}_{ij})$$

where, $\mathbf{S}_{ij} = \mathbf{S}_{ij}^{rated} \sqrt{(2\pi/n)/\sin(2\pi/n)}$ and $n = 6$.

DG Operating Constraints

Constraint (6.11) ensures that the power flow from DG does not exceed its rated DG capacity.

$$\sum_{\phi \in \{a,b,c\}} P_{ij}^{\phi} \leq \delta_{ij} P_G^{max}, \quad \sum_{\phi \in \{a,b,c\}} Q_{ij}^{\phi} \leq \delta_{ij} Q_G^{max} \quad (6.11)$$

6.2.4 Overall Problem

We define a multi-objective restoration problem using a weighted combination of the two previously defined objective functions in (6.12).

Final Optimal Configuration

Maximize:

$$\left(\alpha \sum_{i \in \mathcal{V}_S} \sum_{\phi \in \{a,b,c\}} w_i s_i P_{Li}^{\phi} - \beta \left(\sum_{e \in \mathcal{E}_S^s} (1 - \delta_e) - \sum_{e \in \mathcal{E}_S^t} \delta_e \right) - \gamma \sum_{e \in \mathcal{E}_S^v} \delta_e \right). \quad (6.12)$$

Subject to: (6.4) - (6.11)

where:

$$\tilde{\mathbf{r}}_e = \text{Real}\{\alpha\alpha^H\} \otimes \mathbf{r}_e + \text{Im}\{\alpha\alpha^H\} \otimes \mathbf{x}_e, \tilde{\mathbf{x}}_e = \text{Real}\{\alpha\alpha^H\} \otimes \mathbf{x}_e + \text{Im}\{\alpha\alpha^H\} \otimes \mathbf{r}_e, \alpha = [1 \quad e^{-j2\pi/3} \quad e^{j2\pi/3}]^T$$

$$S_e = S_e^{rated} \sqrt{(2\pi/n)/\sin(2\pi/n)} \text{ and } n = 6$$

$$a_{\phi} = \sum_{i=1}^{32} b_i u_{tap,i}^{\phi} \text{ and } \sum_{i=1}^{32} u_{tap,i}^{\phi} = 1$$

6.3 Results and Discussions

The effectiveness of the proposed approach is validated using a multi-feeder 1069-bus test system consisting of four R3-12.47-2 PNNL taxonomy feeders connected using several tie switches [130]. The restoration problem is formulated as an MILP that can be solved using off-the-shelf solvers. The restoration formulation is modeled using PuLP modeling

functions and solved using CPLEX 12.6 solver. The simulation is carried out on a PC with 3.4 GHz CPU and 16 GB RAM.

The taxonomy feeder R3-12.47-2 represents a moderately populated urban area. The total load on the feeder is 4366.955 kW and 1299.206 kVAr. Four identical feeders are replicated to obtain the four-feeder 1069-bus distribution system where feeders are interconnected using seven normally open tie switches (see Figure 6.3). With a total of 1069 multi-phase physical buses (3444 single-phase buses), 152 sectionalizing switches, 190 possible cycles, and 122,586 number of normal operational radial topologies the 1069-bus test case is a sufficiently large-scale model. We also incorporate several grid-forming utility-owned DGs in test case. To ensure the ability to transfer the load to other feeders, the feeder loading is limited to 70%, consequently, the feeder transformer capacity is 6.7 MVA. This system is assumed to be operating in a peak load condition. Kindly refer to [119] for additional discussions.

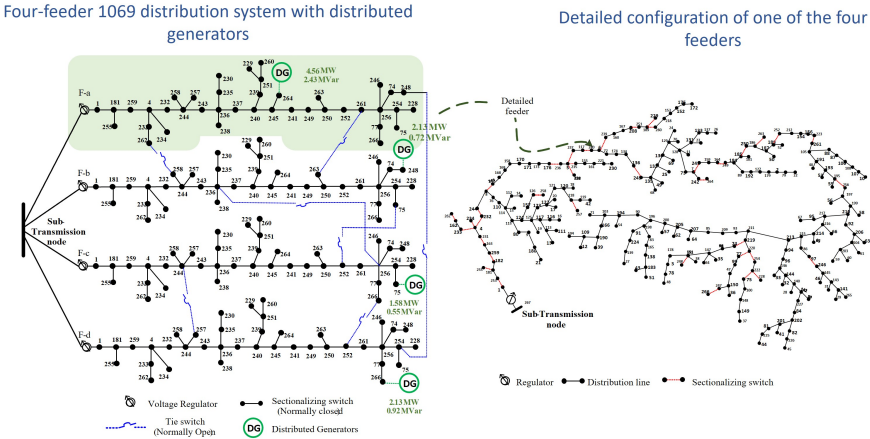


Figure 6.3: Simplified one-line diagram of the multi-feeder 1069-bus distribution system with seven additional tie switches and four DGs.

6.3.1 Restoration During Typical Outages

First, we simulate typical outage scenarios with a few lines at fault. Here, all loads are assumed to be equally critical for restoration. Table 6.1 and Table 6.2 demonstrate the effectiveness of the proposed approach

Table 6.1: Restoration strategy for the four-feeder 1069-bus test case with and without DGs, [119].

Event Detail	Case 1: Switching Schemes without DGs		Restored Load (kW)
	Open	Close	
F: 253-181 (F-c) T: 267-1 (F-c) I: 259-182 (F-c) Loss: 4366.95 kW	219-74 (F-a) 222-75 (F-b) 185-250 (F-b)	248-254 (F-a and F-d) 75-252 (F-b and F-c) 236-256 (F-b and F-c) 261-263 (F-a and F-b)	3904.56
F: 187-50 (F-b) T: 185-250 (F-b) I: 188-252 (F-b) & 186-263 (F-b) Loss: 3564.73 kW	195-256 (F-c)	236-256 (F-b and F-c) 75-252 (F-b and F-c)	3548.32
F: 135-132 (F-d) T: 136-245 (F-d) I: 128-73 (F-d) Loss: 4102.80 kW	220-254 (F-d) 5-237 (F-b) 195-256 (F-c)	248-254 (F-a and F-d) 266-252 (F-c and F-d) 75-252 (F-b and F-c) 236-256 (F-b and F-c)	2984.16

Table 6.2: Restoration strategy for the four-feeder 1069-bus test case with and without DGs [119].

Event Detail	Case 2: Switching Schemes with DGs		Restored load (kW)
	Open	Close	
F: 253-181 (F-c) T: 267-1 (F-c) I: 259-182 (F-c) Loss: 4366.95 kW	219-74 (F-b) 220-77 (F-c) 220-254 (F-c) 223-261 (F-c) 220-254(F-d)	DG-248 (F-b) DG-75 (F-c) 248-254 (F-a and F-d) 236-256 (F-b and F-c) 266-252 (F-c and F-d) 244-257 (F-c and F-c)	4197.55
F: 187-50 (F-b) T: 185-250 (F-b) I: 188-252 (F-b) & 186-263 (F-b) Loss: 3564.73 kW	195-256 (F-c)	236-256 (F-b and F-c) 75-252 (F-b and F-c)	3548.32
F: 135-132 (F-d) T: 136-245 (F-d) I: 128-73 (F-d) Loss: 4102.80 kW	220-254 (F-d) 220-254 (F-c) 195-256 (F-c)	248-254 (F-a and F-d) 266-252 (F-c and F-d) DG-75 (F-c) DG-266 (F-d)	3465.16

using multiple fault cases. We compare the restoration results for two different cases: Case I assumes restoration without using DG-assisted intentional islanding; Case II assumes restoration with DG-assisted

intentional islanding. The notation **F**, **T**, and **I** denote faulted line, tripped switch and isolation candidate, respectively, for a particular event.

In Scenario-1, a fault is simulated near feeder F-c (Line 253-181). This results in the tripping of the upstream switch, 267-1. Fault isolation is initiated to isolate the faulty part of the feeder. In this case, an additional switch in F-c is opened (259-183) to isolate the faulted zone. As a result of this outage, a total of 4366.95 kW of the load is under outage. After fault isolation, the optimization-based restoration algorithm is run to generate a switching scheme to restore the outaged load. The optimal restoration plan includes opening three sectionalizing switches and closing 4 tie switches resulting in the restoration of 3904.56 kW (see Table 6.1). Next, we simulate the same outage scenario allowing for intentional islanding using grid-forming DGs. Unlike the previous case, the resulting optimal restoration plan restores 4197.55 kW of the outaged loads requiring 11 switching operations and the formation of two DG-supplied islands (See Table 6.2). Note that in this case, the DGs located in F-b and F-c form intentional islands. This frees some capacity for the feeder-head transformer allowing it to restore additional loads.

In Scenario-2, we simulate a mid-feeder fault in F-b. The fault results in the opening of Switch 185-250. Two additional sectionalizing switches (188-252 and 186-263) are opened to isolate the faulted section to ensure that the fault is not fed during the restoration process. This outage leads to a total loss of 3564.3 kW of load. The optimal restoration plan for this scenario entails opening one sectionalizing switch and closing two sectionalizing switches (see Table 6.1). In this case, the optimal restoration plan is able to pick up all outage loads except the one on the faulted section. Thus, this case does not require any additional DG support to restore loads resulting in the same optimal solutions for both cases (see Table 6.2).

In Scenario-3, we simulate a fault in F-d. The corresponding switches that tripped off for protection and fault isolation are shown in Table 6.1. This event leads to an outage of 4102.80 kW. The optimal restoration plan for this case includes load transfer between F-b and F-c with the help of tie-switches. The restoration plan (without DG islanding) can

pick 2984.16 kW of loads (see Table 6.1). When DG islanding is allowed, the optimal restoration plan is able to pick up additional loads restoring a total of 3465 kW. In this case, the optimal restoration plan includes island formation using DGs in feeders F-c and F-d (see Table 6.2).

6.3.2 Restoration During an Extreme Event

In this section, we demonstrate the effectiveness of the proposed approach during extreme event scenarios. Multiple case studies discussed below demonstrate the applicability of the proposed optimization-based restoration algorithm in supplying critical loads using all available feeder resources, including grid-forming DGs.

DG Islanding and Impact of Tie Switches

We simulate an extreme event scenario resulting in a substation fault that disconnects all feeders from the main grid. Thus, all customers within the test system experience a loss of electric power supply. Besides, we also assume that multiple distribution lines are damaged due to the extreme event scenario (see Figure 6.4). In this case, the goal is to optimally utilize the DGs to restore the power supply for the critical loads. Here, due to capacity limits of DGs, we have prioritized the restoration of critical loads over non-critical loads. The critical load zones are represented by green patches in Figure 6.4. Using the proposed approach, the available DGs form self-sustained islands by picking up the critical loads with higher priority. Four different islands are formed where each DG picks up the priority loads based on respective operational and connectivity constraints (see Figure 6.4). On average, it takes 12.23 seconds to obtain a feasible restoration plan.

To demonstrate the performance of the proposed restoration approach, we further perform the following case studies: Case I with no tie switches and Case II with all seven tie switches available for restoration. The results for both cases are shown in Figure 6.5. For the case without engaging tie-switches, each DG only restores the critical loads in their own feeders. A total weighted load of 6734.265 kW is restored in the network. Note that the critical loads in F-a and F-d are not restored as paths between the respective DGs and loads are disrupted due to faults

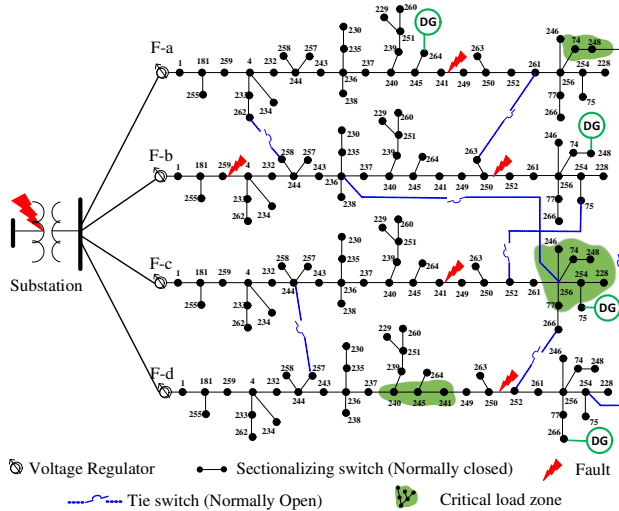


Figure 6.4: Test distribution system after a major disaster. The substation is at fault and multiple distribution system components are damaged [119].

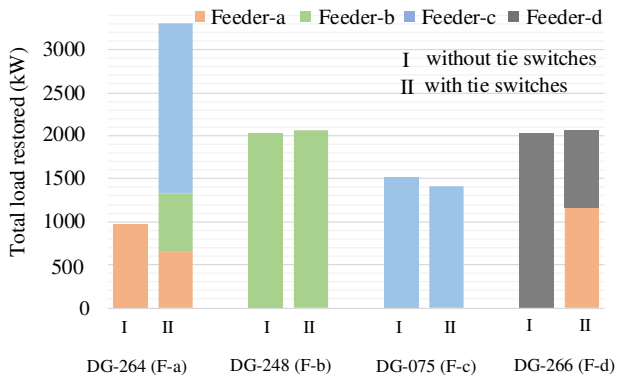


Figure 6.5: Total load picked up by each DG in different feeders for a given disaster scenario in Figure 6.4. In case II, DG at a particular feeder restores loads in another feeder by increasing its operational boundary using tie switches [119].

within the distribution system (see Figure 6.4). Also, due to the limited capacity of DG, the critical load in F-c is only partially restored. On the contrary, DG-264 in F-a has unused excess capacity. In this case, the unavailability of the paths from DGs to critical loads makes it impossible

to supply all critical loads. In Case II, all seven tie switches are engaged in the restoration process. Unlike the previous case, the DGs are able to expand their electrical boundaries forming larger islanded networks with the help of tie switches (see Fig 6.5). In this case, the total amount of restored load increases to 9130.11 kW. Thus, tie switches help better restore critical services by providing added operational flexibility.

Next, to further assess the performance of the proposed approach, we simulate several random faults within the distribution network and obtain optimal restoration plans. The simulated scenarios mimic the varying damage severity in the distribution system during the disaster condition. Specifically, five different scenarios are simulated where, randomly, the following number of lines are assumed to be damaged in the distribution system: 5, 10, 15, 20, and 25. The total load restored based on the optimal restoration plan for each case and with and without tie switches are shown in Figure 6.6. It is observed that DGs prove to be less effective in restoring critical loads as the physical damage in the distribution system increases. This is because damage in the distribution system renders the priority loads unreachable by DGs, reducing the restoration performance. As expected, well-placed tie switches are able to increase the restored loads by leveraging alternate restoration paths (See Figure 6.6). These simulation results validate that the restoration performance is improved in post-disaster conditions using active islanding methods and with the help of tie switches.

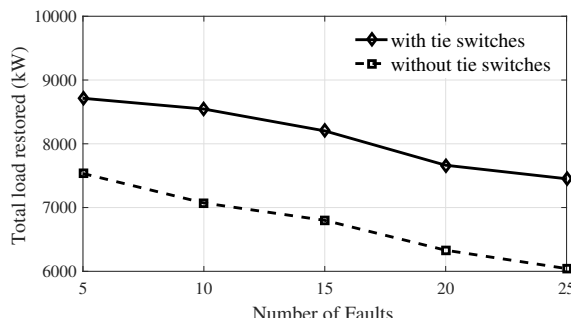


Figure 6.6: Impact of damages on restoration plan (random faults simulated with and without considering tie switches) [119].

6.4 GridAPPS-D Integration of FLISR Application

The acceptance of advanced applications by the utility companies requires a rigorous proof-of-concept regarding the ease of integration within the Advanced Distribution Management System (ADMS) environment and their benefits to the industry [41]. In what follows, we demonstrate the development and integration of a model-based FLISR with the proposed DG-assisted Restoration algorithm within an ADMS environment [120]. The proposed application is implemented on the GridAPPS-D platform – an open-source, standards-based platform designed to support the development of advanced distribution systems applications developed by the Pacific Northwest National Laboratory (PNNL) [92]. The GridAPPS-D platform provides a control and communication-rich environment to develop and demonstrate advanced distribution systems applications that integrate DGs, microgrids, alternate control strategies, and diverse model-based and data-driven algorithms.

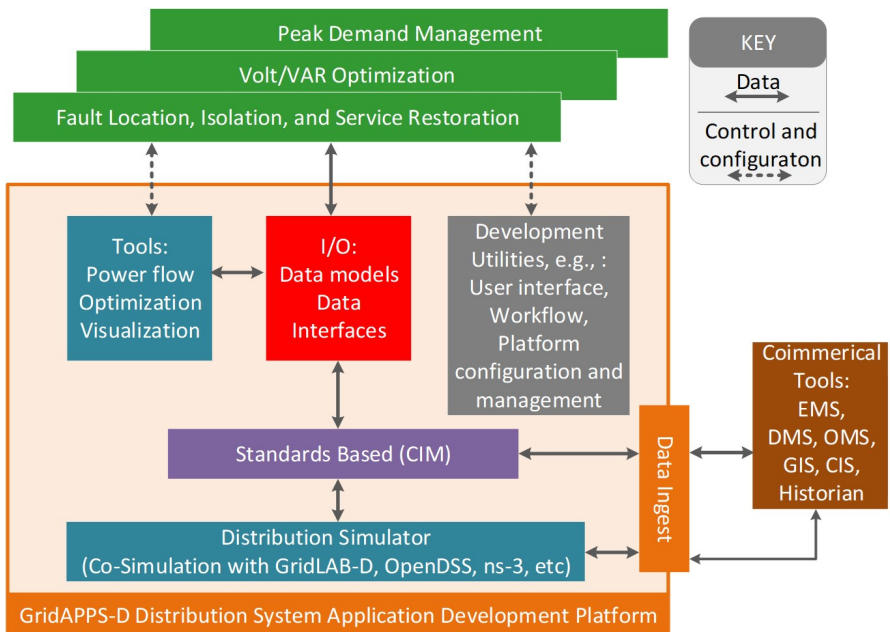


Figure 6.7: GridAPPS-D Platform [92].

Figure 6.7 depicts the logical functionality and conceptual architecture of the GridAPPS-D platform in relation to the application developer and commercial tools. The platform utilizes two different classes of data flow; 1) “Control” and configuration data enabling the application developer to manage the platform (dashed line) and 2) network and real-time measurement data specific to an application (solid line). Here, “Data Ingest” module provides the ability to exchange data with the existing sub-systems such as energy management systems (EMS), OMS, GIS, data historians, and so forth. The key feature of this framework is standards-based data representation using a common information model (CIM) thus providing application developers with a standardized approach to data. With these functionalities, GridAPPS-D supports the full suite of distribution management applications, such as voltage and reactive power optimization, fault location isolation and service restoration, economic dispatches, and optimization routines.

The platform currently runs in a Linux virtual machine through docker containers [39]. The application is started and run through the browser interface. Figure 6.8 shows the visualization of the test feeder currently running on the platform. Additionally, to visualize the topology of the feeder, the platform also allows the user to plot complex power flow in all AC line segments (VA), phase to neutral voltage (PNV) at each node, and regulator tap or switch status (Pos). The tabs show different functionalities of the platform such as simulation, events, and application. The “Events” tab shows if any event is currently active in the test system and the “Applications” tab shows the name of the application currently running on the platform. The alarm tab shows if any action has taken place to toggle the devices such as a switch, capacitor, and regulator taps. Simulation status allows the operator to see whether the actions are well carried out and verify if the application is running smoothly.

6.4.1 Fault Location Isolation and Service Restoration (FLISR)

A FLISR application performs three related actions to restore the power supply after an outage: locate the fault using triggered protection devices and smart meter pings or customer calls, isolate the fault by opening

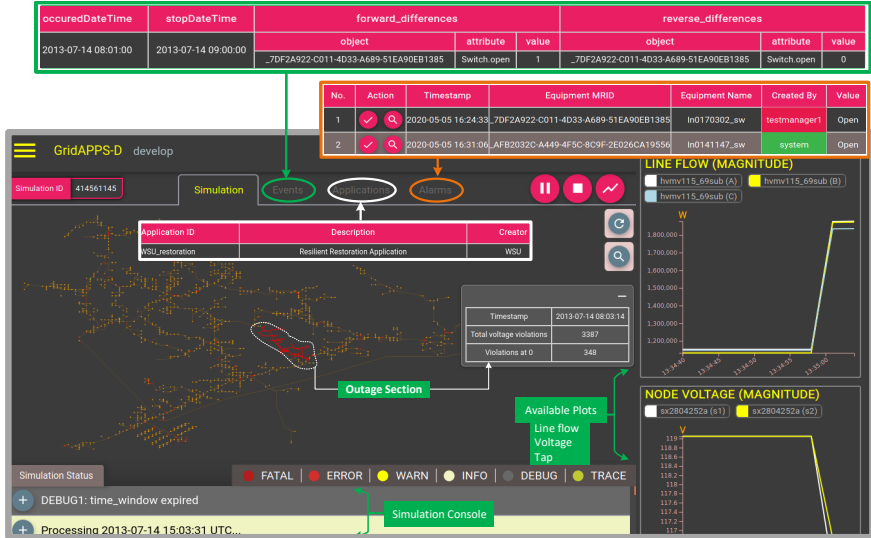


Figure 6.8: Modified IEEE 8500-node running in the platform [120].

the appropriate switching devices, and restore the power supply to the healthy feeders using feeder reconfiguration and intentional islanding using DERs. The overall architecture of the proposed FLISR application is shown in Figure 6.9. Kindly refer to [120] for additional details on each module.

The realization of an autonomous FLISR application requires measurement and control-rich environment that provides post-fault situational awareness and the ability to remotely deploy the decisions for restoration. A successful deployment relies on the ADMS that enables real-time communication and data exchange between the several sub-systems employed by the distribution companies to 1) provide distribution system condition monitoring during normal and outaged conditions, 2) obtain the statuses of available network components and grid resources, and 3) estimate the load demand and their priorities. The figure depicts a schematic for the interactions among the distribution system's operational sub-system to enable the proposed FLISR application.

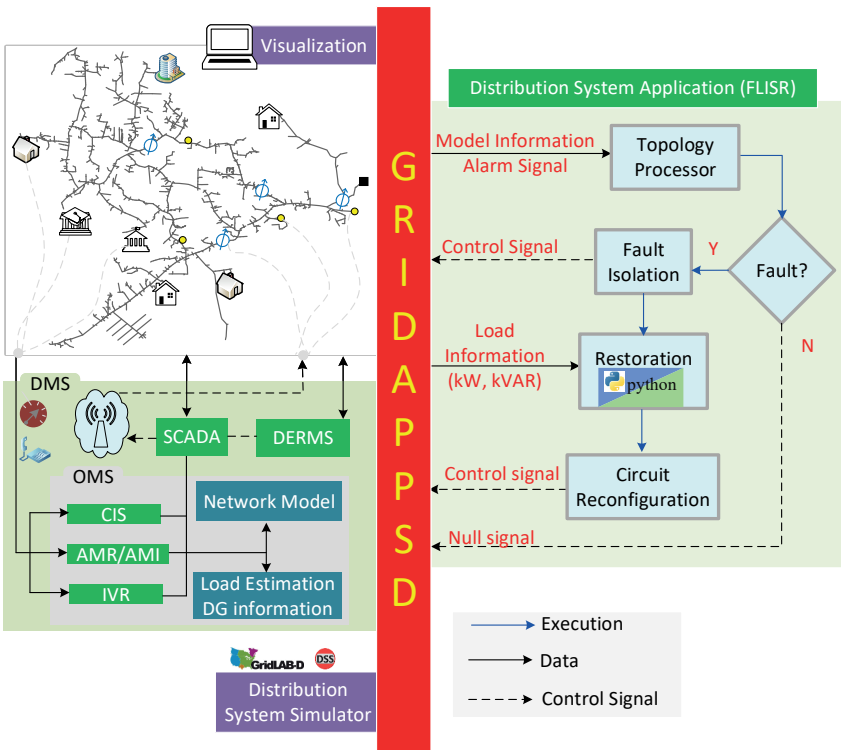


Figure 6.9: FLISR architecture on the GridAPPS-D platform and integration of proposed application to the GridAPPS-D platform. GOSS/FNCS is the PNNL's platform for data exchange among subsystems. GOSS: GridOPTICS Software System; FNCS: Framework for network simulation [120].

The FLISR architecture is deployed in GridAPPS-D platform. This requires integrating other related data and decision-support systems such as DERMS, SCADA, OMS, GIS, AMI, CIS. In the GridAPPS-D platform, a “Data Ingest” provides the ability to exchange data with the existing systems/sub-systems. The information required by an application is obtained via executing relevant queries on the GridAPPS-D platform. Here, the Grid Optics Software System (GOSS) is used to manage the platform data and the message bus, while the Framework for Network Co-simulation (FNCS) handles the time clock and the message traffic between platform and application [32], [54], [57]. In

the GridAPPS-D platform, the network data originates from a three-phase unbalanced distributor simulator driven by GridLAB-D. The information collection and processing is done with a relevant query from the platform. For sending control signals, JSON files are created based on the attributes and device types. Kindly refer to [120] for additional details regarding the information collection and dispatch of the control commands in the GridAPPS-D platform.

6.4.2 GridAPPS-D Integration and Case Studies

The proposed FLISR application is tested on the modified IEEE 8500-node test system [102] (see Figure 6.10). The D-Net library [114] allows modeling power distribution networks and constructing an optimization problem as described in Section 3. The simulation is carried out on a PC of Intel Core i7-6700 @ 3.4 GHz processor with 16 GB RAM. The FLISR application is developed in a python programming language where optimization for service restoration is modeled and solved using PuLP's modeling functions, which will then call a solver [113], [115].

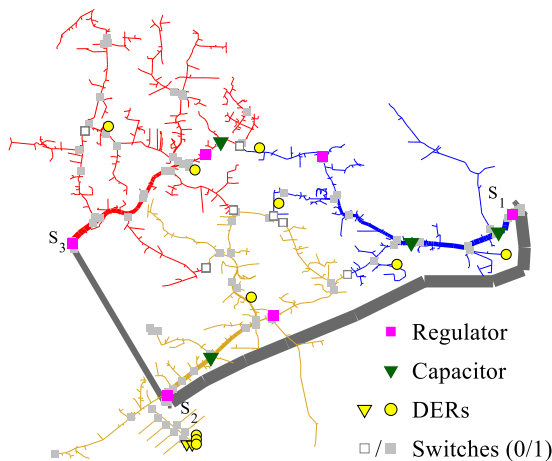


Figure 6.10: IEEE 9500-node test case. Different color lines indicate part of three feeders (s_1 , s_2 , and s_3) [120].

The performance of the application is tested using multiple test scenarios. Here, we demonstrate one specific scenario with multiple faults

including a substation outage requiring intentional islanding using grid-forming DGs. Three different faults are simulated including one near S_1 (See Figure 6.11a). In response, the three nearest upstream switches are tripped. Additionally, the DGs in the isolated area are switched off. All the customers supplied by S_1 and a few by S_2 are out of service as shown in Figure 6.11b. With these actions, there is an outage area that consists of 316 customers. Upon triggering the FLISR application, the three faults are isolated by opening 4 different switches. Once isolation is done, restoration algorithm finds the candidate switches to operate in order to restore service in the outage area. Three tie switches are closed such that a portion of S_1 is supplied from S_3 and S_2 whereas the outage section of S_2 is restored by itself. In addition to the feeder reconfiguration, two intentional islands are formed supplied by two DGs with the grid-forming capability to restore the critical loads in their neighborhood (see Figure 6.11c). Diesel generator restores 10 customers including one big critical load at node “L3234149”. Similarly, the LNG engine restores 9 customers by forming an island. With these switching actions and DG control signals, 166 out of 316 customers are restored. 166 customers observe an outage for around 4 minutes only while the remaining 150 customers are not supplied until the faults are repaired.

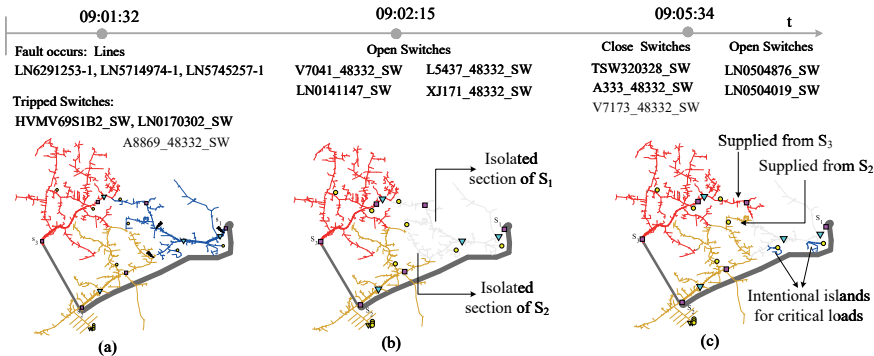


Figure 6.11: Simulation of an example event. The colored segments represent the substation they belong to. (a) Fault at several lines, (b) Isolated area because of fault, and (c) Isolated area supplied by closing two tie switches from s_2 and s_3 and islanding of two DGs [120].

6.5 Summary and Discussions

Distribution system restoration (DSR) is a critical application to ensure the growing service reliability and resilience expectations from the increasingly complex power distribution systems. In this section, we introduced a D-OPF formulation for the restoration of a large-scale three-phase unbalanced power. The approach actively integrates DGs into restoration to support intentional islands and improve resilience during extreme event scenarios. It is demonstrated that the proposed optimization-based DSR module can effectively maximize the total load restored using all available resources, including DGs. Additionally, the formulation can handle multiple sources (feeders or DGs) without significantly increasing the computational complexity. A DG-supplied intentional island that is formed in the aforementioned restoration approach can be thought of as a small single-source microgrid employed to restore additional critical loads during an extreme event. In this case, a single grid-forming resource operates in isochronous mode and maintains a stable islanded operation. The DG used for restoration can be clean or fossil-fuel-based generators as long as they can operate in isochronous mode.

The emerging smart grid technologies, such as remote-controlled switches and DG islanding, pose additional complexity to the service restoration problem, especially under cold load pick-up (CLPU) conditions. Thus, the sequence of operation for the complete restoration and recovery process needs to be studied to better execute these advanced algorithms with due consideration to DG energization and CLPU events. Additional work is needed to synchronize multiple DG-assisted islands and connect those to the grid. Such advanced restoration mechanisms require managing intentional island supplied by multiple grid-forming/grid-supporting DGs. Possible solutions include using distributed/decentralized secondary controller that is collocated with the grid-forming DGs and used for voltage and frequency restoration to enable the formation and operation of such multi-source dynamically formed islands. These and associated concerns have been addressed in some recent work. Kindly refer to [117], [126] for additional details.

7

Conclusions and Future Directions

With the advancement in smart grid technology and increasing penetrations of distributed generators (DGs), the electric power distribution system is rapidly transforming into an active network with bidirectional power flow. Massive penetrations of uncertain, variable, and DGs at the grid-edge (medium and low voltage power distribution systems) greatly threaten the power grid's reliability and resilience. Maintaining the integrity of the power grid under adverse and highly uncertain operating conditions requires novel grid management and response strategies. Consequently, power grid optimization has drawn significant attention at distribution levels. The literature on OPF formulations from the bulk power grid/transmission systems is not directly applicable to the distribution systems because of radial feeders, high R/X ratio, and large variations in bus voltage magnitudes. Consequently, several researchers have proposed distribution OPF (D-OPF) formulations. This monograph introduced multiple D-OPF formulations and the approach to cast distribution systems applications as D-OPF problem. The monograph also discussed the applications of D-OPF, for example, where DGs/DERs are used for provisioning grid services.

Although significant efforts have been made, a combination of fundamental challenges needs addressing to optimally manage distribution-connected millions of controllable grid-edge resources. In what follows, we summarize some emerging topics and future research directions.

7.1 Algorithmic Challenges with Grid-Edge Optimization

The grid-edge optimization problem, which requires real-time control and coordination of numerous DERs/DGs, is not amenable to the current optimization algorithms. To make matters even more difficult, the problem's nonconvexity, heterogeneity, and variety of control modes make it even more difficult to develop scalable optimization models for grid-edge optimization. Additional challenges arise when incorporating various grid-edge technologies, such as smart inverters, battery energy storage systems, secondary voltage controllers, and so on, that introduce integer variables into the underlying optimization problem. Furthermore, grid-edge resources introduce uncertainties as a result of a lack of appropriate models and data or limited forecasting capability (solar/wind generation), which should be systematically incorporated into the optimization framework. This calls for computationally tractable models for large-scale optimization under uncertainty. The intertemporal constraints resulting from the optimization of battery energy resources require a multi-time period formulation, further increasing the problem scale, especially under uncertainty. Given the size and complexity of the grid-edge optimization problem, it may be prudent to divide it into smaller subproblems and employ reasonable approximations. It may also be beneficial to use distributed or hierarchical optimization to reduce the computing requirements on the central agent.

7.1.1 Scalable D-OPF Models

D-OPF models have been based mainly on two power flow formulations: the bus injection model (BIM) and the branch flow model (BFM). Although the bus injection model applies to general radial/mesh feeders, the branch flow model is more suitable for modeling radial distribution feeders. Both BIM and BFM-based D-OPF models in their original

form are non-convex and non-linear programming problems (NLP); they are, therefore difficult to solve. To address this concern, several relaxed models have been proposed in the literature that tackle the problem of non-convexity using convex relaxation techniques or linear approximation methods. The convex relaxations result in an SDP or SOCP formulation that is of reduced complexity compared to the non-linear D-OPF model. However, the conditions for the exactness of the solution obtained from the relaxed models warrant further analysis. Specifically, the relaxed D-OPF model (SDP or SOCP) may yield AC-infeasible solutions. This motivates the evaluation of the existing formulations for AC feasibility using standard distribution feeders for different objective functions and operational scenarios. A recent work presents the numerical evaluation of the performance of these formulations with different choices of objective functions and network sizes [67]. This paper also provides interesting visualization to understand the solution space for different approximate/relaxed D-OPF models. Finally, as most of the relaxed problems for unbalanced D-OPF were found to be AC-infeasible, several iterative algorithms have also been proposed to obtain AC-feasible solutions, for example, [66], [68].

Conventionally, Volt/VAr regulation is achieved through control of legacy grid devices such as on-load tap changers (OLTCs), voltage regulators (VRs), and switched capacitors. However, with the inclusion of legacy devices, the DOPF problem renders a mixed-integer non-linear programming (MINLP); therefore, it is not scalable [148]. The computational complexity of MINLP Volt/VAr optimization problems is reduced in several ways. For example, in [84] only one LTC at the substation transformer is considered; however, this is valid only for European systems as multiple LTCs are common in North American feeders. Integer variables are relaxed in [15], [36], [108], [123] and rounding heuristics are used in [36], [108] to obtain discrete settings of the LTCs and CAPs. However, rounding heuristics are combinatorial in nature that prohibit scalability. A linear grid model is used in [99] to reduce computational complexity, which renders the Volt/VAr optimization as a MILP problem. In [84], [134], [153], computational efficiency of second-order cone programming (SOCP) is leveraged along with integer control of LTCs, which makes the resulting mixed-integer SOCP (MISOCP) Volt/VAr

optimization problem better tractable than the MINLP counterpart [134]. Similarly, in [3] integer LTC variables are added to a Semi-definite Programming (SDP) OPF which makes the resulting problem mixed-integer SDP (MISDP). However, the state-of-the-art methods [3], [84], [99], [108], [123], [134] on the optimal dispatch of discrete LTCs and CAPs are demonstrated using small feeders only.

7.1.2 Distributed Algorithms for Scalability

Another approach to scaling D-OPF problems for large feeders is to use decomposition approaches such as the Augmented Lagrangian Method (ALM) and its variant, the Alternating Direction Method of Multipliers (ADMM) [24], [95]. In a series of early papers, Baldick *et al.* [9], [75], [76] applied a linearized ALM to a regional decomposition of ACOPF. Peng and Low applied ADMM to certain convex relaxations of ACOPF on radial networks [110]–[112]. Along with computational advantages, the distributed methods can be used to coordinate the decisions of physically distributed agents, provide added robustness to single-point failure, and reduce communication overheads [125]. However, the generic distributed optimization algorithms, such as ADMM, do not guarantee convergence for a general nonconvex optimization problem. Specific to the D-OPF problem, the existing methods require a large number of message-passing rounds among the agents (on the order of 10^2 – 10^3) to converge for a single-step optimization [90], [93]. When used for distributed coordination, many communication rounds or message-passing events among distributed agents increase the time of convergence (ToC) and result in significant delays in decision-making. Some of these challenges are mitigated using distributed online controllers; however, they also take several time steps to track the optimal decisions [14], [19], [60], [121]. To address these challenges, a recent work developed a distributed algorithm for the optimization of radial distribution systems based on the equivalence of networks principle [124], [125]. The use of problem structure in our distributed algorithm results in a significant reduction in the number of message-passing rounds needed to converge to an optimal solution by orders of magnitude ($\sim 10^2$). This results in significant advantages over the generic application of distributed optimization

techniques for distributed computing or distributed coordination in radial power distribution systems. Additional work is needed on problem-specific decomposition for even more difficult D-OPF problems, such as with multi-period optimization and optimization under uncertainty.

7.2 Learning-for-Control for DGs/DERs Coordination

With the growing complexity and scale of grid-edge, the use of mathematical optimization approaches is limited as they are slow and do not scale well especially when optimizing under uncertainty. Another major limitation of optimization-based approaches is the need for the frequent state information for the entire distribution system, which is cost-prohibitive. Given the challenges of purely model-based optimization methods, data-driven model-free reinforcement learning (RL) approaches have recently emerged as an attractive alternative to solving distribution-level OPF problems. A detailed survey summarizing the applications of RL methods in power grid operation and control is provided in [51], [157]. These methods learn scalable operational strategies from interactions with a system-like simulation model driven by a large amount of operating data that can be further utilized for optimizing in new operating conditions. RL methods present great improvements in solving complex multivariate systems and have been employed in various power system optimization problems, such as electricity market planning, household control, battery energy arbitrage, and scheduling the charging of electric vehicles, emergency control, demand control and system restoration [45], [144]. One of the applications of deep RL that has lately gained a lot of interest is the voltage regulation of the distribution systems [27], [28], [38], [62], [136], [139], [145], [147], [154], [158], [159]. Specifically, deep RL has been utilized to control capacitors, voltage regulators, and smart inverters to regulate voltages and reduce power losses. Unfortunately, existing model-free RL algorithms ignore the crucial information embedded in the physics-based model of the power distribution systems and may thus compromise the optimizer performance and pose scalability challenges. In more recent works, including power systems model information in neural networks has shown to improve the performance of the OPF problems [31], [82]. Another

recent work uses imitation learning algorithms to speed up the RL training using model-based approximate D-OPF solutions [79]. The synergistic integration of physics-based information into data-driven approaches is an active area of research in power grid optimization.

7.3 Open-source Grid Optimization Packages/Simulator Interface

A significant gap exists between the theory and implementation of power grid optimization techniques, which is exacerbated by the integration of grid-edge technologies. The lack of extensive benchmarking of existing algorithms using real-world systems and scenarios poses a major challenge to technology adoption, especially at the distribution level. Addressing this challenge requires open-source grid optimization packages and their seamless integration with open-source power grid simulators and/or emulators. Recent work addressed these challenges by developing libraries for common D-OPF algorithms using centralized optimization techniques on the Julia platform [48]. Parallel and distributed computing architectures are more promising than centralized methods for scalable optimization. However, their adoption by the power systems community requires appropriate open-source toolkits that can demystify algorithm development in a high-performance computing (HPC) environment. However, the ongoing efforts in this domain have been limited to bulk grid optimization. For example, the DOE-funded initiative, ExaSGD, is developing highly parallel algorithms to solve security-constrained OPF problems for the bulk transmission grid. Likewise, the development of the Exascale Grid Optimization toolkit (ExaGO) for solving large-scale transmission grid optimization problems on parallel and distributed architectures is promising for scalable OPF development and adoption. The existing literature, however, lacks open-source toolkits for grid-edge optimization that can leverage emerging massively parallel architecture such as GPUs.

Likewise, within the learning for control paradigm and the use of RL for grid-edge control, the existing work includes specialized frameworks to model the power system's simulation environment and the interface to the RL library. To this end, each RL implementation requires specialized wrappers for the specific power grid environment

that are not available open-source. Thus, research in this domain is hindered by the unavailability of a suitable open-source wrapper to allow seamless integration of open-source RL libraries with open-source distribution system simulators such as OpenDSS. Some recent efforts have been made to address this challenge. For example, the work in [61] from PNNL presents an open-source platform called Reinforcement Learning for Grid Control (RLGC) for RL applications in power system controls. This tool (RLGC) uses InterPSS as a power system simulator and a Java program as a control module, and the RL algorithms are from OpenAI Gym. Py4J works as a communication between Python and Java. Another recent work develops an open-source OpenDSS-RL wrapper that serves as a user-friendly and readily available tool with minimal customization for the researchers interested in exploring the applications of RL algorithms for power distribution systems [80]. This open-source platform interfaces the OpenAI gym environment (an open-source repository for RL algorithms) with OpenDSS (an open-source distribution system simulator), enabling the seamless application of reinforcement learning (RL) algorithms for power distribution systems using a standardized environment. Additional efforts are needed to seamlessly interface the vast open-source library of machine learning algorithms to power grid simulators.

Acknowledgements

The authors would gratefully acknowledge financial support from several funding agencies that made this research and archival work possible:

- National Science Foundation (NSF) under grant number ECCS #1944142,
- National Science Foundation (NSF) under grant number ECCS #2001732,
- U.S. Department of Energy and Pacific Northwest National Lab (PNNL) under Contract DE-AC05-76RL01830,
- U.S. Department of Energy’s Office of Energy Efficiency and Renewable Energy (EERE) under the Solar Energy Technologies Office Award Number DE-EE0008774,
- U.S. Department of Energy’s Advanced Research Projects Agency-Energy (ARPA-E) grant DE-AR0000694,
- Department of Energy National Nuclear Security Administration under Award Number DE- NA0004016,
- U.S. Department of Energy and Electric Power Research Institute under the project titled “Grid Ready Energy Analytics Training (GREAT) with Data”.

Several sections of this monograph are part of years of research and experimentation work conducted by the authors’ students. Specifically, the authors would like to acknowledge:

- Dr. Rahul Ranjan Jha (General Engineer at ComEd) for his contribution on unbalanced D-OPF models, algorithm development, and applications to Conservation Voltage Reduction and Volt-VAR optimization (Sections 3 and 5).
- Dr. Shiva Poudel (Research Engineer at PNNL) for his contribution on resilient distribution system operations and applications to power distribution system restoration (Section 6).
- Dr. Rabayet Sadnan (Reserach Engineer at PNNL) for his contributions to scaling unbalanced D-OPF models using distributed algorithms (Sections 3 and 7).
- Dr. Mohammad Ostadijafari (Software Engineer at GE Digital) for his contribution on control and coordination of grid-edge resources for demand response from Grid-interactive Efficient Buildings (Section 7)
- Dr. Alper Savasci (Florida International University) for his contributions on mixed-integer DOPF formulation and numerical studies (Section 4)
- Ms. Adedoyin Inaojai (PhD Student, Florida International University) for her contributions on mixed-integer DOPF formulation and numerical studies (Section 4), and Battery Energy Storage Model (Section 2).

Dubey acknowledges her collaborators Dr. Chen-Ching Liu, Dr. Anjan Bose, and Dr. Kevin Schneider for numerous discussions and their contributions on multiple related peer-reviewed research articles. Paudyal acknowledges collaboration with Dr. Sukumar Kamalasadan (University of North Carolina Charlotte) within a sponsored project (DE-EE0008774), and with Dr. Mads Almassalkhi (University of Vermont) within a sponsored project (DE-AR0000694).

References

- [1] Y. P. Agalgaonkar, B. C. Pal, and R. A. Jabr, “Distribution voltage control considering the impact of pv generation on tap changers and autonomous regulators,” *IEEE Transactions on Power Systems*, vol. 29, no. 1, 2014, pp. 182–192. doi: [10.1109/TPWRS.2013.2279721](https://doi.org/10.1109/TPWRS.2013.2279721).
- [2] H. Ahmadi and J. R. Martí, “Linear current flow equations with application to distribution systems reconfiguration,” *IEEE Transactions on Power Systems*, vol. 30, no. 4, 2015, pp. 2073–2080.
- [3] I. Alsaleh, L. Fan, and M. Ma, “Mixed-integer sdp relaxation-based volt/var optimization for unbalanced distribution systems,” in *2019 IEEE Power Energy Society General Meeting (PESGM)*, pp. 1–5, 2019.
- [4] I. Alsaleh and L. Fan, “Multi-time co-optimization of voltage regulators and photovoltaics in unbalanced distribution systems,” *IEEE Transactions on Sustainable Energy*, vol. 12, no. 1, 2021, pp. 482–491. doi: [10.1109/TSTE.2020.3007045](https://doi.org/10.1109/TSTE.2020.3007045).
- [5] K. B. Ardani, E. O’Shaughnessy, and P. D. Schwabe, “Coordinating distributed energy resources for grid services: A case study of pacific gas and electric,” 2018.

- [6] Australia's OpEN project, *Open Energy Networks, An Energy Networks Australia and AEMO joint project*, 2022. URL: <https://www.energynetworks.com.au/projects/open-energy-networks/#open-reports-and-publications>.
- [7] X. Bai and H. Wei, "Semi-definite programming-based method for security-constrained unit commitment with operational and optimal power flow constraints," *IET Generation, Transmission Distribution*, vol. 3, no. 2, Feb. 2009, pp. 182–197. DOI: [10.1049/iet-gtd:20070516](https://doi.org/10.1049/iet-gtd:20070516).
- [8] X. Bai, H. Wei, K. Fujisawa, and Y. Wang, "Semidefinite programming for optimal power flow problems," *International Journal of Electrical Power & Energy Systems*, vol. 30, no. 6, 2008, pp. 383–392. URL: <https://www.sciencedirect.com/science/article/pii/S0142061507001378>.
- [9] R. Baldick, B. H. Kim, C. Chase, and Y. Luo, "A Fast Distributed Implementation of Optimal Power Flow," *IEEE Transactions on Power Systems*, vol. 14, no. 3, 1999, pp. 858–864. DOI: [10.1109/59.780896](https://doi.org/10.1109/59.780896).
- [10] M. Baran and F. F. Wu, "Optimal sizing of capacitors placed on a radial distribution system," *IEEE Transactions on Power Delivery*, vol. 4, no. 1, 1989, pp. 735–743.
- [11] M. Baran and F. Wu, "Network reconfiguration in distribution systems for loss reduction and load balancing," *IEEE Transactions on Power Delivery*, vol. 4, no. 2, 1989, pp. 1401–1407. DOI: [10.1109/61.25627](https://doi.org/10.1109/61.25627).
- [12] M. E. Baran and M.-Y. Hsu, "Volt/var control at distribution substations," *IEEE Transactions on Power Systems*, vol. 14, no. 1, 1999, pp. 312–318.
- [13] A. K. Barnes, V. Martinelli, and J. Simonelli, "A local voltage regulator that improves energy savings under advanced volt-var control," in *2014 IEEE PES T&D Conference and Exposition*, pp. 1–5, 2014. DOI: [10.1109/TDC.2014.6863259](https://doi.org/10.1109/TDC.2014.6863259).
- [14] N. Bastianello, A. Ajalloeian, and E. Dall'Anese, "Distributed and inexact proximal gradient method for online convex optimization," *arXiv preprint arXiv:2001.00870*, 2020.

- [15] M. Bazrafshan, N. Gatsis, and H. Zhu, “Optimal power flow with step-voltage regulators in multi-phase distribution networks,” *IEEE Transactions on Power Systems*, vol. 34, no. 6, 2019, pp. 4228–4239.
- [16] M. Bazrafshan and N. Gatsis, “Comprehensive modeling of three-phase distribution systems via the bus admittance matrix,” *IEEE Transactions on Power Systems*, vol. 33, no. 2, 2017, pp. 2015–2029.
- [17] A. Bernstein, C. Wang, E. Dall’Anese, J. Le Boudec, and C. Zhao, “Load flow in multiphase distribution networks: Existence, uniqueness, non-singularity and linear models,” *IEEE Transactions on Power Systems*, vol. 33, no. 6, 2018, pp. 5832–5843. DOI: [10.1109/TPWRS.2018.2823277](https://doi.org/10.1109/TPWRS.2018.2823277).
- [18] A. Bernstein and E. Dall’Anese, “Linear power-flow models in multiphase distribution networks,” in *2017 IEEE PES Innovative Smart Grid Technologies Conference Europe (ISGT-Europe)*, IEEE, pp. 1–6, 2017.
- [19] A. Bernstein and E. Dall’Anese, “Real-time feedback-based optimization of distribution grids: A unified approach,” *IEEE Transactions on Control of Network Systems*, vol. 6, no. 3, 2019, pp. 1197–1209.
- [20] A. Bokhari, A. Alkan, R. Dogan, M. Diaz-Aguiló, F. de León, D. Czarkowski, Z. Zabar, L. Birenbaum, A. Noel, and R. E. Uosef, “Experimental determination of the ZIP coefficients for modern residential, commercial, and industrial loads,” *IEEE Transactions on Power Delivery*, vol. 29, no. 3, Jun. 2014, pp. 1372–1381. DOI: [10.1109/TPWRD.2013.2285096](https://doi.org/10.1109/TPWRD.2013.2285096).
- [21] A. Bokhari, A. Raza, M. Diaz-Aguiló, F. de León, D. Czarkowski, R. E. Uosef, and D. Wang, “Combined effect of CVR and DG penetration in the voltage profile of low-voltage secondary distribution networks,” *IEEE Transactions on Power Delivery*, vol. 31, no. 1, Feb. 2016, pp. 286–293. DOI: [10.1109/TPWRD.2015.2422308](https://doi.org/10.1109/TPWRD.2015.2422308).

- [22] S. Bolognani and S. Zampieri, “On the existence and linear approximation of the power flow solution in power distribution networks,” *IEEE Transactions on Power Systems*, vol. 31, no. 1, Jan. 2016, pp. 163–172. DOI: [10.1109/TPWRS.2015.2395452](https://doi.org/10.1109/TPWRS.2015.2395452).
- [23] S. Bolognani and F. Dörfler, “Fast power system analysis via implicit linearization of the power flow manifold,” in *2015 53rd Annual Allerton Conference on Communication, Control, and Computing (Allerton)*, IEEE, pp. 402–409, 2015.
- [24] S. Boyd, N. Parikh, E. Chu, B. Peleato, and J. Eckstein, “Distributed optimization and statistical learning via the alternating direction method of multipliers,” *Foundations and Trends® in Machine Learning*, vol. 3, no. 1, 2011, pp. 1–122. DOI: [10.1561/2200000016](https://doi.org/10.1561/2200000016).
- [25] S. Bruno, S. Lamonaca, G. Rotondo, U. Stecchi, and M. La Scala, “Unbalanced three-phase optimal power flow for smart grids,” *IEEE Transactions on Industrial Electronics*, vol. 58, no. 10, 2011, pp. 4504–4513. DOI: [10.1109/TIE.2011.2106099](https://doi.org/10.1109/TIE.2011.2106099).
- [26] M. B. Cain, R. P. O’Neill, A. Castillo, *et al.*, “History of Optimal Power Flow and Formulations,” *Federal Energy Regulatory Commission*, vol. 1, 2012, pp. 1–36.
- [27] D. Cao, W. Hu, J. Zhao, Q. Huang, Z. Chen, and F. Blaabjerg, “A multi-agent deep reinforcement learning based voltage regulation using coordinated pv inverters,” *IEEE Transactions on Power Systems*, vol. 35, no. 5, 2020, pp. 4120–4123.
- [28] D. Cao, J. Zhao, W. Hu, F. Ding, Q. Huang, Z. Chen, and F. Blaabjerg, “Data-driven multi-agent deep reinforcement learning for distribution system decentralized voltage control with high penetration of pvs,” *IEEE Transactions on Smart Grid*, 2021.
- [29] A. Castillo and D. F. Gayme, “Grid-scale energy storage applications in renewable energy integration: A survey,” *Energy Conversion and Management*, vol. 87, 2014, pp. 885–894.
- [30] A. Castillo, P. Lipka, J.-P. Watson, S. S. Oren, and R. P. O’Neill, “A successive linear programming approach to solving the IV-ACOPF,” *IEEE Transactions on Power Systems*, vol. 31, no. 4, 2016, pp. 2752–2763.

- [31] Y. Chen and B. Zhang, “Learning to solve network flow problems via neural decoding,” *arXiv preprint arXiv:2002.04091*, 2020.
- [32] S. Ciraci, J. Daily, J. Fuller, A. Fisher, L. Marinovici, and K. Agarwal, “Fnscs: A framework for power system and communication networks co-simulation,” in *Proceedings of the symposium on theory of modeling & simulation-DEVS integrative*, pp. 1–8, 2014.
- [33] D. Montenegro, J. Taylor, and R. Dugan, “Open source unified power flow controller model for quasi-static time series simulation,” in *Proc. CIGRE U.S. Nat. Committee, Grid Future Symposium, Philadelphia, PA, USA*, Nov. 2016.
- [34] E. Dall’Anese, H. Zhu, and G. B. Giannakis, “Distributed optimal power flow for smart microgrids,” *IEEE Transactions on Smart Grid*, vol. 4, no. 3, 2013, pp. 1464–1475. DOI: [10.1109/TSG.2013.2248175](https://doi.org/10.1109/TSG.2013.2248175).
- [35] E. Dall’Anese, S. V. Dhople, B. B. Johnson, and G. B. Giannakis, “Decentralized optimal dispatch of photovoltaic inverters in residential distribution systems,” *IEEE Transactions on Energy Conversion*, vol. 29, no. 4, Dec. 2014, pp. 957–967. DOI: [10.1109/TEC.2014.2357997](https://doi.org/10.1109/TEC.2014.2357997).
- [36] N. Daratha, B. Das, and J. Sharma, “Coordination between oltc and svc for voltage regulation in unbalanced distribution system distributed generation,” *IEEE Transactions on Power Systems*, vol. 29, no. 1, 2014, pp. 289–299.
- [37] S. V. Dhople, S. S. Guggilam, and Y. C. Chen, “Linear approximations to ac power flow in rectangular coordinates,” in *2015 53rd Annual Allerton Conference on Communication, Control, and Computing (Allerton)*, pp. 211–217, 2015. DOI: [10.1109/ALLERTON.2015.7447006](https://doi.org/10.1109/ALLERTON.2015.7447006).
- [38] R. Diao, Z. Wang, D. Shi, Q. Chang, J. Duan, and X. Zhang, “Autonomous voltage control for grid operation using deep reinforcement learning,” in *2019 IEEE Power & Energy Society General Meeting (PESGM)*, IEEE, pp. 1–5, 2019.
- [39] Docker, *Docker—Build, Ship and Run Any App, Anywhere*. Docker Inc., San Francisco, CA, USA. 2018.

- [40] W. Driscoll. (2018). “U.S. utilities test distributed energy management,” URL: <https://pv-magazine-usa.com/2018/12/14/u-s-utilities-test-distributed-energy-management/> (accessed on 03/03/2023).
- [41] A. Dubey, A. Bose, M. Liu, and L. N. Ochoa, “Paving the way for advanced distribution management systems applications: Making the most of models and data,” *IEEE Power and Energy Magazine*, vol. 18, no. 1, 2020, pp. 63–75.
- [42] A. Dubey and S. Santoso, “Electric vehicle charging on residential distribution systems: Impacts and mitigations,” *IEEE Access*, vol. 3, 2015, pp. 1871–1893. DOI: [10.1109/ACCESS.2015.2476996](https://doi.org/10.1109/ACCESS.2015.2476996).
- [43] A. Dubey and S. Santoso, “On estimation and sensitivity analysis of distribution circuit’s photovoltaic hosting capacity,” *IEEE Transactions on Power Systems*, vol. 32, no. 4, 2017, pp. 2779–2789. DOI: [10.1109/TPWRS.2016.2622286](https://doi.org/10.1109/TPWRS.2016.2622286).
- [44] A. Dubey, S. Santoso, and A. Maitra, “Understanding photovoltaic hosting capacity of distribution circuits,” in *2015 IEEE Power & Energy Society General Meeting*, pp. 1–5, 2015. DOI: [10.1109/PESGM.2015.7286510](https://doi.org/10.1109/PESGM.2015.7286510).
- [45] R. El Helou, D. Kalathil, and L. Xie, “Fully decentralized reinforcement learning-based control of photovoltaics in distribution grids for joint provision of real and reactive power,” *IEEE Open Access Journal of Power and Energy*, vol. 8, 2021, pp. 175–185.
- [46] M. Farivar and S. H. Low, “Branch flow model: Relaxations and convexification: Part I,” *IEEE Transactions on Power Systems*, vol. 28, no. 3, Aug. 2013, pp. 2554–2564. DOI: [10.1109/TPWRS.2013.2255317](https://doi.org/10.1109/TPWRS.2013.2255317).
- [47] M. Farivar, R. Neal, C. Clarke, and S. Low, “Optimal inverter VAR control in distribution systems with high PV penetration,” in *2012 IEEE Power and Energy Society General Meeting*, pp. 1–7, Jul. 2012. DOI: [10.1109/PESGM.2012.6345736](https://doi.org/10.1109/PESGM.2012.6345736).
- [48] D. M. Fobes, S. Claeys, F. Geth, and C. Coffrin, “Powermodels-distribution.jl: An open-source framework for exploring distribution power flow formulations,” *Electric Power Systems Research*, vol. 189, 2020, p. 106 664. DOI: <https://doi.org/10.1016/j.epsr.2020.106664>.

- [49] K. Forsten, “Green circuits: Distribution efficiency case studies,” EPRI, Palo Alto, CA: 2011. 1023518., Tech. Rep., 2011.
- [50] L. Gan and S. H. Low, “Convex relaxations and linear approximation for optimal power flow in multiphase radial networks,” in *Power Systems Computation Conference (PSCC), 2014*, IEEE, pp. 1–9, 2014.
- [51] Y. Gao and N. Yu, “Deep reinforcement learning in power distribution systems: Overview, challenges, and opportunities,” in *2021 IEEE Power & Energy Society Innovative Smart Grid Technologies Conference (ISGT)*, IEEE, pp. 1–5, 2021.
- [52] P. A. N. Garcia, J. L. R. Pereira, S. Carneiro, V. M. da Costa, and N. Martins, “Three-phase power flow calculations using the current injection method,” *IEEE Transactions on Power Systems*, vol. 15, no. 2, May 2000, pp. 508–514. DOI: [10.1109/59.867133](https://doi.org/10.1109/59.867133).
- [53] T. Gonen, *Electric power distribution engineering*. CRC press, 2015.
- [54] I. Gorton, J. Yin, B. Akyol, S. Ciraci, T. Critchlow, Y. Liu, T. Gibson, P. Sumit, S. Poorva, and M. Vlachopoulou, “Gridoptics (tm) a novel software framework for integrating power grid data storage, management and analysis,” in *2013 46th Hawaii International Conference on System Sciences*, IEEE, pp. 2167–2176, 2013.
- [55] B. Green, “Grid Strategy 2011: Conservation Voltage Reduction and Volt VAR Optimization in the Smart Grid,” EPRI, Palo Alto, CA: 2011. 1024482., Tech. Rep., 2010.
- [56] GridLAB-D. (2017). “GridLAB-D, The Next-Generation Simulation Software,” URL: <https://www.gridlabd.org/>.
- [57] GridOPTICS Software System (GOSS), *Pacific Northwest National Laboratory*. URL: <https://github.com/GRIDAPPSD/GOSS-GridAPPS-D>.
- [58] S. S. Guggilam, E. Dall’Anese, Y. C. Chen, S. V. Dhople, and G. B. Giannakis, “Scalable optimization methods for distribution networks with high PV integration,” *IEEE Transactions on Smart Grid*, vol. 7, no. 4, 2016, pp. 2061–2070.

- [59] T. T. Hashim, A. Mohamed, and H. Shareef, “A review on voltage control methods for active distribution networks,” *Electrical review*, 2012.
- [60] X. Hu, Z.-W. Liu, G. Wen, X. Yu, and C. Li, “Branch-wise parallel successive algorithm for online voltage regulation in distribution networks,” *IEEE Transactions on Smart Grid*, vol. 10, no. 6, 2019, pp. 6678–6689.
- [61] Q. Huang, R. Huang, W. Hao, J. Tan, R. Fan, and Z. Huang, “Adaptive power system emergency control using deep reinforcement learning,” *IEEE Transactions on Smart Grid*, vol. 11, no. 2, 2019, pp. 1171–1182.
- [62] R. Huang, Y. Chen, T. Yin, X. Li, A. Li, J. Tan, W. Yu, Y. Liu, and Q. Huang, “Accelerated deep reinforcement learning based load shedding for emergency voltage control,” *arXiv preprint arXiv:2006.12667*, 2020.
- [63] M. Huneault and F. Galiana, “A survey of the optimal power flow literature,” *IEEE Transactions on Power Systems*, vol. 6, no. 2, 1991, pp. 762–770. DOI: [10.1109/59.76723](https://doi.org/10.1109/59.76723).
- [64] A. Inaolaji, A. Savasci, and S. Paudyal, “Distribution grid optimal power flow in unbalanced multiphase networks with volt-var and volt-watt droop settings of smart inverters,” *IEEE Transactions on Industry Applications*, vol. 58, no. 5, 2022, pp. 5832–5843. DOI: [10.1109/TIA.2022.3181110](https://doi.org/10.1109/TIA.2022.3181110).
- [65] R. Jabr, “Radial distribution load flow using conic programming,” *IEEE Transactions on Power Systems*, vol. 21, no. 3, 2006, pp. 1458–1459. DOI: [10.1109/TPWRS.2006.879234](https://doi.org/10.1109/TPWRS.2006.879234).
- [66] R. R. Jha and A. Dubey, “Exact distribution optimal power flow (d-opf) model using convex iteration technique,” in *2019 IEEE Power Energy Society General Meeting (PESGM)*, pp. 1–5, Aug. 2019. DOI: [10.1109/PESGM40551.2019.8974080](https://doi.org/10.1109/PESGM40551.2019.8974080).
- [67] R. R. Jha, A. Inaolaji, B. D. Biswas, A. Suresh, A. Dubey, S. Paudyal, and S. Kamalasadan, “Distribution grid optimal power flow (d-opf): Modeling, analysis, and benchmarking,” *IEEE Transactions on Power Systems*, 2022, pp. 1–14. DOI: [10.1109/TPWRS.2022.3204227](https://doi.org/10.1109/TPWRS.2022.3204227).

- [68] R. R. Jha and A. Dubey, “Network-level optimization for unbalanced power distribution system: Approximation and relaxation,” *IEEE Transactions on Power Systems*, vol. 36, no. 5, 2021, pp. 4126–4139. DOI: [10.1109/TPWRS.2021.3066146](https://doi.org/10.1109/TPWRS.2021.3066146).
- [69] R. R. Jha, A. Dubey, C.-C. Liu, and K. P. Schneider, “Bi-level volt-var optimization to coordinate smart inverters with voltage control devices,” *IEEE Transactions on Power Systems*, vol. 34, no. 3, 2019, pp. 1801–1813.
- [70] X. Jiang, Y. Zhou, W. Ming, P. Yang, and J. Wu, “An overview of soft open points in electricity distribution networks,” *IEEE Transactions on Smart Grid*, vol. 13, no. 3, 2022, pp. 1899–1910. DOI: [10.1109/TSG.2022.3148599](https://doi.org/10.1109/TSG.2022.3148599).
- [71] V. Kekatos, L. Zhang, G. B. Giannakis, and R. Baldick, “Fast localized voltage regulation in single-phase distribution grids,” in *2015 IEEE International Conference on Smart Grid Communications (SmartGridComm)*, pp. 725–730, Nov. 2015. DOI: [10.1109/SmartGridComm.2015.7436387](https://doi.org/10.1109/SmartGridComm.2015.7436387).
- [72] W. H. Kersting, “Distribution system modeling and analysis,” in *Electric Power Generation, Transmission, and Distribution: The Electric Power Engineering Handbook*, CRC press, 2018, pp. 26–1.
- [73] V. Khadkikar, “Enhancing electric power quality using upqc: A comprehensive overview,” *IEEE Transactions on Power Electronics*, vol. 27, no. 5, 2012, pp. 2284–2297. DOI: [10.1109/TPEL.2011.2172001](https://doi.org/10.1109/TPEL.2011.2172001).
- [74] S. Khushalani, J. M. Solanki, and N. N. Schulz, “Optimized restoration of unbalanced distribution systems,” *IEEE Transactions on Power Systems*, vol. 22, no. 2, 2007, pp. 624–630.
- [75] B. H. Kim and R. Baldick, “Coarse-Grained Distributed Optimal Power Flow,” *IEEE Transactions on Power Systems*, vol. 12, no. 2, 1997, pp. 932–939. DOI: [10.1109/59.589777](https://doi.org/10.1109/59.589777).
- [76] B. H. Kim and R. Baldick, “A Comparison of Distributed Optimal Power Flow Algorithms,” *IEEE Transactions on Power Systems*, vol. 15, no. 2, 2000, pp. 599–604. DOI: [10.1109/59.867147](https://doi.org/10.1109/59.867147).

- [77] J. Kirk, “Count loops in a graph,” MathWorks, 2020. URL: <https://www.mathworks.com/matlabcentral/fileexchange/10722-count-loops-in-a-graph>.
- [78] D. Kovaleski. (2022). “Dominion Energy Virginia taps Generac Grid Services for distributed energy resource management,” URL: <https://dailyenergyinsider.com/news/36507-dominion-energy-virginia-taps-generac-grid-services-for-distributed-energy-resource-management/> (accessed on 03/03/2023).
- [79] G. Krishnamoorthy and A. Dubey, “Reinforcement learning for battery energy storage dispatch augmented with model-based optimizer,” *CoRR*, vol. abs/2109.01659, 2021. arXiv: [2109.01659](https://arxiv.org/abs/2109.01659). URL: <https://arxiv.org/abs/2109.01659>.
- [80] G. Krishnamoorthy, A. Dubey, and A. H. Gebremedhin, “An open-source environment for reinforcement learning in power distribution systems,” in *2022 IEEE Power & Energy Society General Meeting (PESGM)*, pp. 1–5, 2022. doi: [10.1109/PESGM48719.2022.9916862](https://doi.org/10.1109/PESGM48719.2022.9916862).
- [81] Y. Kumar, B. Das, and J. Sharma, “Service restoration in distribution system using non-dominated sorting genetic algorithm,” *Electric Power Systems Research*, vol. 76, no. 9-10, 2006, pp. 768–777.
- [82] H. Lange, B. Chen, M. Berges, and S. Kar, “Learning to solve ac optimal power flow by differentiating through holomorphic embeddings,” *arXiv preprint arXiv:2012.09622*, 2020.
- [83] J. Lei, Y. Deng, Y. He, and B. Zhang, “Network reconfiguration in unbalanced distribution systems for service restoration and loss reduction,” in *Power Engineering Society Winter Meeting, 2000. IEEE*, IEEE, vol. 4, pp. 2345–2350, 2000.
- [84] P. Li, C. Zhang, Z. Wu, Y. Xu, M. Hu, and Z. Dong, “Distributed adaptive robust voltage/var control with network partition in active distribution networks,” *IEEE Transactions on Smart Grid*, vol. 11, no. 3, 2020, pp. 2245–2256.
- [85] Q. Li and V. Vittal, “Non-iterative enhanced SDP relaxations for optimal scheduling of distributed energy storage in distribution systems,” *IEEE Transactions on Power Systems*, vol. 32, no. 3, 2017, pp. 1721–1732.

- [86] Z. Li, X. Chen, K. Yu, Y. Sun, and H. Liu, “A hybrid particle swarm optimization approach for distribution network reconfiguration problem,” in *PES GM-Conversion and Delivery of Electrical Energy in the 21st Century, 2008 IEEE*, IEEE, pp. 1–7, 2008.
- [87] C.-C. Liu, S. J. Lee, and S. Venkata, “An expert system operational aid for restoration and loss reduction of distribution systems,” *IEEE Transactions on Power Systems*, vol. 3, no. 2, 1988, pp. 619–626.
- [88] Y. Liu, J. Bebic, B. Kroposki, J. de Bedout, and W. Ren, “Distribution system voltage performance analysis for high-penetration pv,” in *2008 IEEE Energy 2030 Conference*, pp. 1–8, 2008. DOI: [10.1109/ENERGY.2008.4781069](https://doi.org/10.1109/ENERGY.2008.4781069).
- [89] S. H. Low, “Convex relaxation of optimal power flow Part II: Exactness,” *IEEE Transactions on Control of Network Systems*, vol. 1, no. 2, Jun. 2014, pp. 177–189. DOI: [10.1109/TCNS.2014.2323634](https://doi.org/10.1109/TCNS.2014.2323634).
- [90] S. Magnússon, P. C. Weeraddana, and C. Fischione, “A distributed approach for the optimal power-flow problem based on admm and sequential convex approximations,” *IEEE Transactions on Control of Network Systems*, vol. 2, no. 3, 2015, pp. 238–253.
- [91] B. McMillan, P. Guido, O. Leitermann, V. Martinelli, A. Gonzaga, and R. McFetridge, “Application of power electronics lv power regulators in a utility distribution system,” in *2015 IEEE Rural Electric Power Conference*, pp. 43–47, 2015. DOI: [10.1109/REPC.2015.15](https://doi.org/10.1109/REPC.2015.15).
- [92] R. B. Melton, K. P. Schneider, E. Lightner, T. E. Mcdermott, P. Sharma, Y. Zhang, F. Ding, S. Vadari, R. Podmore, A. Dubey, R. W. Wies, and E. G. Stephan, “Leveraging standards to create an open platform for the development of advanced distribution applications,” *IEEE Access*, vol. 6, 2018, pp. 37361–37370. DOI: [10.1109/ACCESS.2018.2851186](https://doi.org/10.1109/ACCESS.2018.2851186).
- [93] B. Millar and D. Jiang, “Smart grid optimization through asynchronous, distributed primal dual iterations,” *IEEE Transactions on Smart Grid*, vol. 8, no. 5, 2016, pp. 2324–2331.

- [94] K. N. Miu, H.-D. Chiang, and R. J. McNulty, “Multi-tier service restoration through network reconfiguration and capacitor control for large-scale radial distribution networks,” *IEEE Transactions on Power Systems*, vol. 15, no. 3, 2000, pp. 1001–1007.
- [95] D. K. Molzahn, F. Dörfler, H. Sandberg, S. H. Low, S. Chakrabarti, R. Baldick, and J. Lavaei, “A survey of distributed optimization and control algorithms for electric power systems,” *IEEE Transactions on Smart Grid*, vol. 8, no. 6, 2017, pp. 2941–2962.
- [96] D. K. Molzahn and I. A. Hiskens, “A survey of relaxations and approximations of the power flow equations,” *Foundations and Trends® in Electric Energy Systems*, vol. 4, no. 1-2, 2019, pp. 1–221. DOI: [10.1561/3100000012](https://doi.org/10.1561/3100000012).
- [97] J. Momoh, R. Adapa, and M. El-Hawary, “A review of selected optimal power flow literature to 1993. i. nonlinear and quadratic programming approaches,” *IEEE Transactions on Power Systems*, vol. 14, no. 1, 1999, pp. 96–104. DOI: [10.1109/59.744492](https://doi.org/10.1109/59.744492).
- [98] National Academies of Sciences, Engineering, and Medicine, *Enhancing the Resilience of the Nation’s Electricity System*. National Academies Press, 2017.
- [99] N. Nazir and M. Almassalkhi, “Receding-horizon optimization of unbalanced distribution systems with time-scale separation for discrete and continuous control devices,” in *2018 Power Systems Computation Conference (PSCC)*, pp. 1–7, 2018.
- [100] Y. Ngo, H. Arant, C. Bilby, and A. Grice, “Investing for the future: How small utilities are finding success with advanced distribution management systems,” *IEEE Power and Energy Magazine*, vol. 18, no. 1, 2020, pp. 34–42.
- [101] OpenDSS, *Electric Power Research Institute (EPRI), Simulation Tool-OpenDSS*, 2008.
- [102] Pacific Northwest National Laboratory (PNNL), *Gridapps-d documentation-data model*, 2021. URL: <https://gridappsd.readthedocs.io/en/master/overview/index.html>.

- [103] H. V. Padullaparti, Q. Nguyen, and S. Santoso, “Advances in volt-var control approaches in utility distribution systems,” in *2016 IEEE Power and Energy Society General Meeting (PESGM)*, pp. 1–5, Jul. 2016. DOI: [10.1109/PESGM.2016.7741366](https://doi.org/10.1109/PESGM.2016.7741366).
- [104] H. V. Padullaparti, P. Chirapongsananurak, S. Santoso, and J. A. Taylor, “Edge-of-grid voltage control: Device modeling, strategic placement, and application considerations,” *IEEE Power and Energy Technology Systems Journal*, vol. 4, no. 4, 2017, pp. 106–114. DOI: [10.1109/JPETS.2017.2750479](https://doi.org/10.1109/JPETS.2017.2750479).
- [105] H. V. Padullaparti, S. Jothibasu, S. Santoso, and G. Todeschini, “Increasing feeder pv hosting capacity by regulating secondary circuit voltages,” in *2018 IEEE Power & Energy Society General Meeting (PESGM)*, pp. 1–5, 2018. DOI: [10.1109/PESGM.2018.8586615](https://doi.org/10.1109/PESGM.2018.8586615).
- [106] H. V. Padullaparti, M. Lwin, and S. Santoso, “Optimal placement of edge-of-grid low-voltage svcs in real-world distribution circuits,” in *2017 IEEE Workshop on Power Electronics and Power Quality Applications (PEPQA)*, pp. 1–6, 2017. DOI: [10.1109/PEPQA.2017.7981646](https://doi.org/10.1109/PEPQA.2017.7981646).
- [107] H. V. Padullaparti, Q. Nguyen, and S. Santoso, “Advances in volt-var control approaches in utility distribution systems,” in *2016 IEEE Power and Energy Society General Meeting (PESGM)*, pp. 1–5, 2016. DOI: [10.1109/PESGM.2016.7741366](https://doi.org/10.1109/PESGM.2016.7741366).
- [108] S. Paudyal, C. A. Cañizares, and K. Bhattacharya, “Optimal Operation of Distribution Feeders in Smart Grids,” *IEEE Trans. on Ind. Electron.*, vol. 58, no. 10, Oct. 2011, pp. 4495–4503.
- [109] S. Paudyal, C. A. Cañizares, and K. Bhattacharya, “Three-phase distribution opf in smart grids: Optimality versus computational burden,” in *2011 2nd IEEE PES International Conference and Exhibition on Innovative Smart Grid Technologies*, pp. 1–7, Dec. 2011. DOI: [10.1109/ISGTEurope.2011.6162628](https://doi.org/10.1109/ISGTEurope.2011.6162628).
- [110] Q. Peng and S. H. Low, “Distributed Algorithm for Optimal Power Flow on a Radial Network,” in *53rd IEEE Conference on Decision and Control*, pp. 167–172, 2014. DOI: [10.1109/CDC.2014.7039376](https://doi.org/10.1109/CDC.2014.7039376).

- [111] Q. Peng and S. H. Low, “Distributed Algorithm for Optimal Power Flow on an Unbalanced Radial Network,” in *2015 54th IEEE Conference on Decision and Control (CDC)*, pp. 6915–6920, 2015. DOI: [10.1109/CDC.2015.7403309](https://doi.org/10.1109/CDC.2015.7403309).
- [112] Q. Peng and S. H. Low, “Distributed Optimal Power Flow Algorithm for Radial Networks, I: Balanced Single Phase Case,” *IEEE Transactions on Smart Grid*, vol. 9, no. 1, 2018, pp. 111–121. DOI: [10.1109/TSG.2016.2546305](https://doi.org/10.1109/TSG.2016.2546305).
- [113] S. Poudel, *GridAPPS-D Restoration Application*, 2019. URL: <https://github.com/shpoudel/WSU-Restoration>.
- [114] S. Poudel, *Network data structure of distribution feeders from OpenDSS*, 2019. URL: <https://github.com/shpoudel/D-Net>.
- [115] S. Poudel, *WSU-Restoration Application Documentation*, 2019. URL: <https://wsu-restoration.readthedocs.io/en/latest/>.
- [116] S. Poudel and A. Dubey, “Critical load restoration using distributed energy resources for resilient power distribution system,” *IEEE Transactions on Power Systems*, vol. 34, no. 1, 2019, pp. 52–63. DOI: [10.1109/TPWRS.2018.2860256](https://doi.org/10.1109/TPWRS.2018.2860256).
- [117] S. Poudel and A. Dubey, “A two-stage service restoration method for electric power distribution systems,” *IET Smart Grid*, vol. 4, no. 5, Mar. 2021. DOI: [10.1049/stg2.12021](https://doi.org/10.1049/stg2.12021).
- [118] S. Poudel, A. Dubey, and A. Bose, “Risk-based probabilistic quantification of power distribution system operational resilience,” *IEEE Systems Journal*, vol. 14, no. 3, 2020, pp. 3506–3517. DOI: [10.1109/JSYST.2019.2940939](https://doi.org/10.1109/JSYST.2019.2940939).
- [119] S. Poudel, A. Dubey, and K. P. Schneider, “A generalized framework for service restoration in a resilient power distribution system,” *IEEE Systems Journal*, vol. 16, no. 1, 2022, pp. 252–263. DOI: [10.1109/JSYST.2020.3011901](https://doi.org/10.1109/JSYST.2020.3011901).
- [120] S. Poudel, P. Sharma, A. Dubey, and K. P. Schneider, “Advanced FLISR with intentional islanding operations in an ADMS environment using GridAPPS-D,” *IEEE Access*, vol. 8, 2020, pp. 113 766–113 778. DOI: [10.1109/ACCESS.2020.3003325](https://doi.org/10.1109/ACCESS.2020.3003325).
- [121] G. Qu and N. Li, “Optimal distributed feedback voltage control under limited reactive power,” *IEEE Transactions on Power Systems*, vol. 35, no. 1, 2019, pp. 315–331.

- [122] H. Ren, R. R. Jha, A. Dubey, and N. N. Schulz, “Extremum-seeking adaptive-droop for model-free and localized volt-var optimization,” *IEEE Transactions on Power Systems*, vol. 37, no. 1, 2022, pp. 179–190. DOI: [10.1109/TPWRS.2021.3093831](https://doi.org/10.1109/TPWRS.2021.3093831).
- [123] B. A. Robbins, H. Zhu, and A. D. Domínguez-García, “Optimal tap setting of voltage regulation transformers in unbalanced distribution systems,” *IEEE Transactions on Power Systems*, vol. 31, no. 1, 2016, pp. 256–267.
- [124] R. Sadnan and A. Dubey, “Real-time distributed control of smart inverters for network-level optimization,” in *2020 IEEE International Conference on Communications, Control, and Computing Technologies for Smart Grids (SmartGridComm)*, IEEE, pp. 1–6, 2020.
- [125] R. Sadnan and A. Dubey, “Distributed optimization using reduced network equivalents for radial power distribution systems,” *IEEE Transactions on Power Systems*, 2021.
- [126] R. Sadnan, S. Poudel, A. Dubey, and K. P. Schneider, “Layered coordination architecture for resilient restoration of power distribution systems,” *IEEE Transactions on Industrial Informatics*, 2022, pp. 1–1. DOI: [10.1109/TII.2022.3177464](https://doi.org/10.1109/TII.2022.3177464).
- [127] M. D. Sankur, R. Dobbe, E. Stewart, D. S. Callaway, and D. B. Arnold, “A linearized power flow model for optimization in unbalanced distribution systems,” *arXiv preprint arXiv:1606.04492*, 2016.
- [128] A. Savascı, A. Inaolaji, and S. Paudyal, “Two-stage volt-var optimization of distribution grids with smart inverters and legacy devices,” *IEEE Transactions on Industry Applications*, vol. 58, no. 5, 2022, pp. 5711–5723. DOI: [10.1109/TIA.2022.3183182](https://doi.org/10.1109/TIA.2022.3183182).
- [129] A. Savascı, A. Inaolaji, S. Paudyal, and S. Kamalasadan, “Efficient distribution grid optimal power flow with discrete control of legacy grid devices,” in *2021 IEEE Power & Energy Society General Meeting (PESGM)*, pp. 1–5, 2021. DOI: [10.1109/PESGM46819.2021.9638228](https://doi.org/10.1109/PESGM46819.2021.9638228).
- [130] K. P. Schneider, Y. Chen, D. Engle, and D. Chassin, “A taxonomy of north american radial distribution feeders,” in *IEEE PES General Meeting, 2009*, IEEE, pp. 1–5, 2009.

- [131] K. P. Schneider, B. A. Mather, B. C. Pal, C. W. Ten, G. J. Shirek, H. Zhu, J. C. Fuller, J. L. R. Pereira, L. F. Ochoa, L. R. de Araujo, R. C. Dugan, S. Matthias, S. Paudyal, T. E. McDermott, and W. Kersting, “Analytic considerations and design basis for the ieee distribution test feeders,” *IEEE Transactions on Power Systems*, vol. 33, no. 3, May 2018, pp. 3181–3188. DOI: [10.1109/TPWRS.2017.2760011](https://doi.org/10.1109/TPWRS.2017.2760011).
- [132] K. P. Schneider, J. C. Fuller, F. K. Tuffner, and R. Singh, “Evaluation of conservation voltage reduction (CVR) on a national level,” PNNL, Richland, WA (US), Tech. Rep., 2010.
- [133] K. Schneider, D. Enge, Y. Chen, S. Thompson, D. Chassin, and R. Pratt, “Modern grid initiative distribution taxonomy,” November 2008.
- [134] S. R. Shukla, S. Paudyal, and M. R. Almassalkhi, “Efficient distribution system optimal power flow with discrete control of load tap changers,” *IEEE Transactions on Power Systems*, vol. 34, no. 4, 2019, pp. 2970–2979.
- [135] X. Su, M. A. S. Masoum, and P. J. Wolfs, “Optimal pv inverter reactive power control and real power curtailment to improve performance of unbalanced four-wire lv distribution networks,” *IEEE Transactions on Sustainable Energy*, vol. 5, no. 3, Jul. 2014, pp. 967–977. DOI: [10.1109/TSTE.2014.2313862](https://doi.org/10.1109/TSTE.2014.2313862).
- [136] X. Sun and J. Qiu, “Two-stage volt/var control in active distribution networks with multi-agent deep reinforcement learning method,” *IEEE Transactions on Smart Grid*, 2021.
- [137] Y. T. Tan and D. S. Kirschen, “Impact on the power system of a large penetration of photovoltaic generation,” in *2007 IEEE Power Engineering Society General Meeting*, pp. 1–8, 2007. DOI: [10.1109/PES.2007.385563](https://doi.org/10.1109/PES.2007.385563).
- [138] L. Thurner, A. Scheidler, F. Schäfer, J.-H. Menke, J. Dollichon, F. Meier, S. Meinecke, and M. Braun, “Pandapower—an open-source python tool for convenient modeling, analysis, and optimization of electric power systems,” *IEEE Transactions on Power Systems*, vol. 33, no. 6, 2018, pp. 6510–6521. DOI: [10.1109/TPWRS.2018.2829021](https://doi.org/10.1109/TPWRS.2018.2829021).

- [139] J.-F. Toubeau, B. Bakhshideh Zad, M. Hupez, Z. De Grève, and F. Vallée, “Deep reinforcement learning-based voltage control to deal with model uncertainties in distribution networks,” *Energies*, vol. 13, no. 15, 2020, p. 3928.
- [140] F. C. Trindade, T. S. Ferreira, M. G. Lopes, and W. Freitas, “Mitigation of fast voltage variations during cloud transients in distribution systems with pv solar farms,” *IEEE Transactions on Power Delivery*, vol. 32, no. 2, 2017, pp. 921–932.
- [141] K. Turitsyn, P. Sulc, S. Backhaus, and M. Chertkov, “Local control of reactive power by distributed photovoltaic generators,” in *Proc. First IEEE International Conference on Smart Grid Communications*, pp. 79–84, 2010.
- [142] K. Turitsyn, P. Sulc, S. Backhaus, and M. Chertkov, “Options for control of reactive power by distributed photovoltaic generators,” *Proceedings of the IEEE*, vol. 99, no. 6, 2011, pp. 1063–1073. DOI: [10.1109/JPROC.2011.2116750](https://doi.org/10.1109/JPROC.2011.2116750).
- [143] UK Open Networks Project, *UK Open Networks 2017-2022*, <https://www.energynetworks.org/creating-tomorrows-networks/open-networks/2017-2022>, 2022.
- [144] B. Wang, Y. Li, W. Ming, and S. Wang, “Deep reinforcement learning method for demand response management of interruptible load,” *IEEE Transactions on Smart Grid*, vol. 11, no. 4, 2020, pp. 3146–3155.
- [145] S. Wang, J. Duan, D. Shi, C. Xu, H. Li, R. Diao, and Z. Wang, “A data-driven multi-agent autonomous voltage control framework using deep reinforcement learning,” *IEEE Transactions on Power Systems*, vol. 35, no. 6, 2020, pp. 4644–4654.
- [146] W. Wang and N. Yu, “Chordal conversion based convex iteration algorithm for three-phase optimal power flow problems,” *IEEE Transactions on Power Systems*, vol. 33, no. 2, Mar. 2018, pp. 1603–1613. DOI: [10.1109/TPWRS.2017.2735942](https://doi.org/10.1109/TPWRS.2017.2735942).
- [147] W. Wang, N. Yu, Y. Gao, and J. Shi, “Safe off-policy deep reinforcement learning algorithm for volt-var control in power distribution systems,” *IEEE Transactions on Smart Grid*, vol. 11, no. 4, 2019, pp. 3008–3018.

- [148] Z. Wang, J. Wang, B. Chen, M. M. Begovic, and Y. He, “Mpc-based voltage/var optimization for distribution circuits with distributed generators and exponential load models,” *IEEE Transactions on Smart Grid*, vol. 5, no. 5, 2014, pp. 2412–2420.
- [149] Z. Wang, D. S. Kirschen, and B. Zhang, “Accurate semidefinite programming models for optimal power flow in distribution systems,” *arXiv preprint arXiv:1711.07853*, 2017.
- [150] Z. Wang and J. Wang, “Self-healing resilient distribution systems based on sectionalization into microgrids,” *IEEE Transactions on Power Systems*, vol. 30, no. 6, 2015, pp. 3139–3149.
- [151] J.-P. Watson, A. F. Castillo, P. U. Lipka, S. U. Oren, and R. F. O’Neill, “A current-voltage successive linear programming approach to solving the ACOPF.,” Sandia National Lab.(SNL-NM), Albuquerque, NM (United States), Tech. Rep., 2014.
- [152] W. L. Winston, M. Venkataraman, and J. B. Goldberg, *Introduction to mathematical programming*, vol. 1. Thomson/Brooks/Cole Duxbury; Pacific Grove, CA, 2003.
- [153] W. Wu, Z. Tian, and B. Zhang, “An exact linearization method for OLTC of transformer in branch flow model,” *IEEE Transactions on Power Systems*, vol. 32, no. 3, 2017, pp. 2475–2476.
- [154] Q. Yang, G. Wang, A. Sadeghi, G. B. Giannakis, and J. Sun, “Two-timescale voltage control in distribution grids using deep reinforcement learning,” *IEEE Transactions on Smart Grid*, vol. 11, no. 3, 2019, pp. 2313–2323.
- [155] Z. Yang, H. Zhong, A. Bose, T. Zheng, Q. Xia, and C. Kang, “A linearized OPF model with reactive power and voltage magnitude: A pathway to improve the mw-only DC OPF,” *IEEE Transactions on Power Systems*, vol. 33, no. 2, 2018, pp. 1734–1745.
- [156] A. S. Zamzam, N. D. Sidiropoulos, and E. Dall’Anese, “Beyond relaxation and newton–raphson: Solving AC OPF for multi-phase systems with renewables,” *IEEE Transactions on Smart Grid*, vol. 9, no. 5, 2018, pp. 3966–3975. DOI: [10.1109/TSG.2016.2645220](https://doi.org/10.1109/TSG.2016.2645220).

- [157] D. Zhang, X. Han, and C. Deng, “Review on the research and practice of deep learning and reinforcement learning in smart grids,” *CSEE Journal of Power and Energy Systems*, vol. 4, no. 3, 2018, pp. 362–370.
- [158] J. Zhang, Y. Li, Z. Wu, C. Rong, T. Wang, Z. Zhang, and S. Zhou, “Deep-reinforcement-learning-based two-timescale voltage control for distribution systems,” *Energies*, vol. 14, no. 12, 2021, p. 3540.
- [159] Y. Zhang, X. Wang, J. Wang, and Y. Zhang, “Deep reinforcement learning based volt-var optimization in smart distribution systems,” *IEEE Transactions on Smart Grid*, vol. 12, no. 1, 2020, pp. 361–371.
- [160] C. Zhao, E. Dall-Anese, and S. Low, “Convex relaxation of OPF in multiphase radial networks with wye and delta connections,” National Renewable Energy Lab.(NREL), Golden, CO (United States), Tech. Rep., 2017.
- [161] H. Zhu and H. J. Liu, “Fast local voltage control under limited reactive power: Optimality and stability analysis,” *IEEE Transactions on Power Systems*, vol. 31, no. 5, Sep. 2016, pp. 3794–3803. DOI: [10.1109/TPWRS.2015.2504419](https://doi.org/10.1109/TPWRS.2015.2504419).